TWO-LAYER SLOT COATING:

STUDY OF DIE GEOMETRY AND INTERFACIAL REGION

TWO-LAYER SLOT COATING:

STUDY OF DIE GEOMETRY AND INTERFACIAL REGION

By

SHAWN DAVID TAYLOR, B.Eng. Mgt.

A Thesis

Submitted to the School of Graduate Studies

in Partial Fulfillment of the Requirements

for the Degree

Master of Engineering

McMaster University

July 1997

Master of Engineering (1997)	McMaster University
Chemical Engineering	Hamilton, Ontario

TITLE:	Two-Layer Slot Coating: Study of Die Geometry and Interfacial Region
AUTHOR:	Shawn David Taylor, B.Eng.Mgt. (McMaster University)
SUPERVISOR:	Dr. A. N. Hrymak
NUMBER OF PAGES:	xvii, 150

ABSTRACT

The two-layer slot coating method is commonly used in industry to apply multiple layers of miscible liquids onto a moving substrate. Previous experimental work using a standard flat die face geometry has shown that tiny recirculations exist within the coating bead. Recirculations near the interfacial region may cause convective mixing of the two liquid layers and thus, defects in the final coated material. Previous studies on the interfacial region between the two miscible liquids have assumed that diffusional and convective mixing of the two layers can be ignored and that an 'interface' of zero surface tension exists between the two layers. This work attempts to show that observable mixing does occur between layers of miscible liquid and that the convective mixing can be minimized by changing the geometry of the die face between the two slots.

Flow visualizations using particles and two different coloured dyes were performed on the standard square die face geometry. Result show that vortices exist in the coating bead under all the test conditions, either at the downstream shoulder of the die or in the interfacial region near upstream feed slot. The presence of the vortices at these positions, as well as the position of the separation line, was partially determined by the ratio of top layer viscosity to bottom layer viscosity, among other factors.

Visualizations were also done using various geometries for the centre block: knife, groove, and bullet referring to the shape of the different blocks. The knife geometry decreased the performance of the two slot coater, causing problems such as oscillations of the upstream meniscus and invasions of the top layer into the bottom layer feed slot. The performance of the groove geometry was very similar to the standard square geometry

except for the occurrence of an extra tiny vortex inside the groove itself. The bullet centre block eliminated the vortices in the interfacial region and provided limited control of the region's shape and position.

The commercial CFD package FIDAP™ was used to simulate a two dimensional Newtonian model of the two slot coating bead under the same operating conditions used in the experiments. Variations in liquid properties across the interfacial region were calculated by defining viscosity as a function of false species concentration, where the isoconcentration contours were then used to define the interfacial region. The simulation showed excellent agreement with the square and groove geometries, and reasonable agreement with the knife and bullet geometries. The simulations indicate that a vortex forms in the interfacial region near the upstream feed slot for viscosity ratios of 4:1 to 10:1. The vortex caused convective mixing between the liquid layers for all geometries; however, the mixing was reduced or eliminated by the knife, groove and bullet geometries at a viscosity ratio of 10:1.

ACKNOWLEDGMENTS

I would first like to express my deepest appreciation to my supervisor, Andrew Hrymak, for the insight and enthusiasm that he brought to this work as well as his guidance in building my professional career. I would also like to thank him for not losing his temper when I 'accidentally rolled' our small Argon-Ion laser.

I would like to acknowledge the financial support of the Natural Sciences and Engineering Research Council of Canada, the Xerox Research Centre of Canada, and McMaster University. I would like to thank the Ontario Laser & Lightwave Research Centre at the University of Toronto for the use of their Argon-Ion laser.

Thank you to the employees of Xerox Research Centre of Canada for their support during my time at XRCC. I am especially gratefully to Maya Stevanovic, Art Jones, Dave MacKinnon, and Greg Kovacs for their contributions to this theses.

Thank you to ***everyone*** in the Department of Chemical Engineering at McMaster University for your friendship and support over the last seven years. I am especially grateful to the following people: Ċeline Bellehumeur, Victor Bravo, Justyna Derkach, Jim Dickson, Sara Gallo-O'Toole, Paul Gatt, Shaffiq Jaffer, Julie McLachlan, Barb Owen, Alberto Rincon, Farhad Sharif, Vasileios Sidiropoulos, Gord Slater, John Vlachopoulos, Philip Wood, Donald Woods, and Alex MacGregor (for the two black eyes from hockey).

Thank you to my family for always giving me guidance and encouragement when I needed it.

Finally, I want to thank my fiancée Tara for her continuing love and support throughout this work.

TABLE OF CONTENTS

TABLE OF CONTENTS

TABLE OF CONTENTS

LIST OF FIGURES

LIST OF FIGURES

LIST OF FIGURES

LIST OF FIGURES

LIST OF FIGURES

LIST OF TABLES

LIST OF SYMBOLS

C	concentration of false species
Ca	Capillary number
D	downstream region of coating bead
f(x)	general function for velocity
F	film forming region of coating bead
$\hat{F}$	unit vector in direction of gravity
g	acceleration of gravity
gap	coating gap
H	heel or upstream region of coating bead
$\hat{i}$	unit vector in x-direction
I	intermediate region of coating bead
$\overline{\overline{I}}$	identity matrix
$\hat{j}$	unit vector in y-direction
L	characteristic length
m	top layer to bottom layer viscosity ratio
$\hat{n}$	unit normal
p	pressure
Q	flow rate per unit length
r	radius of curvature
Re	Reynolds number

s	line of meniscus
S	feed slot region of coating bead
St	Stokes number
t	wet thickness
$\hat{t}$	tangent unit vector
$\overline{\overline{T}}$	stress tensor
u	x-velocity component
$\overline{u}$	velocity vector
U	web speed
$\overline{U}$	dimensionless velocity vector
v	y-velocity component
vac	vacuum pressure
$\overline{W}$	solution vector
x	coordinate vector (x,y,z)
y	coordinate vector (x,y,z)
z	coordinate vector (x,y,z)

Greek Symbols

α	false species diffusivity
β	slip coefficient
γ	relaxation factor

λ	wave length
μ	viscosity
θ	contact angle
ρ	density
σ	surface tension
τ	shear stress

Subscripts

1	meniscus number 1 in Young-Laplace equation
2	meniscus number 2 in Young-Laplace equation
A	top liquid layer
air	property of air
atm	atmospheric
B	bottom liquid layer
d	downstream
dyn	dynamic
i	index
L	lower layer
max	maximum absorption wavelength
ref	reference
s	solid surface
u	upstream

U upper layer

vac vacuum

w web surface

Superscripts

T transpose

* calculated solution vector

Mathematical Symbols

d/dy derivative

δ/δx partial derivative

Δ difference

∇ gradient

• dot product

: double-dot product

CHAPTER 1

SLOT COATING FUNDAMENTALS

1.1 Introduction

The process of coating has been defined as the displacement of gas at a solid surface by a layer of liquid (Scriven and Suszynski, 1990). A number of methods have been developed for applying liquid layers to a moving substrate, such as curtain, dip, roll and slide coating. A comprehensive review of these methods can be found in Cohen and Gutoff (1992).

All of the processes discussed by Cohen and Gutoff are capable of applying, at minimum, a single layer for every substrate pass through the applicator equipment. In many applications, such as floor coverings and paper, only one coating may be necessary. Other products like photographic film require many layers that are very thin and precise in final thickness. Products requiring such precise thickness control are coated using premetered coating machines, examples being curtain, slide, and slot coaters. These machines use a pump to deliver a measured amount of liquid through a die or hopper that distributes the liquid as a thin film on the moving solid surface. The thickness of the liquid layer is determined by the flow rate and not by the properties of the coating fluids (Cohen and Gutoff, 1992).

At one time, it was customary to coat only a single layer with each pass through the premetered coating machine and apply the next layer after the previous one had dried. It was believed that this prevented mixing of adjacent layers (Russell, 1956). However, coating only one layer at a time is costly in both time and duplicate equipment. To reduce these costs, a number of variations on premetered coaters have been developed to apply several liquid layers in a single pass. Table 1.1 lists patents covering some of the variations in premetered coating design.

The focus of this work is the analysis of the die design of a premetered two-slot coater. Particular attention is given to the effects of different separator shapes between the two liquids on the flow field of the coating bead. The coating bead is defined as the liquid-filled region between the die and the web (or substrate). The occurrence of film defects are often directly related to the flow structure within the bead. By controlling the shape of the die, we should be able to control the flow structure and thus reduce or eliminate many film defects.

The main difficulty in every model for the flow within slot coaters has been defining the boundary conditions, particularly in the regions of fluid-fluid-solid and fluid-fluid interfaces. This chapter will review the forces affecting the bead of slot coaters followed by a discussion of the fluid models for the single- and double-layer slot coaters. The major features of a two-slot coater are defined in Figure 1.1. The features of the single slot coater are the same except that the centre piece and the interfacial region do not exist.

Table 1.1: Patents covering variations in premetered coating die design.

Inventor	Patent	Year	Description of Design
Russell	US 2,761,418	1956	Up to four liquid layers brought into contacted inside a die and extruded onto the web through a single flat faced slot.
Beck	US 2,901,770	1959	Flat faced two slot coater applying liquid at an angle of 0° to 30° to the direction of the web surface.
Bartlett et. al.	US 2,932,855	1960	Flat faced two and four slot coater with die faces set at varying angles to the web surface.
Miller and Wheeler	US 3,206,323	1965	Two slot coater with liquid layers contacted inside the die with knife shaped separator piece.
Cameron and Wills	US 3,413,143	1968	Flat faced three slot coater for coating two liquid layers. Bottom layer thickness controlled by drawing extra liquid up the middle slot.
Ishiwata et. al.	US 3,573,965	1971	Flat faced two and four slot coater set perpendicular to web surface with increasing liquid layer viscosity from the bottom to the top layer.
Nagai and Uchida	US 3,584,600	1971	Flat faced four slot coater with downstream die face at least 5 times longer than length of the other die faces.
Kageyama and Yoshida	UK 2 120 132	1986	Single slot coater with the downstream die face cut to create a varying gap height.
Shibata et. al.	US 4,681,062	1987	Single slot coater with rounded die faces.
Chino et. al.	US 5,030,484	1991	Two slot coater with liquid layers making contact inside the die. Flat separator piece interchangeable rounded or pointed tipped pieces.
Umemura	US 5,097,792	1992	Two slot coater with rounded centre and downstream die faces.

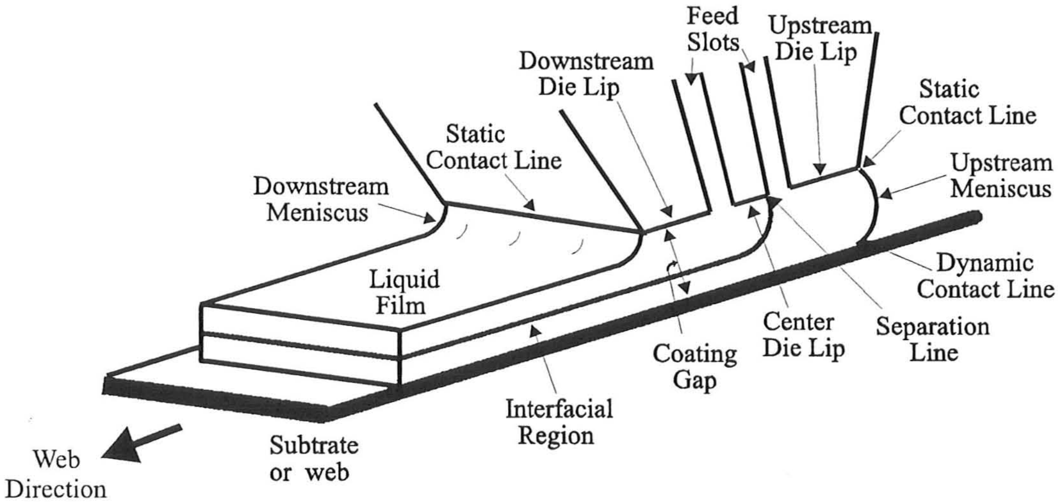

Figure 1.1: Main features of a two slot coating bead.

1.2 Forces Affecting the Coating Bead

The key to obtaining a uniform coating is to balance the forces that affect the bead. When a balanced or stable bead is achieved, the flow structure becomes predominantly two dimensional and independent of time. Cohen and Gutoff (1992) identified the main forces that affect the stability of a coating bead and classified each force as either *destabilizing,* which tends to lift the upstream meniscus off the web, or *stabilizing,* that tends to hold the bead against the web.

Destabilising Forces

Viscous drag is the main destabilizing force within the coating bead. The sudden pull of the liquid across the coating gap by the large viscous drag tends to pull the liquid apart. The shear stress, τ_{xy}, for a Newtonian fluid is expressed as:

$$\tau_{xy} = \mu \frac{du}{dy} \tag{1.1}$$

where μ is the fluid viscosity, u is the velocity in the web direction and y is normal to the web surface (Figure 1.2). The total drag is obtained by integrating the shear stress along the web from the dynamic contact line to a point downstream where $\tau = 0$.

Air film momentum becomes important at higher web speeds where it becomes difficult to displace the air trapped along the surface of the web. Due to the no-slip condition, air at the surface of the web moves at the web velocity. Hence, a very thin layer of air remains at the web surface pushing the bead away from the web and causing an increase in the dynamic contact angle, the angle made when the upper meniscus comes into contact with the moving web. When this angle reaches 180° the bead becomes unstable and the liquid layer entrains air bubbles.

Centrifugal forces created by the rotation of the backing roll tends to throw the liquid off the web. However, this force is considered insignificant due to the low mass of the thin liquid film.

Stabilising Forces

Gravity tends to pull the upstream meniscus down, helping to keep the liquid within the vertical coating gap. Due to the low mass of the thin liquid film, Cohen and Gutoff suggest ignoring the gravity body force in the analysis of the coating bead; however, Sartor (1990) and Scanlan (1990) found gravity to be important in their models.

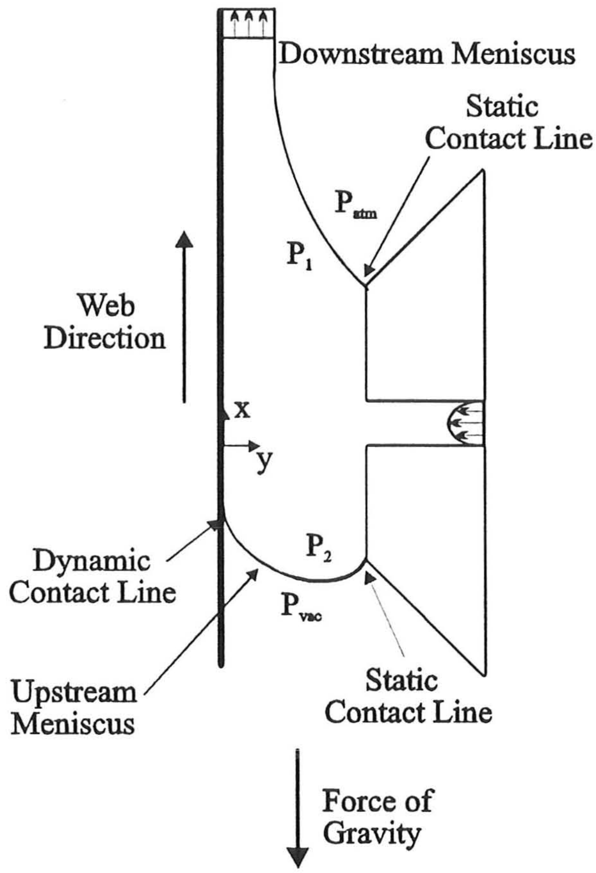

Figure 1.2: Coating bead of a single-slot coater.

The *inertia forces* created by the fluid travelling from the feed port towards the web have only a small effect on stabilising the bead. Slow flow rates and the high viscosities typical of slot coating lead to a small inertia force relative to the dominant viscous force. This is indicated by a Reynolds number less than one (Cohen, 1993):

$$\mathrm{Re} = \frac{\rho UL}{\mu} < 1 \tag{1.2}$$

where ρ is the fluid density, μ is the fluid viscosity, U is a characteristic velocity (usually web speed), and L a characteristic length. The choice of length is typically the coating gap or gap length, although Cohen (1993) simplified the Reynolds number by setting L equal to the final thickness of the liquid layer. The Reynolds number becomes:

$$Re = \frac{\rho Q}{\mu} \tag{1.3}$$

where Q = UL is the flow rate per unit width.

Capillary pressure, created by the two menisci, is the main stabilising force within the bead. The pressure difference across a fluid interface is given by the Young-Laplace equation (Woods, 1995):

$$\Delta p = \sigma\left(\frac{1}{r_1} + \frac{1}{r_2}\right) \tag{1.4}$$

where σ is the surface tension and r_i (i=1,2) are the radii of curvature of any free surface. Since both menisci are two dimensional, $r_2 = 0$. Assuming absolute atmospheric pressure, p_{atm}, outside the downstream meniscus and a radius of curvature $r_1 = r_d$, equation (1.4) becomes:

$$p_{atm} - p_1 = \frac{\sigma}{r_d} \tag{1.5}$$

A similar equation is obtained for the pressure difference across the upstream meniscus:

$$p_2 - p_{vac} = \frac{\sigma}{r_u} \tag{1.6}$$

where p_{vac} is the absolute vacuum pressure below the meniscus of radius $r_l = r_u$. The pressure difference, $p_{atm}-p_{vac} \geq 0$, helps to keep the bead within the coating gap. However, the capillary force only helps over a limited range of surface tensions and flow rates before large viscous forces created by higher web speeds cause the bead to break apart (Higgins, 1980). The range of bead stability can be extended by applying a vacuum below the upstream meniscus (Beguin, 1954).

More complicated equations for the pressure change across a gas-liquid interface have been derived by Higgins (1980) who assumed that the upstream and downstream menisci had circular curvatures. Later experimental work by Sartor (1990) proved that the menisci never have a circular curvature, but appear to be stretched arcs.

Coating Window

When the forces affecting the coating bead are properly balanced, a stable two-dimensional flow field is obtained that results in a uniform coating. If any of the forces become too weak or too strong, transient behaviour will begin to occur within the bead causing defects in the final coating. In some cases, a partial or complete collapse of the bead may occur. The most common defects that are observed include the following:

- *ribbing*: regular or irregular variations in the coating thickness in the cross web direction.
- *rivulets*: severe ribbing where the liquid is coated in a series of thin lines separated by line of dry webbing.
- *barring*: regular or irregular variations in the coating thickness in the web direction.

- *weeping*: a reduction in the coating thickness due to the loss of liquid at the upstream meniscus.
- *air entrainment*: tiny bubbles formed at the upstream meniscus become entrained in the coating flow.

The occurrence of any one of these defects depends on the operating conditions of the coater. The set of conditions under which defect free coatings are obtained is referred to as a *coating* or *operating window*.

1.3 Single Layer Slot Coater

A simple, yet commonly used liquid applicator in industry is the single-layer slot coater. A thorough theoretical study of the bead for Newtonian fluids has been done by Sartor (1990), whose model is briefly presented here. Note that the coordinate axis are defined in Figure 1.2 where $\overline{\mathrm{u}} = (\mathrm{u}, \mathrm{v})$.

1.3.1 Governing Equations

The analysis begins with the general continuity and momentum equations. The transient terms are omitted since the bead is assumed to be at steady state under normal operating conditions. Fluid dynamics in the bead can be assumed to be two dimensional by ignoring the edge effects. The resulting governing equations, in dimensionless form, are as follows:

$$\nabla \bullet \overline{\mathrm{U}} = 0 \qquad (1.7)$$

$$\mathrm{Re}(\overline{\mathrm{U}} \bullet \nabla \overline{\mathrm{U}}) = \nabla \bullet \overline{\mathrm{T}} + \mathrm{St}\hat{\mathrm{F}} \qquad (1.8)$$

where $\overline{U} = \overline{u} / U = (u, v) / U$ is the dimensionless velocity vector, $St = gL^2/\mu U$ is the Stokes number, $\hat{F}$ is the unit vector in the direction of the gravity body force, U is the web speed, μ is the liquid viscosity, and L is a characteristic length (normally the coating gap). While most coating liquids are shear thinning, the analysis can be simplified at this point by assuming the coating is a Newtonian fluid. The total stress tensor, $\overline{\overline{T}}$, can be expressed as the sum of the isotropic pressure term, $\overline{\overline{I}}p$, and the viscous stress term:

$$\overline{\overline{T}} = -\overline{\overline{I}}p + \mu(\nabla\overline{U} + (\nabla\overline{U})^T) \tag{1.9}$$

Equations (1.7) through (1.9) can then be solved numerically once the appropriate boundary conditions have been applied.

1.3.2 Boundary Conditions

The first boundary condition to be specified is the velocity profile at the entrance to the coating bead. The flow of liquid through the feed slot is simply pressure driven flow between two parallel plates. Thus, the classic parabolic velocity profile, $\overline{u} = f(x)(\hat{i}, \hat{j})$, is applied at some distance up the feed slot. At the exit of the bead is the thin uniform film that is carried away by the web. For a distance far enough downstream in the web direction, a natural outflow condition or 'no traction condition' is imposed at the outflow plane:

$$\hat{n} \bullet \overline{\overline{T}} = 0 \tag{1.10}$$

Since there should not be a y-component velocity in the outflow region when the web in moving in the x-direction, an additional constraint is added:

$$\overline{u} \bullet \hat{j} = 0 \tag{1.11}$$

The next set of boundary conditions must be applied to the free surfaces of the upstream and downstream menisci. Assuming that the air near the menisci is inviscid and inertialess, the liquid-gas interface becomes a balance between normal viscous forces, pressure, and surface tension. Taking $\hat{n}$ to be the outward unit normal and $\hat{t}$ as tangential unit vector to the line, s, the force balance can be expressed by the equation:

$$\hat{n} \bullet \overline{\overline{T}} = \frac{1}{Ca}\frac{d\hat{t}}{ds} - \hat{n}p \tag{1.12}$$

where the ratio of viscous to surface tension forces is measured by the capillary number, $Ca=\mu U/\sigma$ and σ is the surface tension of the coating liquid. By specifying atmospheric pressure outside the downstream meniscus, the dimensionless pressure, p, is then set to zero:

$$p = p_{atm} - p_{ref}\left(\frac{L}{\mu U}\right) \tag{1.13}$$

Note that the reference pressure is set equal to the atmospheric pressure. Then equation (1.12) for the downstream and upstream meniscus, respectively, becomes (Scanlan, 1990):

$$\hat{n} \bullet \overline{\overline{T}} = \frac{1}{Ca}\frac{d\hat{t}}{ds} \tag{1.14}$$

$$\hat{n} \bullet \overline{\overline{T}} = \frac{1}{Ca}\frac{d\hat{t}}{ds} - \hat{n}\, p_{vac} \tag{1.15}$$

where p_{vac} is the vacuum pressure applied to the upstream meniscus.

Sartor (1990) also applied the kinematic condition at the gas-liquid interface:

$$\hat{n} \bullet \overline{u} = 0 \tag{1.16}$$

This condition assumes that the liquid is non-volatile and thus, there is no mass transfer across the gas-liquid interface.

Boundary conditions are also applied where the menisci meet a solid surface, either the moving web (referred to as a *dynamic contact line*) or the stationary coating die (referred to as a *static contact line*). To define a contact line in a two dimensional problem, one must choose two degrees of freedom. The possible degrees of freedom to choose from include: the u velocity component, the v velocity component, a relation between u and v, and the contact angle, θ. The contact angle is calculated as follows:

$$\hat{n}_S \bullet \hat{n} = \cos\theta \tag{1.17}$$

where $\hat{n}_S$ is the outward unit normal of the solid surface.

Velocity components u and v are usually set to zero for a static contact line, thus 'pinning' or fixing the position of the free surface. Sartor (1990) chose to pin the upstream and downstream contact lines to upstream and downstream die corners, respectively.

However, in some situations, Sartor (1990) chose to specify a contact angle and one velocity as zero at the upstream 'static' line to allow it move along the inside die face.

At the dynamic contact line, Sartor (1990) chose to specify a dynamic contact angle, θ_{dyn}, and impose Navier's slip boundary relationship:

$$\beta^{-1}\hat{t}_w \bullet (\bar{u} - \bar{u}_w) = \hat{t}_w\, \hat{n}_w : \bar{\bar{T}} \tag{1.18}$$

where the subscript 'w' refers to the web. Sartor (1990) found β=0.01 was a reasonable choice for the slip coefficient.

The dynamic contact angle, θ_{dyn}, can be determined from empirical correlations, such as (Gutoff and Kendrick, 1982):

$$\theta_{dyn} = 6.24\,Ca^{0.22}\left(\frac{\rho\sigma^3}{g\mu^4}\right)^{-0.099}\left(\frac{\mu}{\mu_{air}}\right)^{0.36} \tag{1.19}$$

where Ca is capillary number of the coating liquid. The correlation assumes a squared radius of curvature, r^2=0.90 and reasonably high web velocities. Due to these types of limitations, the dynamic contact angle is sometimes determined from flow visualizations.

The no-slip condition is imposed where the liquid makes contact with the die face or the moving web:

$$\bar{u} = (0,0) \quad \text{or} \quad \bar{u} = (V,0) \tag{1.17}$$

It is well documented that the no-slip condition leads to a singularity at the dynamic contact line (Dussan, 1979). Sartor has followed Silliman's (1979) suggestion of replacing the no slip condition with Navier's slip boundary condition in this region. However, the dynamic wetting process is still not fully understood making it difficult to describe mathematically. A fairly thorough review of dynamic wetting concept, experiments, and a number of possible boundary conditions or equations to solve this problem are given by Dussan (1979).

A graphical summary of Sartor's model is given in Figure 1.3.

1.4 Two Layer Slot Coater

Many products require more than one layer of coating. To help reduce the production costs associated with these products, industry has developed the two-slot coater which is capable of applying multiple layers in a single pass. The flow field of the two-layer bead is complicated by the presence of an interfacial region between the two liquid layers (refer to Figure 1.1). The separation line position, or the point along the die face where the layers first meet, may determine whether the film will have certain defects. For example, Ishizuka (1989) observed streaks in the final coating when the interfacial region invaded the feed slot in slide coaters. To eliminate such defects, it is important to have a good understanding of the flow field within the coating bead. This section reviews the two models that have been developed to predict the flow structure of two slot coating beads at steady state.

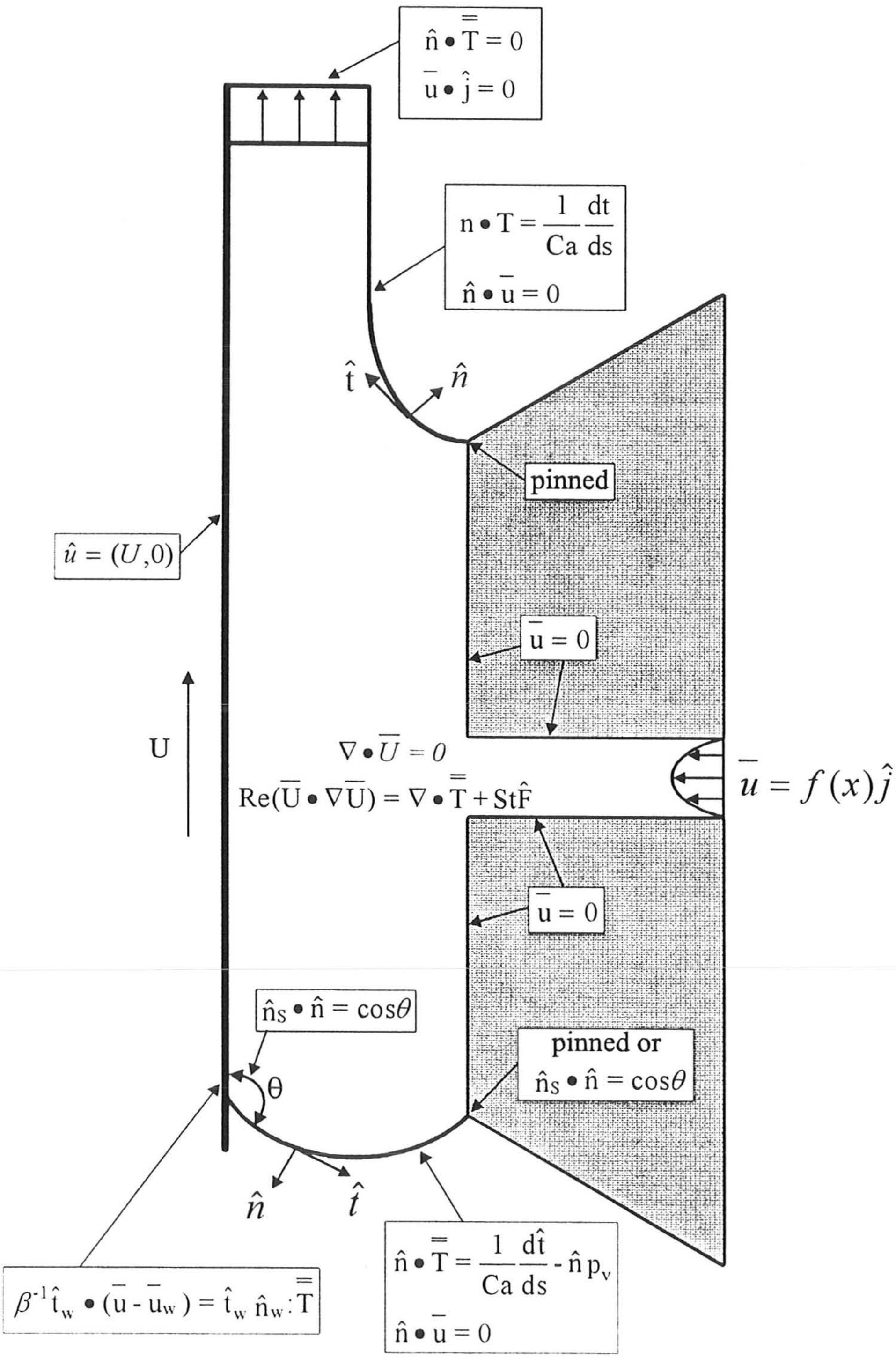

Figure 1.3: The mathematical model of the two dimensional, steady slot coater bead (Sartor, 1990).

1.4.1 Scanlan's Two Dimensional Model

Since the flow field of the two-layer bead is similar to the single-layer bead, Scanlan (1990) used the equations and boundary conditions developed by Sartor (1990). However, the new model required two sets of conservation equations (1.7, 1.8, and 1.9) for the top and for the bottom liquid layers.

Scanlan (1990) recognized that the interfacial region is actually a thin mixing zone between the two layers of miscible liquids. However, he chose to ignore the mixing effects between the layers arguing that the rate of Fickian diffusion is slow compared to the fluid velocity and that no other type of mixing occurred in the interfacial region. The interfacial region could then be assumed to be a liquid-liquid interface. A boundary condition for the interfacial region was then derived from the conservation of linear momentum to balance the normal stresses across an interface for immiscible liquids:

$$\hat{n}_A \bullet \overline{\overline{T}}_A = m(-\hat{n}_B \bullet \overline{\overline{T}}_B) + \frac{1}{Ca_{AB}}\frac{d\hat{t}}{ds} \tag{1.19}$$

where $m=\mu_B/\mu_A$. A and B refer to the top and bottom liquids layers, respectively. Since no interface tension exists between miscible layers, the final term in equation (1.19) could be eliminated. Assuming that both liquids are Newtonian, the equation becomes:

$$-p_A\,\hat{n}_A + \hat{n}_A \bullet [\nabla\bar{u} + (\nabla\bar{u})^T]_A = m(-p_B\,\hat{n}_B + \hat{n}_B \bullet [\nabla\bar{u} + (\nabla\bar{u})^T]_B) \tag{1.20}$$

Scanlan also applied the kinematic condition and no-slip condition along the interface region. Since the unit normal, $\hat{n}$, and unit tangents, $\hat{t}$, are equal and opposite, these conditions simply imply that the velocities on either side of the interface must be equal:

$$\bar{u}_A = \bar{u}_B = \bar{u} \tag{1.21}$$

An expression for the pressure difference across the 'interface' is then obtained by combining equations (1.20) and (1.21):

$$(p_A - p_B)\hat{n}_A = (m - 1)[\hat{n}_B \bullet (\nabla\bar{u} + (\nabla\bar{u})^T)] \tag{1.22}$$

When the viscosities of the two liquids are equal (m=1), this equation predicts a sudden jump in pressure across the 'liquid-liquid interface' which is not physically possible in a miscible system.

Scanlan completed his description of the interfacial region by applying the no-slip condition, $\bar{u} = 0$, at the separation line. The zero velocity at the die face corresponds to a balance in pressure between the two liquids, $p_A=p_B$, at the separation line. A small distance away from the wall, the velocities become non-zero and the pressure change is calculated using equation (1.22). This creates an artificial and sudden change in the pressure difference over a very short distance, leading to a conflict in the balance of normal stresses in the final solution (Dheur and Crochet, 1987). Scanlan suggested integrating the normal stress balance from the interface to the attachment point:

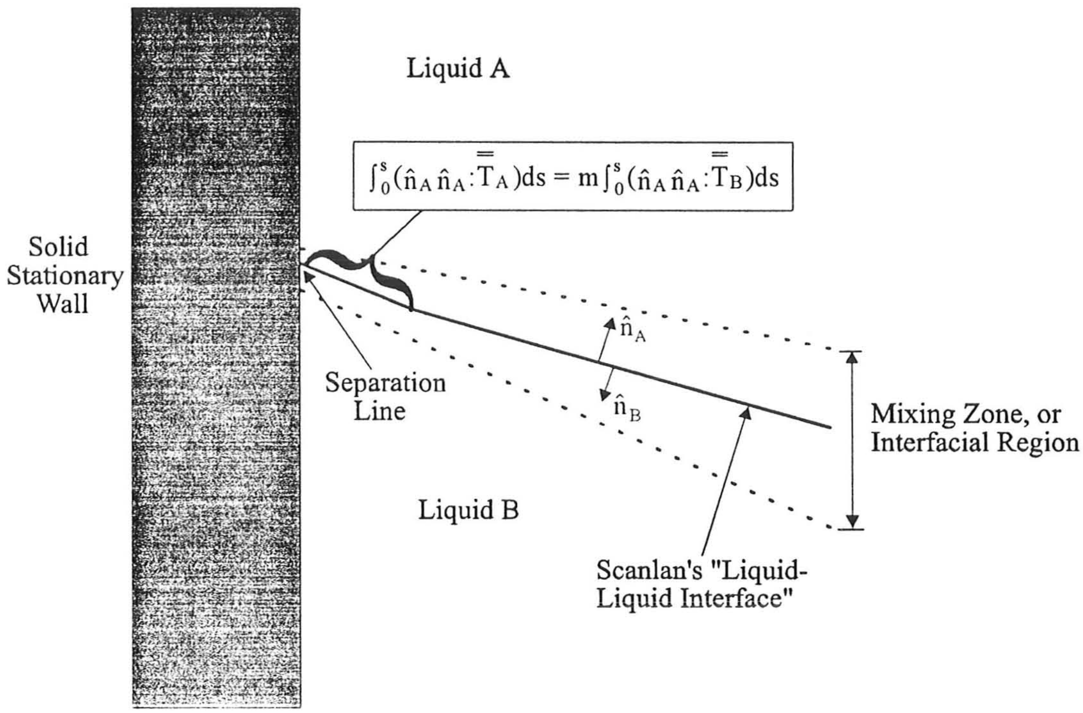

Figure 1.4: Integration of the normal stress in the region of the stationary die face (Scanlan, 1990).

$$\int_0^s(\hat{n}_A\hat{n}_A:\overline{\overline{T}}_A)ds = m\int_0^s(\hat{n}_A\hat{n}_A:\overline{\overline{T}}_B)ds \qquad (1.23)$$

where s is a short distance away from the wall (indicated by the bracket in Figure 1.4). While this method has a physical basis, it is difficult to execute since very small velocities are used in the calculation.

A graphical summary of Scanlan's two-slot coating model is shown in Figure 1.5.

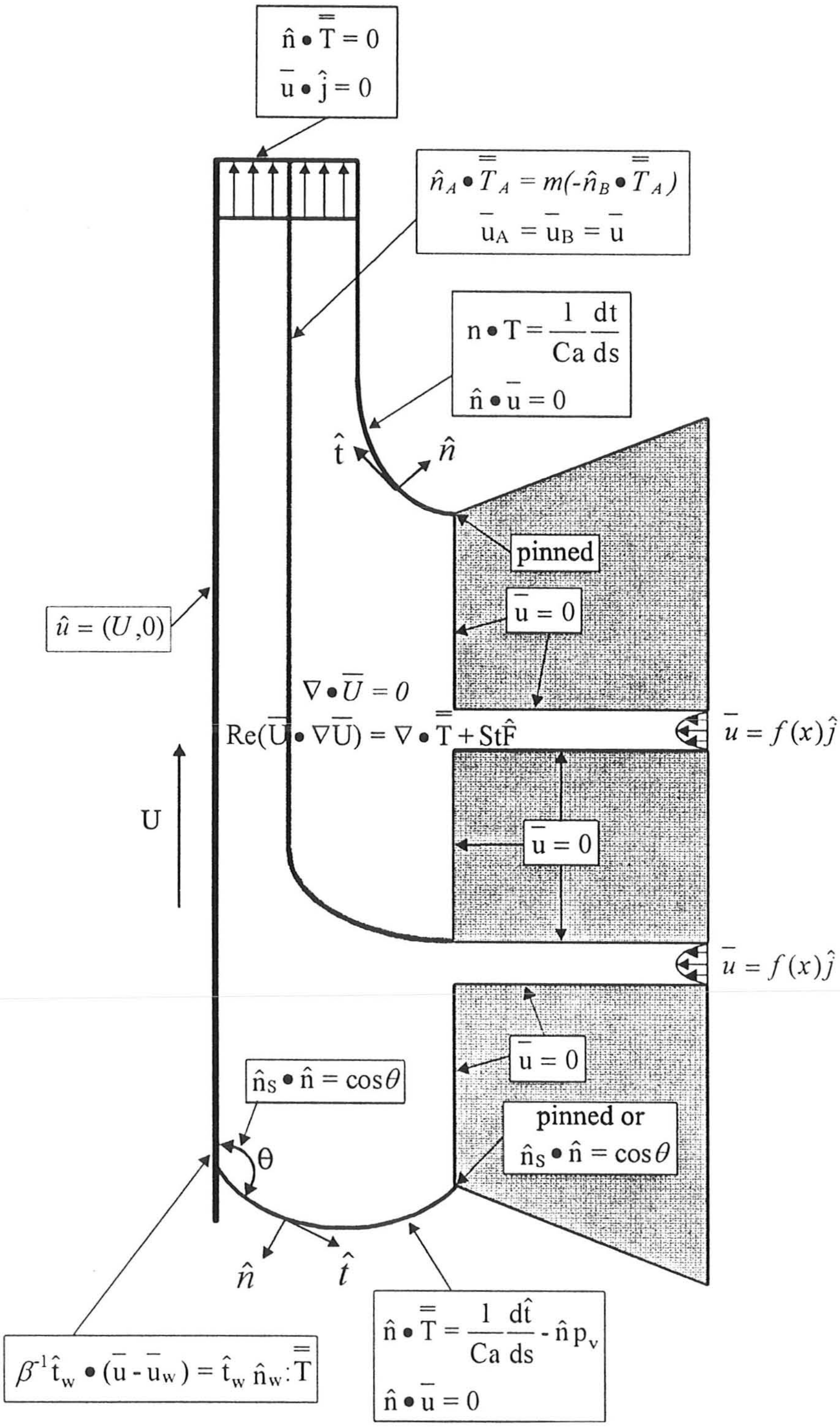

Figure 1.5: The mathematical model of the two dimensional, steady two slot coating bead (Scanlan, 1990).

1.4.2 Cohen's Rectilinear Model

While the dynamics of a slot coating bead is actually three dimensional, Sartor (1990) and Scanlan (1990) have shown that under steady state conditions the flow field is well approximated by a two dimensional model. Cohen (1993) attempted to take a simpler approach by noting that the flow field between the face of each die piece and the web is nearly rectilinear. Ignoring the small two-dimensional flow near the feed slots, the main flow characteristics of the coating bead could be obtained by modelling it as three separate sections. The sections would then be combined to give an approximation of the entire coating bead, as shown in Figure 1.6.

Each section can be modelled as Couette flow of two liquid layers between parallel plates. Ignoring any body forces and convective terms, the Navier-Stokes equations for two Newtonian fluids simplify to become:

$$\frac{\partial p}{\partial x} = \mu_i \frac{\partial^2 u_i}{\partial y^2} \qquad \text{where } i = A, B \tag{1.24}$$

$$\frac{\partial p}{\partial y} = 0 \tag{1.25}$$

By applying the same boundary conditions as Sartor (1990), an analytical solution can be derived for the velocity and pressure profiles. The full derivation of the rectilinear model is given in Appendix A.

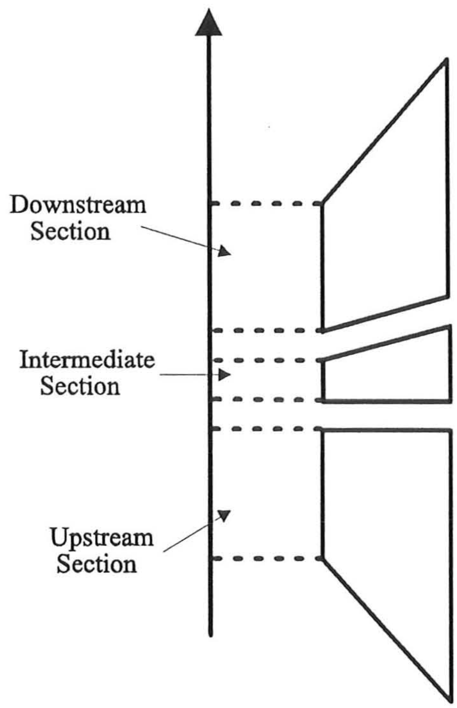

Figure 1.6: The separation of a two slot coating bead into three sections (Cohen, 1993).

The rectilinear model provides some useful insights into the main flow characteristics of the coating bead. For example, it gives an approximate position of the separation line as well as predicting the presence of large recirculation patterns. However, the model falls short in predicting the shape of the two menisci as well as the shape of the interfacial region and it can not predict the occurrence of small recirculation patterns.

1.5 Die Design and Flow Analysis

The objective in designing a multilayer coating is to create a series of distinct, uniform liquid layers stacked on top of one another. Designers follow a number of rules of thumb learned from years of manufacturing experience. For example, the bottom layer should always have the lowest viscosity, the carrier liquids must be miscible in one another, and the density and volatility of each liquid should be matched.

The use of miscible liquids in multilayer coating necessarily implies some degree of slow diffusional mixing between the adjacent liquid layers. Faster, convective mixing of the two liquids can also occur if a vortex exists between the two layers. The volume of mixed material between the two adjacent layers can be referred to as a mixing zone or interfacial region. In ideal coatings, the mixing zone should be almost non-existent so that each layer appears to be completely separated from its adjacent layers. In reality, mixing of the two fluid layers leads to an interfacial region of finite thickness over which the pressure, density, viscosity, and particle concentrations change very rapidly. Such severe gradients are difficult to observe experimentally and are very difficult to model mathematically.

In the case of a two-slot coating bead, Cohen (1993) suggested that the coater can be viewed simply as two single-layer slot coaters operating in sequence where the second layer is deposited immediately after the first layer. This concept is useful for understanding the two-slot coating flow under ideal conditions, such as the coating of two layers of identical fluids where no interfacial region exists. Since it is impossible to exactly match the properties of different liquid layers in a manufacturing environment, it is impossible to eliminate the interfacial region. Thus, the two slot coating bead must be modeled as a simultaneous two liquid flow.

One of the major difficulties in modeling the two slot coater, or any multilayer coater, is how to define the interfacial region between layers of miscible liquids. Both Scanlan (1990) and Cohen (1993) assumed no mass transfer between the layers and thus, proposed that the region behaves like an immiscible liquid-liquid interface with zero surface tension. Smith, van de Ven, and Mason (1980) have proposed a transient surface tension between miscible fluids. They suggest that a finite surface tension exists when the liquids first come into contact and then the tension reduces to zero over time as the two fluids diffuse into one another. The underlying assumption in both of these approaches is that the liquid-liquid interface is a two-dimensional plane (Edwards et. al., 1991; Israelachvili, 1992). In reality, an immiscible liquid-liquid interface has a finite thickness in the range of 10^{-9} m (Yang and Li, 1996) where there is steep gradient in fluid properties. However, the thickness of the surface can be ignored for problems with immiscible liquids. For miscible systems, the thickness of the interfacial region can not be ignored since it becomes quite thick or possibly non-existent as mixing (diffusional and/or convective) eliminates the steep gradient in fluid properties. Thus, the Sartor (1990) and Cohen (1993) models based on an immiscible interface of zero thickness should not be used to model the interfacial region of finite thickness.

A model for the interfacial region could be derived from the work on miscible liquid layers by Joseph (1990) and Galdi et. al. (1991). It was observed that droplets of glycerin in water "give rise at early times to shapes similar to, but not the same [as], pendant drops of immiscible liquids" (Joseph, 1990). Joseph proposed an alternative to surface tension that focused on variations in density, composition, and temperature around the interfacial region. The approach is based on the continuum ideas of Korteweg (1901) to compressible fluids. However, unlike Korteweg who related density to changes in pressure, Joseph suggested that the density in miscible liquid-liquid systems varies with concentration and temperature. The result, for an isothermal system, is an additional stress tensor being added to the Navier-Stokes equations that accounts for stresses created in the fluid system by variations in concentrations. This stress tensor would be negligible in the bulk flow but, would become large around the interfacial region. The two dimensional model of Scanlan (1990) could be modified to incorporate this tensor, although the calculations would become quite difficult.

A third, more empirical approach is to introduce a false species to track the interfacial region (Thompson, 1986; Hrymak and Stevanovic, 1994). The fluid viscosity is made a function of the false species concentration and the concentration throughout the flow field is calculated using the general mass transfer equations. Scanlan's immiscible interface boundary condition can then be replaced by an interfacial region where the properties of the two liquid layers are allowed to change over a short distance. Hrymak and Stevanovic (1994) report an estimate of the interfacial position and shape that responds to changes in operating conditions.

This work builds on the results of Hrymak and Stevanovic (1994), focusing on the effect of the die design on the shape, position, and thickness of the interfacial region in a two layer slot coating bead.

CHAPTER 2

EXPERIMENTAL METHOD

2.1 Introduction

Flow visualizations allow a researcher to examine the shape and form of a flow field and facilitates a conceptual understanding of basic flow structures. Models can then be built and validated using the results from these visualizations. There are a variety of visualization techniques available that provide both qualitative and quantitative information about a flow field. Goldstein (1983) provides a comprehensive review of the different methods available to a researcher. The choice of which method(s) to use depends on the nature of the flow field, the equipment available and the type information the researcher requires. In the case of coating flows, the small dimensions (often less than 1 mm) and the relatively inaccessible, fast moving coating bead limits a researcher without specialized equipment to qualitative visualizations.

Schweizer (1988) used a combination of dyes and hydrogen bubbles illuminated by fiber optic lighting to obtain side views of slide coating flows. The use of hydrogen bubbles limited this method of visualization to liquid layers with identical refractive indices and fluids that can generate hydrogen bubbles (i.e. water/glycerin solutions). Chen (1992) showed that the interface between liquid layers with different optical properties can be visualized by injecting dyes near the interface. Sartor (1990) adapted Schweizer's method to visualize the coating bead of a single slot coater and Cohen (1993) adapted it to a two-slot coater. Cohen also found that the use of hydrogen bubbles prevented the visualization of distinct liquid layers of different refractive indices.

This work uses visualizations to determine the flow structure of a stable two slot coating bead and how this flow field changed under different operating conditions. Particular attention was given to the shape and position of the interfacial region between the upper and lower liquid layers. Observations were also made on other features such as the positions of any recirculations, the static and dynamic contact lines, their apparent contact angles, and the shapes of the upstream and downstream menisci. These results were collected in the form of flow maps, sketches that highlight the basic structures in the coating bead at each operating condition. The flow maps and pictures will be used in a later chapter to validate the numerical model of the coating bead. This chapter outlines the details of the experimental set-up and operating conditions.

2.2 Experimental Set-Up

2.2.1 Coating Process

All visualizations were performed using a modified pilot scale Keegan coater, a schematic of which is shown in Figure 2.1. The coating liquids were pumped individually from the storage tanks under 35 kPa of nitrogen using two Zenith gear pumps (BPB Series and BMC Series, Zenith Pumps Division, Parker Hannifin). The gear pumps

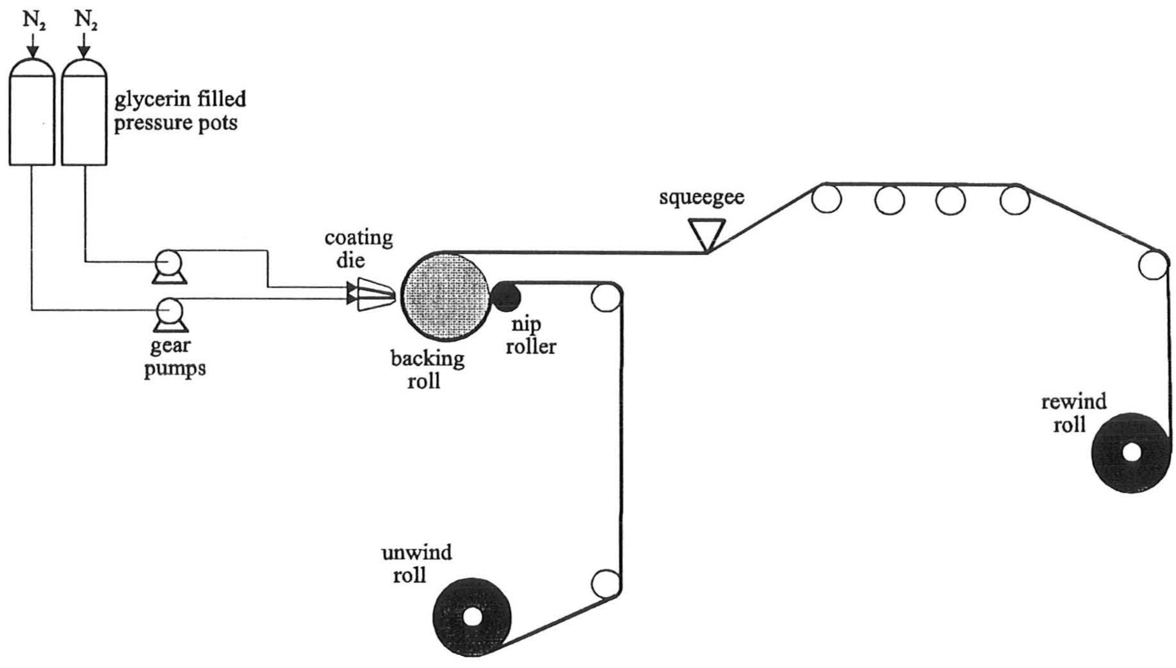

Figure 2.1: Schematic of the coating process.

delivered an accurate, premetered amount of each liquid through Teflon tubing (3/8 inch diameter, Nalge Company) to the coating die. The use of gear pumps ensured precise control of the thickness of each liquid layer.

Each liquid was then distributed and applied by a 7.62 cm (3 inch) wide two slot die onto a 10.16 cm (4 inch) wide strip of aluminized mylar (0.0005 inch thick). The fresh roll of mylar was unwound and proceeded through a series of rollers to one side of a 17.8 cm (7 inch) diameter stainless steel backing roll where a nip roller pressed the webbing firmly against the roll surface. The webbing was then carried to the opposite side of the backing roll where the die applied the coating solutions. The coated mylar was removed from the top of the backing roll and pulled under a rubber squeegee that scraped the liquid from the mylar and collected it in a stainless steel pot for disposal. The 'cleaned' webbing was then sent over a series of rollers to a rewind roll. Even after scrapping, a very thin film of liquid still remained on the web surface. Since the presence of the liquid film would change the surface characteristics of the web, the 'cleaned' mylar was not reused.

The set-up of the unwind and rewind rollers were identical. A variable speed DC motor (Reliance Model FR W56HC, Reliance Electric Co.) drove a belt around a 2.54 cm (1 inch) stainless steel bar that held the rolls of aluminized mylar. Web tension was controlled from the unwind and rewind rollers using magnetic clutches (Magpower Model O-50-S4, Magnetic Power Systems Inc.) located between the motor and belt drive. The line speed was controlled with a variable speed DC motor (Reliance Model FR W56HC, Reliance Electric Co.) connected directly to the backing roll.

2.2.2 Coating Die and Vacuum Box

All visualizations were performed using the 7.62 cm (3 inch) wide two-slot coating die shown in Figure 2.2. The modular die (Liberty Tool Corporation, Rochester, NY) consisted of three stainless steel pieces: an upstream block, a center block and a downstream block. There were four possible center pieces that could be used in the assembly of the die, each piece having a different shaped lip. The die was easily assembled by mounting the upstream block to the top side of the center block with two

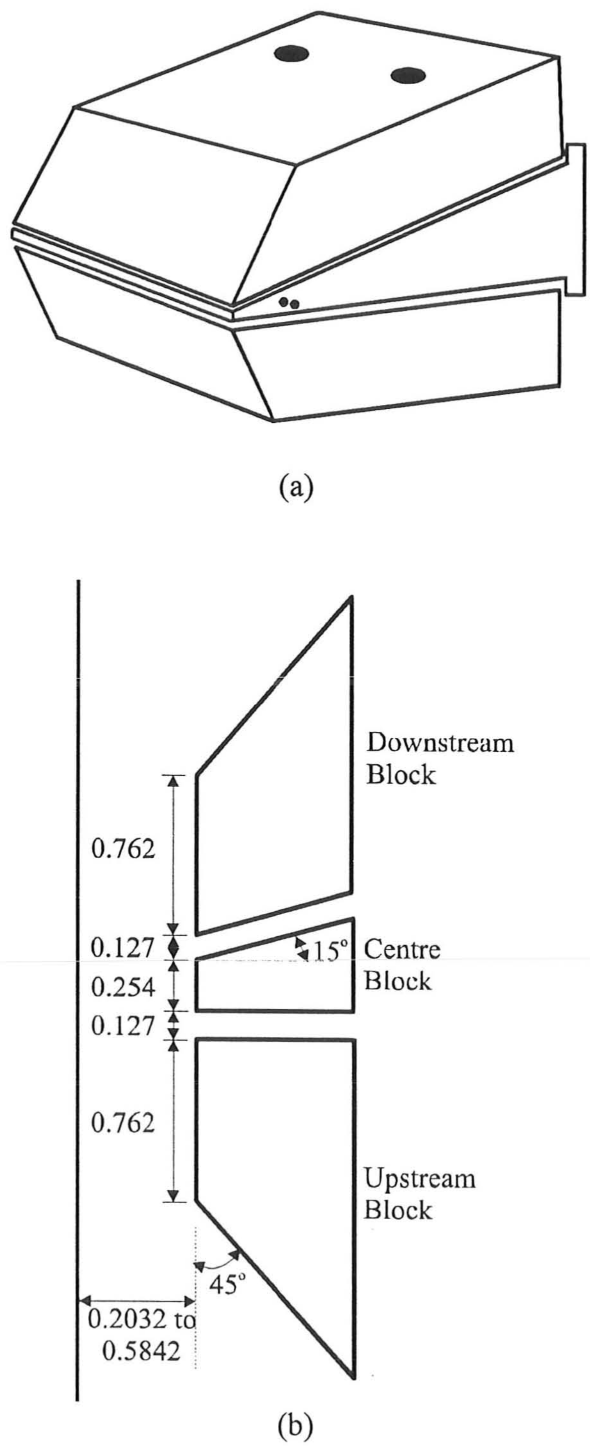

Figure 2.2: The modular two slot coating die (a) and the dimensions of the die lips (b). All dimensions in mm.

assembled by mounting the upstream block to the top side of the center block with two screws and securing the downstream block to the bottom side with two more screws. Plastic shims of various thickness could be inserted between each die piece to obtain any desired feed gap, although the feed gap was held constant at 0.127 mm (0.005 inches). Once assembled, the die was aligned along its side using a polished flat granite stone.

Precise alignment of the die lips was done visually using a video microscope. The video microscope consisted of a microscope lens (Zoom-6000 II, D.O. Industries) connected to a CCD camera (Panasonic, Model GP-kr402) and a colour monitor (Sony Trinitron, Model PVM-1342).

The die was mounted in the custom made vacuum box (Senior Machine, Pickering, Ontario) shown in Figure 2.3. The box was built using four 0.635 cm (1/4 inch) thick aluminum pieces. Side piece A was designed with a curved edge that fits snugly against the surface of the backing roll. The other side piece, B, was cut to fit closely to the side of the backing roll, allowing only enough clearance for a thin liquid film for lubrication. A 0.32 cm (1/8 inch) strip of Teflon (Joint Sealant, Gore-Tex) was placed between the side pieces and the backing roll to prevent scratching of the roll surface and to help maintain the vacuum seal. The bottom piece, C, was designed to fit tightly under the backing roll. A thin sheet of Teflon was added to the tip of the bottom piece to prevent tearing of the mylar and to maintain the vacuum seal. The box was closed by the

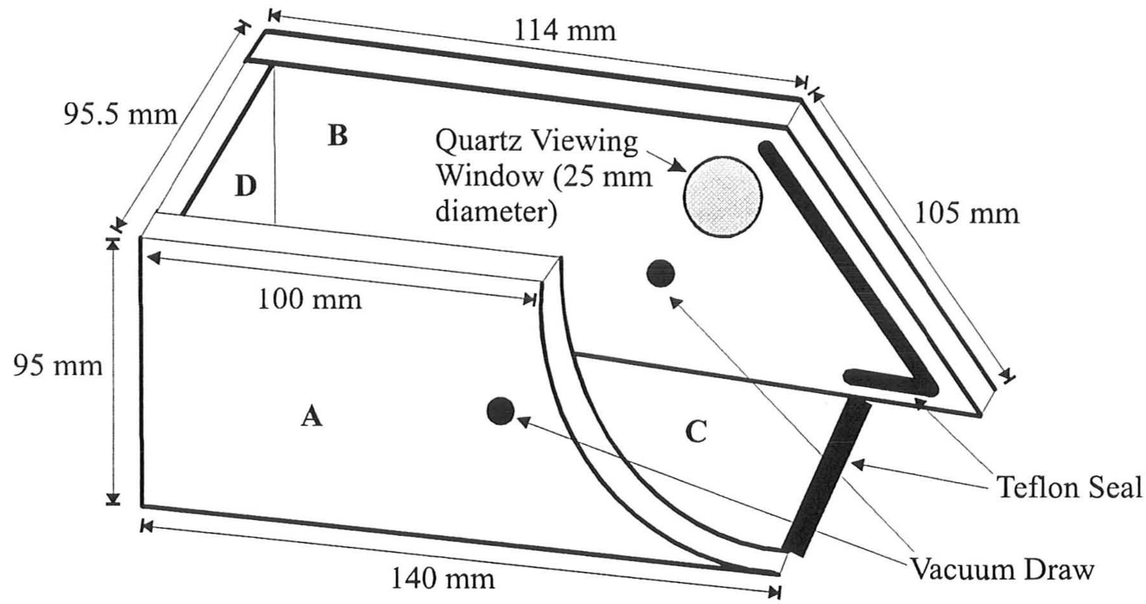

Figure 2.3: Sketch of the vacuum box.

fourth aluminum piece, D, placed behind the die. All four pieces were held together with screws and the seam between each piece was sealed with liquid Teflon sealant (Formula 8, Fluoramics, Inc.).

The die/vacuum box was mounted on a horizontal transverse (Unislide Series A4000, Velmex Inc.) that allowed the whole assembly to be moved towards or away from the backing roll. The vacuum box and transverse were designed to hold the die lips in vertical alignment and thus maintain a zero degree angle of attack to the web. A vacuum pump (Model KLR-85 S, Kinney Vacuum) was used to pull air from the vacuum box through two ports, one on either side of the box. A third port in the bottom of the vacuum box was used to drain away any liquid build-up. The vacuum pressure was measured using a water filled manometer attached to a copper tube positioned just under the coating bead. The copper tube occasionally became clogged with liquid, preventing any measurement of the vacuum pressure.

The coating liquids were fed to the back of the die through holes in the back of the vacuum box. The liquid for the bottom layer was feed through the upstream block and the top layer liquid was fed through the downstream block. Tubular feed channels in the outer blocks carried the liquids to T-shaped manifolds that distributed the coating solutions across the entire width of the die. The manifolds tapered down to the width of the feed slots, where the liquid flow was allowed to become fully developed (parabolic laminar flow) before reaching the coating bead.

The die could have been assembled using any one of four different center blocks. Machining of each block was identical except for the shape of the die lips. The lip shapes are identified in Figure 2.4 as ‘square’, ‘knife’, ‘bullet’, and ‘groove’. The square center block was studied previously by Cohen (1993) for layers of equal viscosity. He found that recirculations existed in almost every coating bead he observed and speculated that a study of the downstream die lip shape may lead to the elimination of some of these recirculations. He also found that the beginning of the interface region (or separation line) would pin to the downstream corner of the center die lip at a top to bottom flow rate ratio of 0.86. As this ratio was increased, Cohen (1993) observed the separation line move

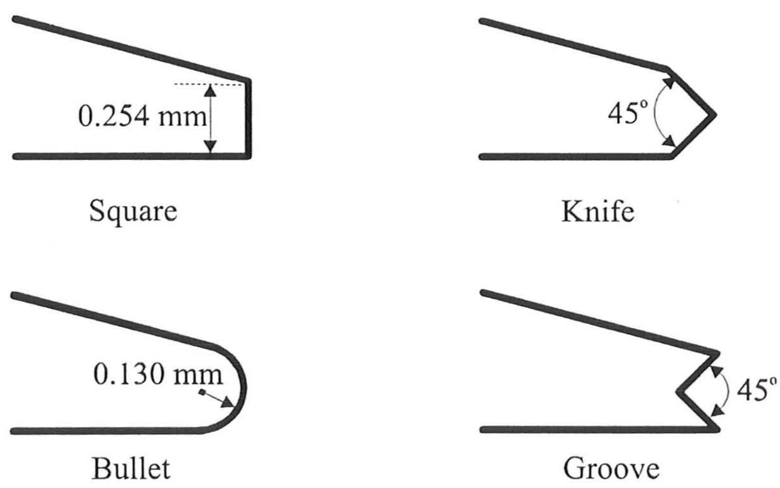

Figure 2.4: The shapes of the die lips of the four centre blocks.

along the die face in the upstream direction until it pinned to the upstream corner of the centre die lip at a flow rate ratio of 1. The separation line remained pinned to the upstream corner at a flow rate ratio of 2.

The square, knife and bullet shaped centre die lips have been studied previously by Chino et al. (1991). Chino contacted the two liquid layers *inside* the coating die before extruding the fluids into a coating bead. The die configuration used by Chino is shown in Figure 2.5 along with the various centre die pieces. It was suggested that a knife or bullet shape at the end of the centre block would prevent the occurrence of 'interfacial turbulence' or mixing of the two liquid layers. The intention of this study was to use the

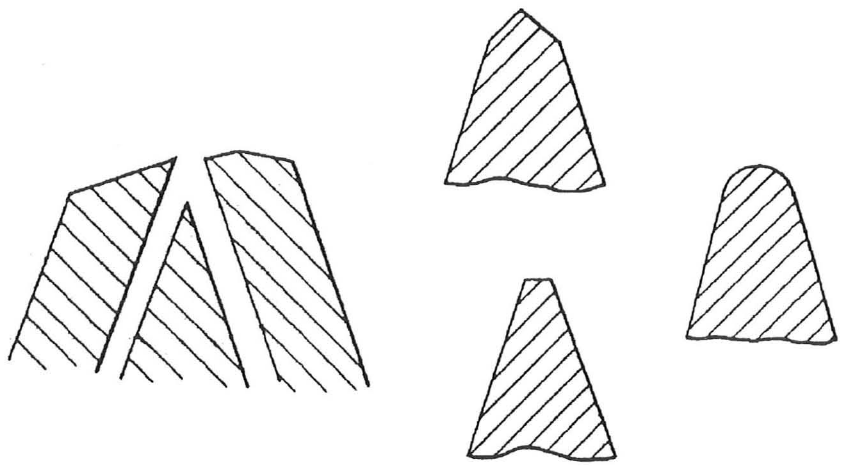

Figure 2.5: Two slot coating die used by Chino et al. (1991). Clockwise from top: knife, bullet, square centre die shapes and two slot die.

knife edge to pin the separation line, preventing it from moving freely along the die face. In contrast, the bullet edge was intended to allow the separation line to move freely and instead control the shape of the interface by maintaining a constant ‘contact angle’.

Curved die faces have appeared in a number of patents, such as Chino et al. (1991). A more recent patent by Umemura et al. (1992) describes a two slot die design where both the centre and downstream die blocks have curved faces (see Figure 2.6). They claim that the curved surface helps to control the final thickness by gradually forcing the liquid into a narrower coating gap.

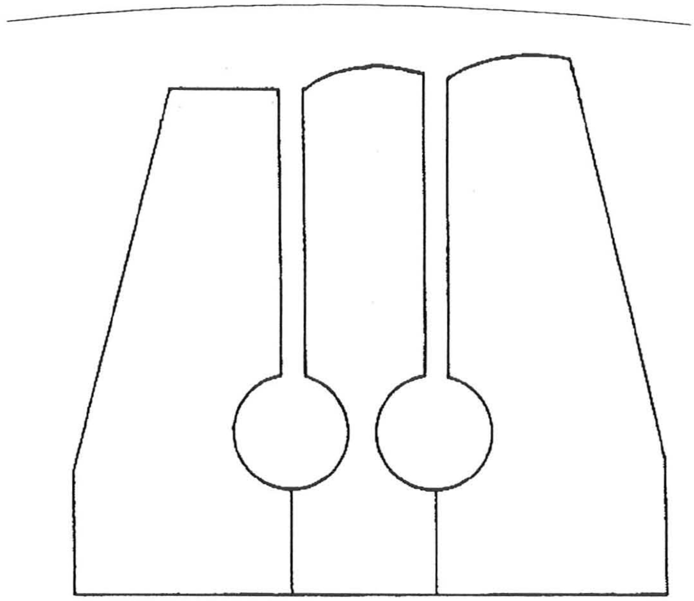

Figure 2.6: Two slot coating die with curved die faces used by Umemura et al. (1992).

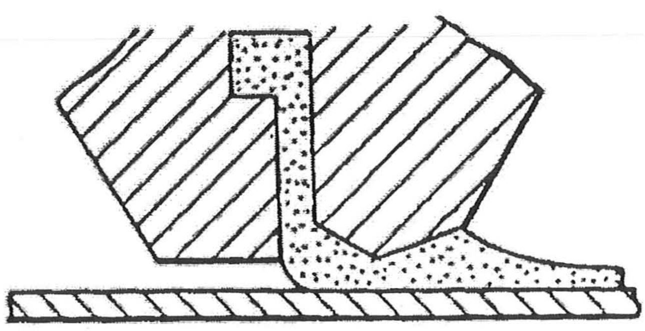

Figure 2.7: Groove shaped die blocks used by Kageyama and Yoshida (1983) for a single slot coater.

The groove shape has also been studied previously by Kageyama and Yoshida (1986) who used varying gap heights to control the pressure gradient within a single-slot coating bead (see Figure 2.7). They claimed that by creating converging and then diverging flow, the pressure gradient inside the coating bead could be increased. This, in turn, would allow the bead to remain stable at higher line speeds and/or allow thinner layers to be coated by adding to the pressure gradient between the upstream and downstream menisci. A conjecture of this work was that the groove would change the pressure gradient under the center block, forcing the interfacial region to remain stationary, either pinning on the upstream or downstream edge or becoming trapped inside the groove itself.

2.2.3 Coating Solutions

Glycerin (CAS# 56-81-5, Fischer Scientific) was chosen as the coating liquid since its Newtonian viscosity was easily adjusted with the addition of water. Due to the strong hydrophilic nature of glycerin, the coating liquids were stored in pressure pots under a pad of nitrogen gas. This prevented absorption of moisture from the air that might of caused the viscosity to decrease over time.

Diluting glycerin with water also decreased the refractive index of the solution. This made visualizations of two layers of different concentrations difficult since it caused some blurring of the liquid-liquid interfacial region. Attempts were made to avoid this problem by increasing the refractive index of the lower viscosity solution using sodium

Table 2.1: Physical properties of glycerol solutions.

	77 %wt Glycerin	96.5 %wt Glycerin
specific gravity	1.19	1.24
viscosity[1]	39 cp	386 cp
refractive index[2]	1.4409	1.4657
static contact angle[3] (stainless steel)	81.2^0	86.6^0
static contact angle (aluminized mylar)	57.6^0	53.2^0

[1] Viscosity measured using a Brookfield Viscometer, Model LVF, Brookfield Engineering Labs Inc. at 24°C.
[2] Refractive index measures using a Multi Scale Automatic Refractometer, Model RFM 81, Bellingham + Stanley Limited at 25°C.
[3] Static contact angles measured using a Noram Instrument App#28, Type 4-1, Lorentzen & Wettre at 23°C.

thiosulfate salt (Cat.# 21,726-3, Aldrich Chemical Company). However, these attempts were unsuccessful since the required concentration of sodium thiosulfate was too high to be used practically (greater than 25% by weight). Composite images of the whole coating bead were finally obtained by focusing the camera on one layer at a time and by using a combination of dye tracers along the interfacial region and particles or fluorescent dye solutions in the bulk flow. Table 2.1 lists the physical properties of the glycerin solutions used in this work.

2.2.4 Coordinate System

The Cartesian coordinate system for the coating bead is given in Figure 2.8. The origin, O, is located on the surface of the substrate at the upstream edge of the coating bead. Let x be in the direction of the moving substrate, y normal to the surface of the substrate, and z in the transverse flow direction. Except at the extreme edges, a stable coating bead is predominately a two dimensional flow field. Hence, this work assumed that there was no flow variation in the z-direction and the bead could then be visualized along any x-y plane.

2.2.5 Flow Visualization Set-Up

Two-dimensional flow fields are usually easy to visualize at a position perpendicular to the direction of flow. However, in the case of the two slot coater, this task became very tedious due to the small dimensions and the large number of reflective surfaces. Clear pictures of the coating bead could only be obtained when all three components (lighting, optics, and tracers) were precisely aligned.

Tracers

Particle tracers were used to visualize the streamlines within the coating flow. A solution of particles was made by mixing a rheoscopic fluid (AQ-1000, Kalliroscope Corporation; an aqueous solution of titanium oxide, aluminum oxide, and mica particles) with glycerin in proportions to match the densities and viscosities of the coating solutions.

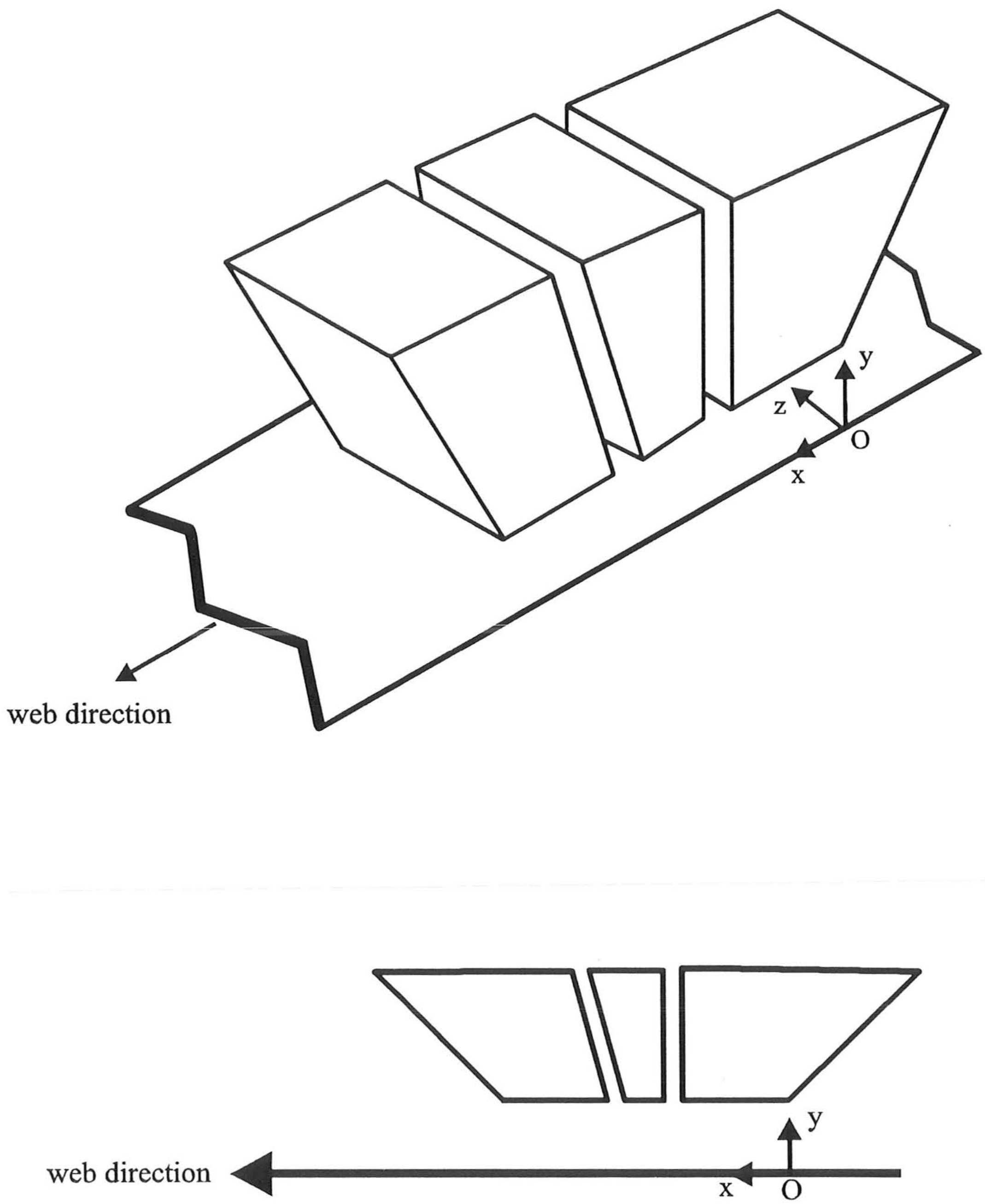

Figure 2.8: Cartesian coordinate system for the two slot coater.

The particle tracer solution was injected into the feed lines at the back of the die, allowing the particles to completely mix with the coating liquids before reaching the die lips. The particle solution was injected at a rate of 0.4 to 1.0 cc/min using disposable syringes (60 cc B-D, Becton-Dickinson & Co.) mounted on a syringe pump (Syringe Infusion Pump 22, Model 22 I/W, Harvard Apparatus).

The interfacial region was visualized using two fluorescent dye tracers: fluorescein disodium salt (Cat.# 108 2536, Eastman Kodak Company, λ_{max} = 493.5 nm) and laser grade sulforhodamine B (Cat.# 136 7499, Eastman Kodak Company, λ_{max} = 558 nm). Both dyes easily dissolved in water and fluoresced when exposed to the blue-green light of an Argon-Ion laser (λ = 458, 477, 488, & 515 nm). Each dye emitted a different colour when excited by the blue-green light; fluorescein emitted a bright yellow-green light while the sulforhodamine appeared an orange-red colour. The best visualization pictures were obtained with concentrations of 2.0 mg/L of fluorescein and 5.0 mg/L of sulforhodamine B.

Solutions of the dye tracers were made by dissolving powdered dyes into samples of the glycerin coating solutions (see Appendix I). Premixing of the dye tracers with the coating liquids prevented any visualization errors caused by density or viscosity differences between the tracer and coating flows. Syringes were used to inject the fluorescent dyes into two dye ports on the side of the center block (Figure 2.9) at a rate of 0.15 to 0.5 cc/min. Each dye exited through the tiny seep holes into the feed channel and became entrained in the flow of the coating liquid.

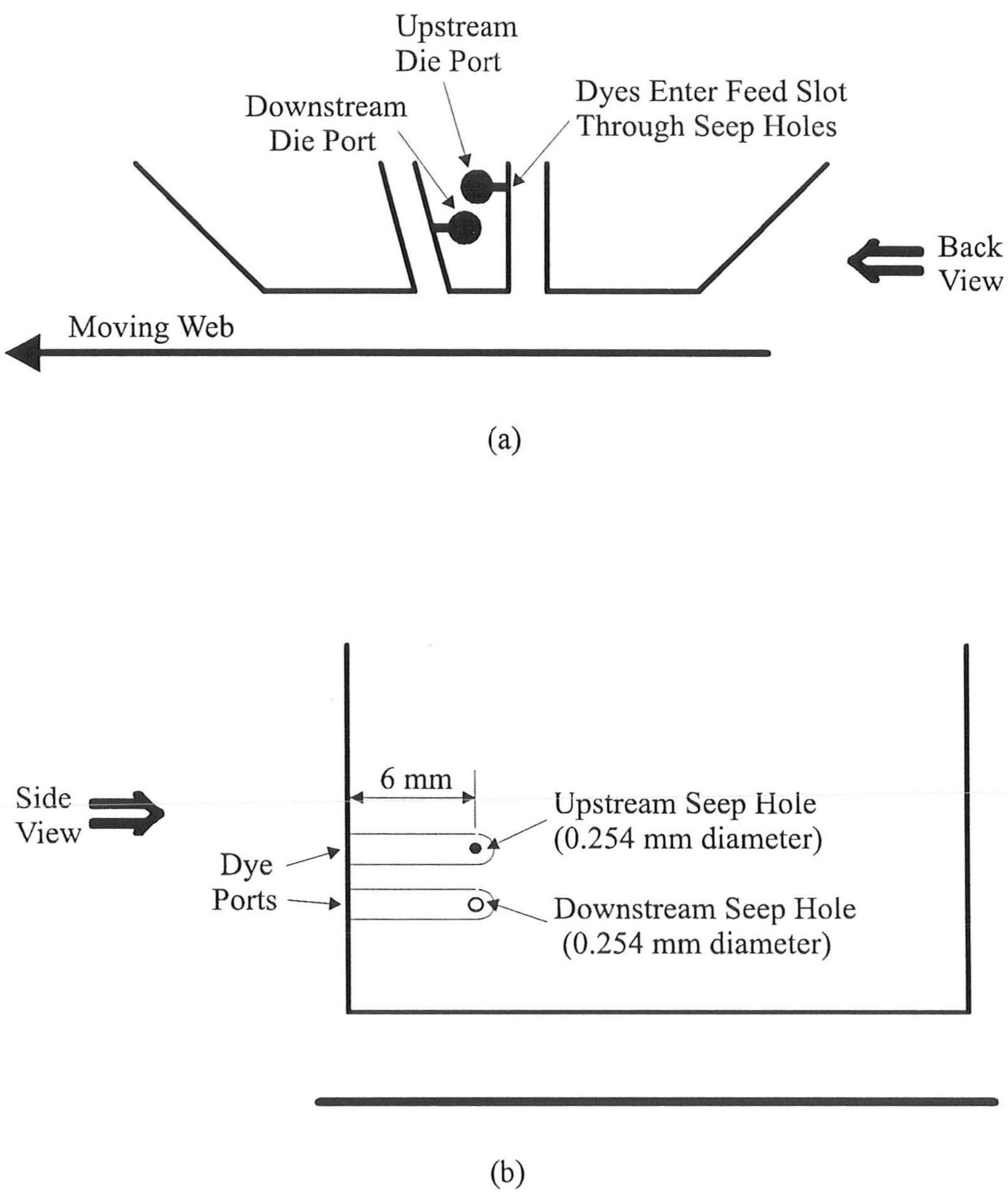

Figure 2.9: Dye injection ports in the side of the center block.
(a) Side view. (b) Back view.

Once into the coating flow, the dye tracers were expected to meet inside the coating bead at the separation line and then follow the interfacial region. The two differently coloured dyes were expected to show that mixing did occur along the interfacial region by combining to create a third colour. The dye tracer solutions were mixed in various proportions inside a test tube and then exposed to the blue-green light to determine the third colour. The results showed that a spectrum of colours from green (fluorescein solution only) to yellow to red (sulforhodamine B solution only) could be created. A solution made from equal amounts of each dye solution emitted a dull yellow colour when exposed to the blue-green light. Thus, equal mixing of the two dye tracers should make the interfacial region appear as a dull yellow region for the flow visualizations.

Visualizations with the 96.5% glycerin solutions caused problems with the injection of the dye tracers. Back pressure prevented the dye solutions from seeping out of the dye ports. In these situations, particles were injected into the higher viscosity top layer and the interface was traced using only the one dye tracer in the low viscosity bottom layer. Additional experiments were conducted with fluorescein mixed directly into the 96.5% glycerin coating solution. This allowed for direct viewing of the individual layers and hence, only the position and shape of the interfacial region.

Lighting and Optics

The plane of visualization was located 6 mm from the edge of the die. This plane was illuminated by a 20 mW Argon-Ion laser (Head Model 5425A-00C-2, Power Supply Model 5400A-115-00-2, Ion Laser Technology) operating in multiline TEM_{oo} mode. The 1-2 mm diameter beam was directed at a mirror mounted directly above the coating gap. The mirror reflected the beam down into the coating bead. The beam entered through the downstream meniscus and bounced off the various reflective surfaces to illuminate the coating bead (Figure 2.10a). The laser light exited the bead through the upstream meniscus and then terminated within the vacuum box. Attempts were made to expand the beam into a thin sheet of light using a cylindrical lens, but the narrow coating gap (less than 1 mm) prevented most of the light sheet from entering the bead. The highest light intensity was obtained by directing the beam itself into the bead at a slight angle (about 10 degrees from the x-axis).

The plane of visualization was viewed through an optically flat quartz lens mounted flush in the side of the vacuum box. A zoom microscope (Zoom 6000 II, D.O Industries) attached to a 35 mm camera (Olympus OM-1) was used to capture images of the coating flow. The camera was positioned perpendicular to the direction of flow and level with the coating bead. The images were recorded on colour film (Fuji Super HG 1600 ISO).

Figure 2.10b shows the arrangement of the lighting and optics for the visualization.

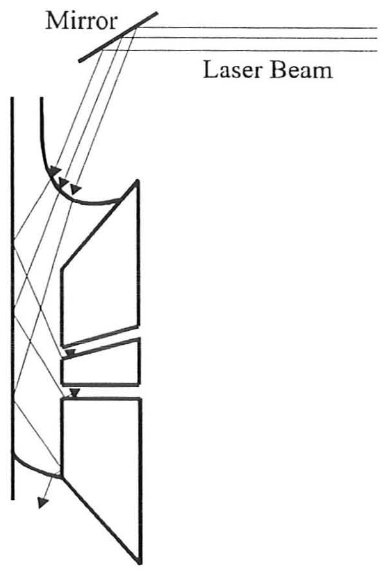

(a)

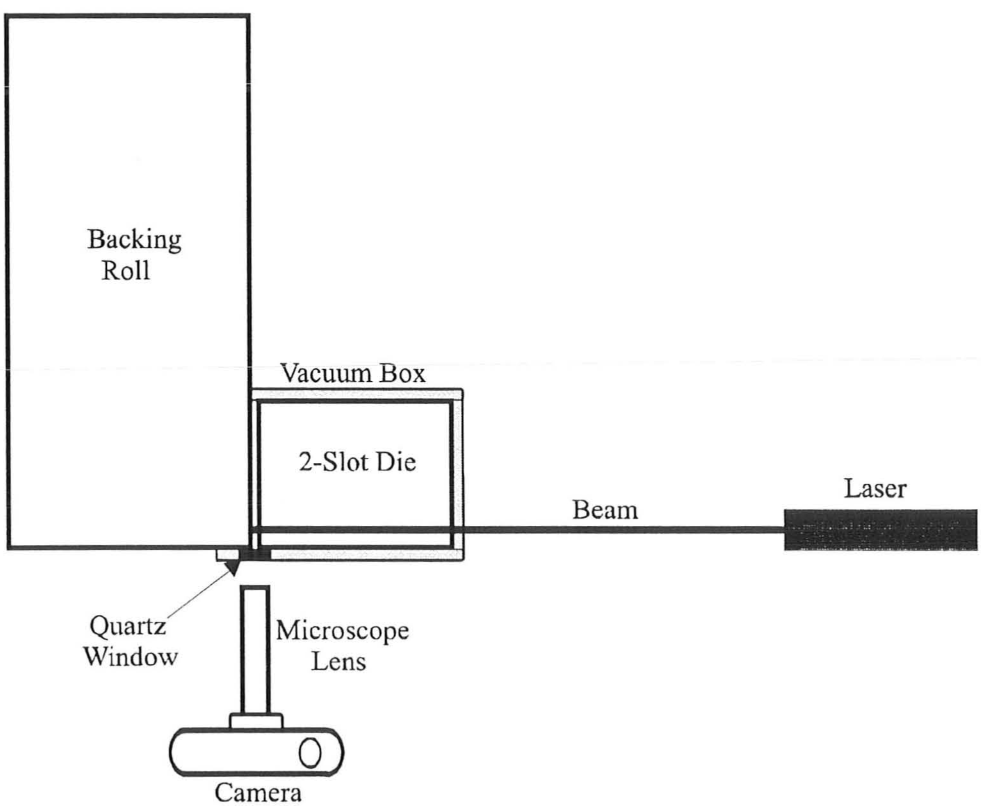

(b)

Figure 2.10: Lighting and optics for the flow visualization. (a) Illumination of coating bead with a laser beam. (b) Top view of laser and camera positions.

2.3 Experimental Conditions

The experiments were broken down into four blocks, one for each center piece geometry. The effects of line speed, viscosity ratio and wet thickness ratio were then studied within each block at predefined levels. The line speed was varied from 0.152 m/s (30 ft/min) to 0.305 m/s (60 ft/min). Attempts were made to visualize higher speeds, but three dimensional flow patterns at the very edge of the bead caused the view of the flow field to become blurred above line speeds greater than 0.33 m/s (65 ft/min). The viscosity ratio, the liquid viscosity in the top layer to the liquid viscosity in the bottom layer, was varied from 1 to 10. The bottom layer was held constant at 39 cp while the top layer viscosity was increased. The wet thickness ratio was varied from 1 to 2.5, where the ratio was defined as the final thickness of the top liquid layer over the final thickness of the bottom liquid layer. Any ratios higher than 2.5 resulted in severe wetting of the downstream shoulder of the die and hence, an unrealistic operating condition. The bottom layer thickness was held constant at 50 μm.

The coating gap was set to a maximum value through trial and error coating experiments with the square geometry at 1:1 viscosity ratio. At coating gaps larger than the maximum value, the bead would become unstable and collapse into the vacuum box. The maximum coating gap was determined to be 305 μm (0.012 inch) for 1:1 wet thickness ratio and 457 μm (0.018 inch) for 2.5:1 wet thickness ratio. To aid in the

Table 2.2: Experimental block for each centre piece geometry.

Run #	Line Speed (m/s)	Wet Thickness Ratio	Viscosity Ratio
1	0.152	1	1
2	0.305	1	1
3	0.152	2.5	1
4	0.305	2.5	1
5	0.152	1	10
6	0.305	1	10
7	0.152	2.5	10
8	0.305	2.5	10

comparison between various visualizations, the gap was held constant at these maximum values. However, some operating conditions required an increased or decreased coating gap to obtain a stable bead or to eliminate severe wetting of the downstream shoulder.

The block design is summarized in Table 2.2. This block was first performed using the square center piece to establish a base set of data that could be compared to Cohen's work and to the results of the other geometries. The block was repeated three more times (once for each center piece) for a total of 32 runs. Additional visualizations of the square geometry were also performed, including repeated runs and runs at 0.254 m/s (50 ft/min). Appendix C provides a summary of all the parameter values for every coating run that was performed.

It is important to note at this point that clear pictures and repeatable results could only be obtained by proper cleaning of the coating apparatus. The extent of cleaning required between runs depended on the operating conditions. When the line speed or wet thickness ratio were adjusted, only cleaning of the die lips and the quartz lens with acetone were required. Changes in viscosity ratio or die geometry required disassembly and cleaning of the die, the vacuum box and the gear pumps. Cleaning of the backing roll was also required to remove any glycerin that may have been deposited onto the side of the roll.

2.4 Start-Up Procedure

There has been speculation that the structure of the flow within the coating bead may depend on the coater's start-up procedure. At present, no evidence of this phenomenon has been seen in the public literature for slot coating flows. However, for the sake of completeness and also for possible future reference, the start-up procedure used in this work is listed below:

1. Check that the camera and laser beam are properly aligned before starting the coater.
2. Set the coating gap to the desired distance.
3. Start the flow of tracer solutions by turning on the syringe pumps. Allow a few minutes for the dye ports to fill with tracer fluid.
4. Once the die tracers are visible in the coating bead, start-up the web at a relatively slow speed (approximately 0.1 m/s).

5. Start the feed to the top layer at about one third the desired flow rate.

6. After the top fluid reaches the coating gap, start the feed to the bottom layer at about one third the desired flow rate.

7. Slowly increase the line speed until a non-uniform coating is obtained.

8. To regain a uniform coating, slowing increase the flow rates of both the top and bottom fluid layers.

9. Continue to iterate steps 7 and 8 until the desired flow rates and line speed are obtained.

10. If a uniform coating still does not exist, slowly increase the vacuum pressure until a uniform coating is obtained.

11. Increase the vacuum pressure until the upstream meniscus is pinned on the upstream corner of the die.

12. Begin taking pictures.

CHAPTER 3

VISUALIZATION RESULTS

This chapter is devoted to presenting the flow visualization results of a two-slot coater, focusing mainly on the interfacial region. The first section describes the coating bead that was observed when the center die piece had a square geometry. This section also covers the effects of wet thickness ratio, viscosity ratio, and line speed on the structure of the flow field. The next three sections discuss the effects on the interfacial region by the different center die lip shapes; knife, bullet and groove. The chapter ends with a few brief comments on experimental observations of the upstream meniscus.

To qualitatively describe the flow field, it is useful to divide the coating bead into a number of regions. The convention used here, adopted by Cohen (1993), is to separate the coating bead into the six regions shown in Figure 3.1. The separation consists of the upstream and downstream feed slot regions, S^U and S^L respectively, the upstream region (or heel), H, the intermediate region, I, a downstream region, D, and a film forming region, F.

3.1 Square Geometry

3.1.1 Layers of Equal Viscosity

The simplest case to describe is the 1:1 viscosity ratio where the two liquid layers have the same glycerin concentration (77%wt) and viscosity (39 cp). Figure 3.2 is an example of such a flow field.

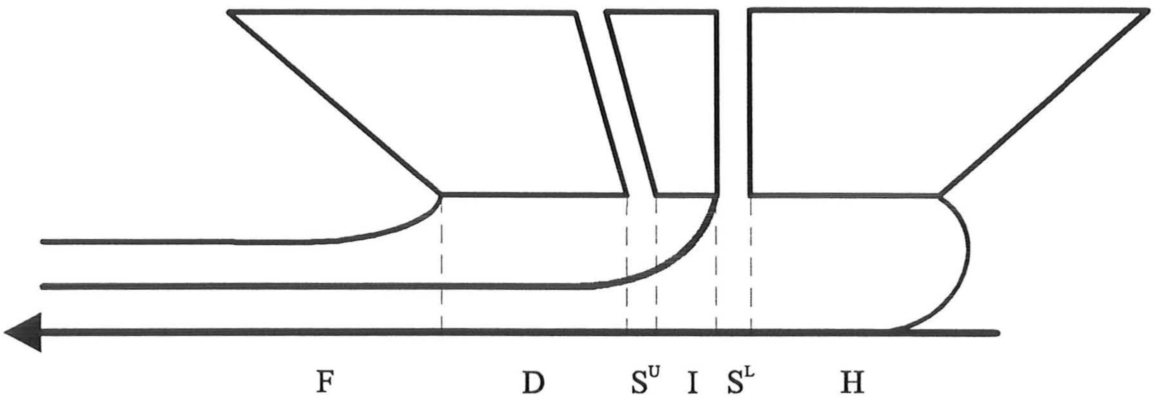

Figure 3.1: Six regions of the two layer slot coating bead: S^U and S^L the feed slots, H upstream region, I intermediate region, D downstream region, and F film forming region.

Top Layer

The liquid for the top layer exited from the downstream feed slot and separated into two portions, one flowing into region I and the other flowing into region D. The first portion of fluid flowed into the intermediate region where it headed upstream until it reached the upstream corner of the center die face. At the corner, the liquid turned a full 180^0 towards the web, filling in a curved pocket region created by the interfacial region, and then accelerated in the web direction. The wide line of fluorescein tracer in region I indicated that the velocity of the liquid was relatively slow, as shown in the bottom photograph of Figure 3.2. The tracer line thinned as the fluid particles accelerated downstream towards the film forming region F.

The second portion of the top layer fluid headed immediately downstream, filling in a large part of the downstream section D and partially wetting the downstream shoulder. All the coating runs (regardless of the shape of the center die lip) with a low viscosity liquid (39 cp) in the top layer saw a set of recirculations form at the downstream die shoulder. The top photograph of Figure 3.2 shows the set included a large vortex (about 900 μm wide by 2300 μm long) centered above the downstream shoulder. This large vortex was connected to a much smaller vortex (about 300 μm diameter) located adjacent to the downstream die face. Both recirculations moved in a clockwise direction. A third, very small vortex rotating in a counter-clockwise direction, exists further up on the downstream shoulder, between the large vortex and static contact line. This third vortex is visible in Figure 3.3 where the wetting of the downstream shoulder was so severe that the recirculation was large enough to be seen.

Wetting of the downstream shoulder is generally avoided in industrial practice. Unpinning of the upstream meniscus increases the chance of ribbing as well as leading to stagnation points or recirculations near the free surface (Cohen, 1993).

The presence of recirculations imply long residence times for coating particles that become trapped by the rotating fluid. For example, Figure 3.4 shows tiny air bubbles that became trapped in the center of the large shoulder vortex during the flow visualizations. The bubbles remained in the observed position for over five minutes before being released back into the bulk of the coating flow.

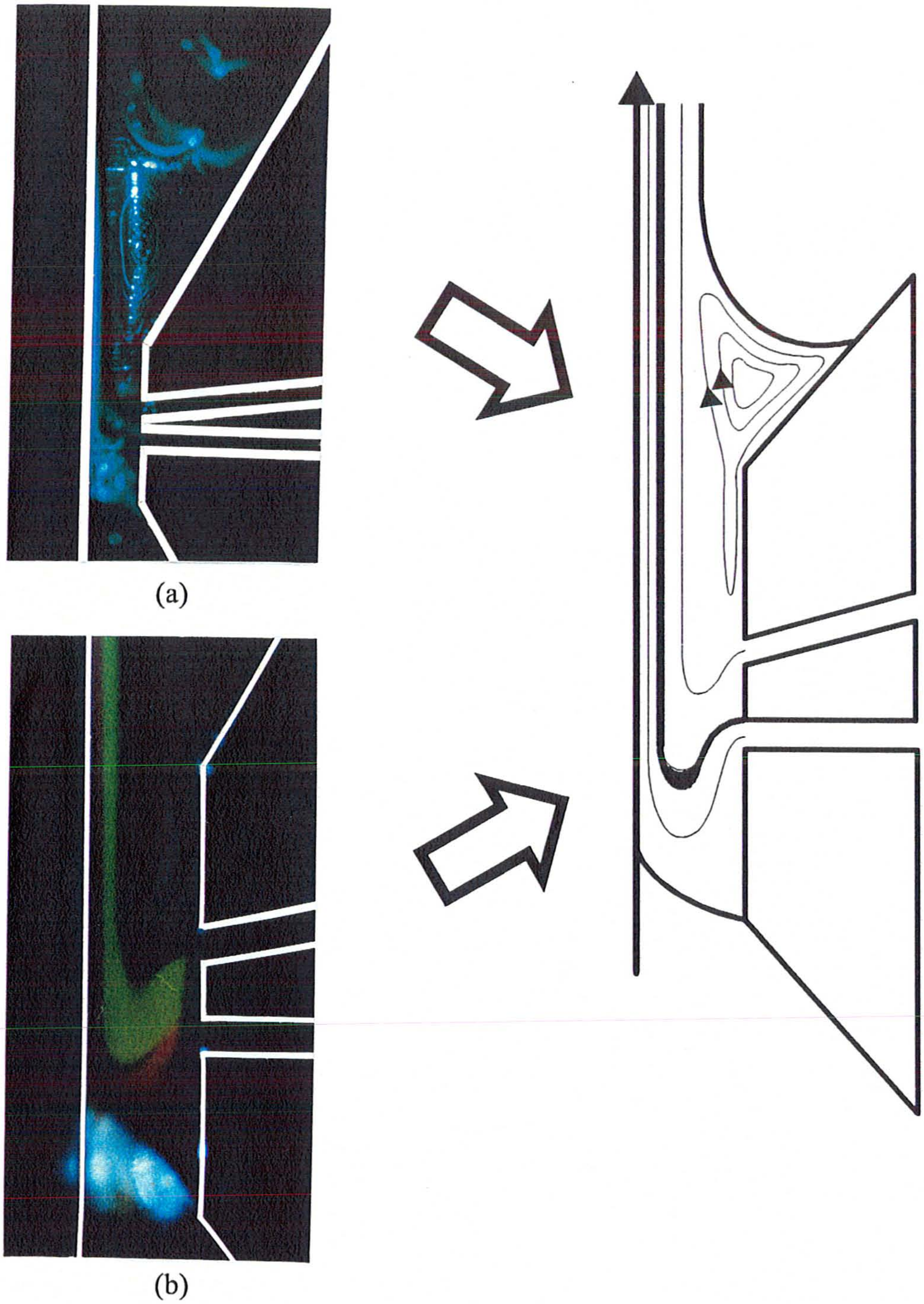

Figure 3.2: Flow structure created by the square geometry for layers of equal viscosity. Photo (a): upper layer thickness, t_U=125 μm, lower layer thickness, t_L=50 μm, upper layer viscosity, μ_U= 38 cp, lower layer viscosity, μ_L=38 cp, vacuum pressure, vac=0 cmH_2O, web speed, U=0.152 m/s, gap=686 μm. Photo (b): t_U=125 μm, t_L=50 μm, μ_U= 39 cp, μ_L=39 cp, vac=0.1 cmH_2O, U=0.152 m/s, gap=457 μm.

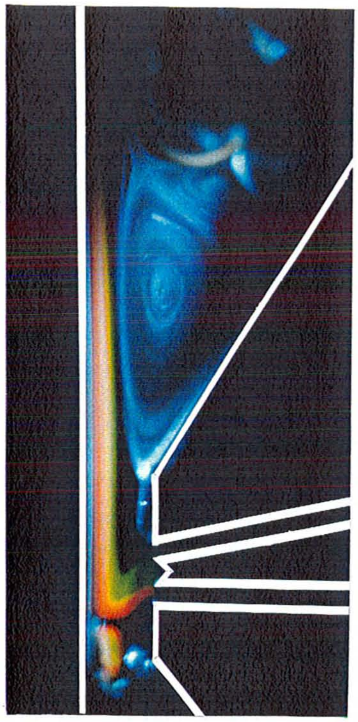

Figure 3.3: Severe wetting of downstream shoulder. t_U=125 μm, t_L=50 μm, μ_U= 39 cp, μ_L=39 cp, vac=0 cmH_2O, U=0.152 m/s, gap=584 μm.

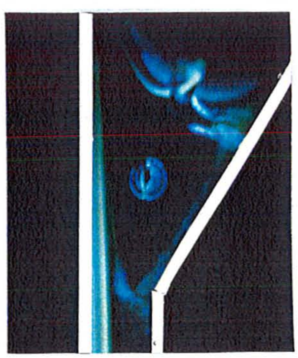

Figure 3.4: Air bubbles trapped in the center of recirculation. t_U=125 μm, t_L=50 μm, μ_U= 38 cp, μ_L=38 cp, vac=0.5 cmH_2O, U=0.152 m/s, gap=508 μm.

Within the coating gap, coating particles that tend to build-up in recirculations are pumped to the edges of the coating flow by the slow z-direction flow in the vortices (Schweizer, 1988). On the downstream shoulder, the recirculation is exposed to the atmosphere. Since coating solutions often use volatile solvents as the carrier fluid, the liquid can quickly evaporate, leaving behind deposits of solid particles. Both cases represent a loss of coating material and hence, a decrease in the final dry coating thickness.

In this work, no operating conditions could be found where the downstream meniscus could be pinned to the corner of the die without causing weeping at the upstream meniscus. Thus, all visualizations show some degree of wetting at the downstream die shoulder. In addition to this work, recirculations on the wetted downstream shoulder were often observed in the visualizations of the slot coater by Sartor (1990) and Cohen (1993). Both claimed that the vortices could be eliminated by pinning the downstream static contact line to the downstream corner of the die. However, this does not mean that the recirculation immediately adjacent to the downstream die face would be eliminated. Both Sartor and Cohen also showed that a vortex often exists at this position when the downstream static contact line is pinned.

Bottom Layer

The liquid for the bottom layer exited from the upstream feed slot S^U and turned immediately upstream. The bottom photograph of Figure 3.2 shows a red line of sulforhodamine B dye tracer following the liquid along the interfacial region. The liquid filled the entire upstream region H, flowing back along the die face to the upstream corner of the die. From this corner, the fluid would turn smoothly towards the web, bending a full 180^0 to form the curved upstream meniscus. The fluid would come into contact with the web at the dynamic contact line, located either parallel to or just downstream of the upstream die corner. The bottom liquid then quickly accelerated in the web direction, forming a thin fluid layer below the top layer. At this point, the bottom layer was close to its final wet thickness of 50 μm.

Interfacial Region

The interfacial region can be seen as a thin black band between the two dye tracers in the bottom photograph of Figure 3.2. The interfacial region appeared to begin from the upstream corner of the center die face. This result agreed with that of Cohen (1993) who observed that the interfacial region pins to the upstream corner of the centre die block when the wet thickness is equal to of greater than 1:1. From the upstream corner, the interfacial region extended perpendicularly into the coating bead. It then turned sharply upstream to form a 180^0 arc as the fluid turned again to move in the web direction. This arc can be thought of as a smoothly curved *pocket* that contains slow moving liquid from the top layer. The pocket often extended into the upstream feed slot region S^U or just beyond the feed slot and into the upstream region H. A slight oscillation of the pocket was often observed at all line speeds (0.152, 0.254, and 0.305 m/s) and at both wet thickness ratios (1:1 and 2.5:1). From region I through to region F, the interfacial region appeared to be parallel to the web remaining about 50 to 60 μm above its surface. Oscillations were not observed downstream of the pocket.

A bright yellow streak along the interfacial region can be seen in some photographs, such as the photo in Figure 3.3. The yellow streak was also observed visually during coating runs of 1:1 viscosity ratio with 0.254 m/s and 0.305 m/s line speeds. The streak was the thickest along the slow moving pocket region and then thinned out as the liquid accelerated in the web direction.

The yellow color was caused by the mixing of the orange-red and green dye colors. While the nature of the mixing was not clear, there are two probable causes of the yellow streak. The first possibility is that diffusion led to the physical mixing of the two dyes tracers to form a band of yellow. Experiments proved that a dull yellow light is emitted when the two dyes are mixed in equal portions. Alternatively, there may have been no physical mixing of the dye particles. In this case, it may be possible that the light emitted from the adjacent tracers combined to appear as a band of yellow light. For this second possibility to be true, the thickness of the yellow line should remain constant. However, it was observed that the yellow band did change thickness, lending support to the idea that mixing of the dye tracers did occur along the interfacial region.

3.1.2 Layers of Different Viscosity

Top Layer

The switch to a 10:1 viscosity ratio (386 cp top layer viscosity over a bottom layer viscosity of 39 cp) for any center block geometry saw the disappearance of the recirculations at the downstream shoulder, as shown in the top photograph of Figure 3.5. The liquid in the top layer could be seen moving smoothly through the downstream and film forming regions.

The Reynolds number for slot coating was previously defined by Cohen (1993) as $Re=\rho Q/\mu$ where Q was the flow rate per unit length of a particular layer. Smooth flow was observed for low Reynolds numbers between 0.048 and 0.12 (μ = 389 cp) while recirculations were observed for higher Reynolds numbers between 0.23 and 0.58 (μ = 39 cp). Hence, the presence of recirculations on the wetted downstream shoulder is related to Reynolds number under the current experimental conditions. Similar observations were made by Kistler and Scriven (1993) whose simulations showed that recirculations would develop on a wetted shoulder of a curtain coater as the Reynolds number was increased.

Interfacial Region

The bottom photograph of Figure 3.5 shows the change in shape and position of the interfacial region when the viscosity ratio was switched to 10:1. With the high viscosity liquid in the top layer, the interfacial region appeared to be pinned to the

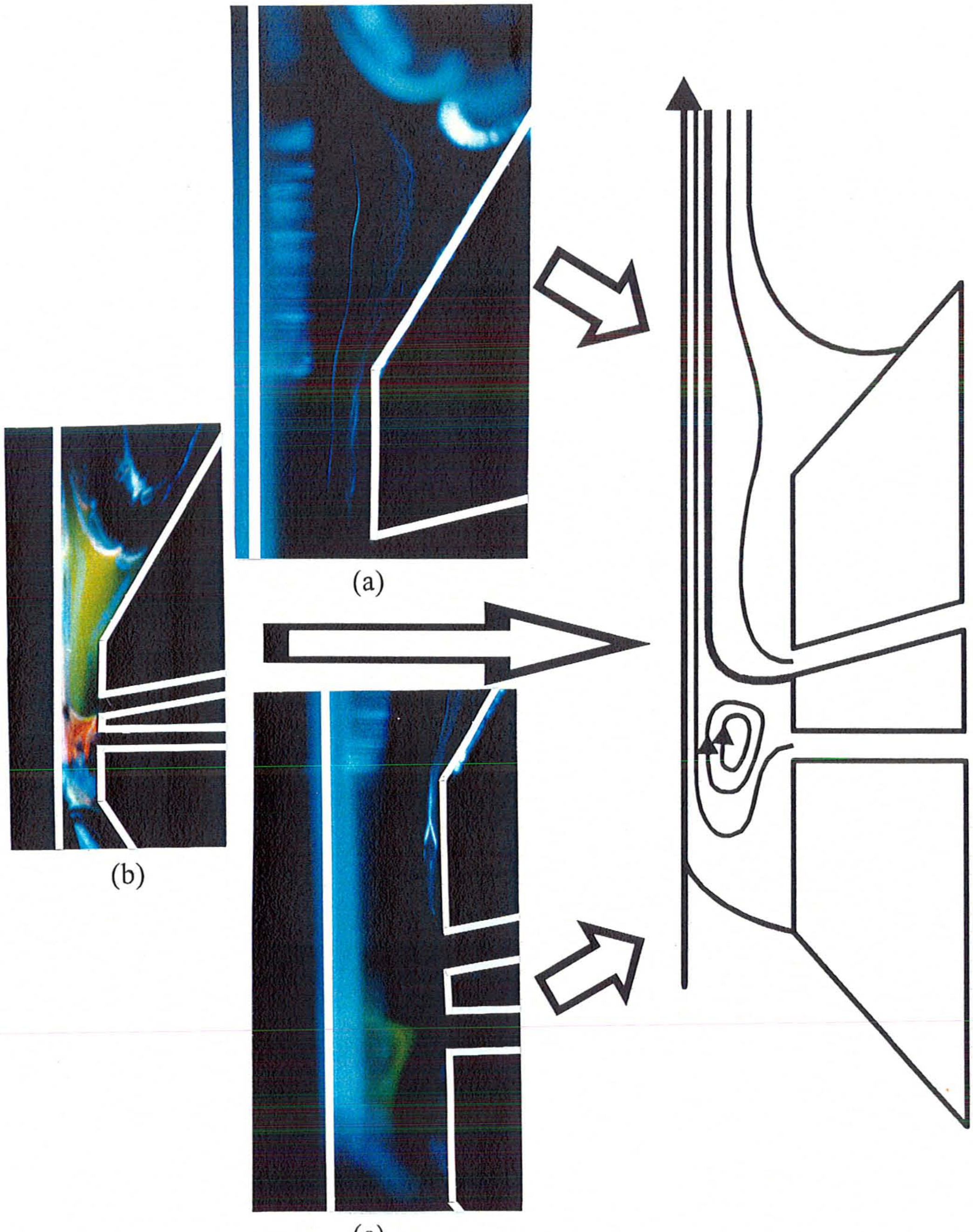

Figure 3.5: Flow structure created by the square geometry for layers of different viscosity. Photo (a): t_U=125 μm, t_L=50 μm, μ_U= 390 cp, μ_L=39 cp, vac=0.6 cmH_2O, U=0.152 m/s, gap=457 μm. Photo (b): t_U=125 μm, t_L=50 μm, μ_U= 390 cp, μ_L=39 cp, vac=0.6 cmH_2O, U=0.152 m/s, gap=457 μm. Photo (c): t_U=125 μm, t_L=50 μm, μ_U= 406 cp, μ_L=35 cp, vac=1.6 cmH_2O, U=0.305 m/s, gap=457 μm.

downstream corner of the center die face. The bottom photograph shows that the interfacial region initially extended straight out from the corner into the coating bead. The region then gradually turned downstream forming an elongated arc that ended when the region was parallel to the web surface.

Back pressure problems at the downstream seep hole prevented the use of both dye tracers, making it impossible to determine the thickness of the interfacial region or to detect mixing between the liquid layers. The change in refractive index between the layers caused blurring along the interfacial region. The blurring made it difficult to determine if there were any oscillations of the interfacial region.

Bottom Layer

The liquid for the bottom layer separated into two portions upon leaving the upstream feed slot. The bulk of the fluid turned upstream, following the same flow pattern that was outlined for the 1:1 viscosity ratio. The remaining liquid filled the intermediate region I under the center die face and formed a large recirculation zone under the center die face, indicated by the orange-red dye in the middle photograph of Figure 3.5. The bottom photograph shows that this zone contained a large vortex centered over regions I and S^U. The whole recirculation zone extended from the interfacial region to a point just inside the upstream region H. This vortex appeared to be rotating in a clockwise direction, following the streamlines of bulk flow of the bottom layer and against the flow direction of the top layer. To meet continuity requirements, a small second vortex rotating counter-clockwise should exist between the large vortex, the interfacial zone and the center die face. Without the second vortex, the large recirculation would be entraining some of the fluid from the top layer. This phenomenon could have been observed as a mix of the green and orange-red tracers in the recirculation zone, but due to back pressure problems at the injection ports, only one tracer was used in the 10:1 viscosity ratio experiments. Further problems of blurring near the interfacial region made it extremely difficult to determine if the second recirculation existed or whether there was entrainment of the two fluid layers mixing in the large vortex.

3.1.3 Vacuum Effects

Vacuum was used below the upstream meniscus for two purposes: to stabilize the bead to obtain a uniform coating and to pull the meniscus down so that the static contact line pinned on the upstream corner of the die. The amount of vacuum required depended on the operating conditions. At a wet thickness ratio of 2.5:1 and 1:1 viscosity ratio, no vacuum was needed for a uniform coating and only a slight vacuum (up to 1.0 cmH_2O) was used to pin the upstream static contact line. Increasing the vacuum above 6.0 cmH_2O caused the bead to become unstable and thus, a uniform coating was no longer maintained. Visualizations with a 10:1 viscosity ratio required even less vacuum pressure (up to 0.5 cmH_2O) to pin the upstream static contact line and the bead became unstable for vacuum pressures greater than 5.5 cmH_2O. Thus, for a 2.5:1 wet thickness ratio, there was about a 6.0 cmH_2O range of vacuum where a uniform coating could be obtained.

The coating runs with 1:1 wet thickness ratio required up to 3.5 cmH_2O of vacuum at a line speed of 0.152 m/s (30 ft/min) and nearly 6.0 cmH_2O at a line speed of 0.305 m/s (60 ft/min) to pin the upstream meniscus. The range of vacuum for a uniform coating could not be determined for 1:1 wet thickness ratio since the maximum obtainable vacuum pressure was 6.5 cmH_2O.

For the 2.5:1 wet thickness ratio, various coating defects occurred outside the 0 to 6.0 cmH_2O range of vacuum pressure. The coating often showed a mix of rivulets and/or barring when no vacuum was present and then switched to air entrainment as a low amount of vacuum was applied. If too much vacuum was applied, the upstream meniscus would begin to swell. Increasing the vacuum above 6.0 cmH_2O would result in weeping, rivulet flow and eventually, a complete collapse of the coating bead with all the liquid running into the vacuum box. Qualitatively, these observations match the coating window obtained by Sartor (1990) for a single slot coater.

In describing the flow for a 1:1 viscosity ratio, the interfacial region was identified as being pinned to the upstream corner of the square center block. This generally occurred when the upstream meniscus was pinned to the upstream corner of the bottom die face. By slightly decreasing the vacuum, it is possible to move the upstream static contact line along the die face towards the upstream feed slot. This in turn allowed the interfacial region to move freely along the face of the center block.

Figure 3.6 shows the effect of vacuum on the shape and position of the interfacial region. The photograph of Figure 3.6a was taken at a relatively low vacuum where the interfacial region was pinned to the downstream corner of center block. At this point, the

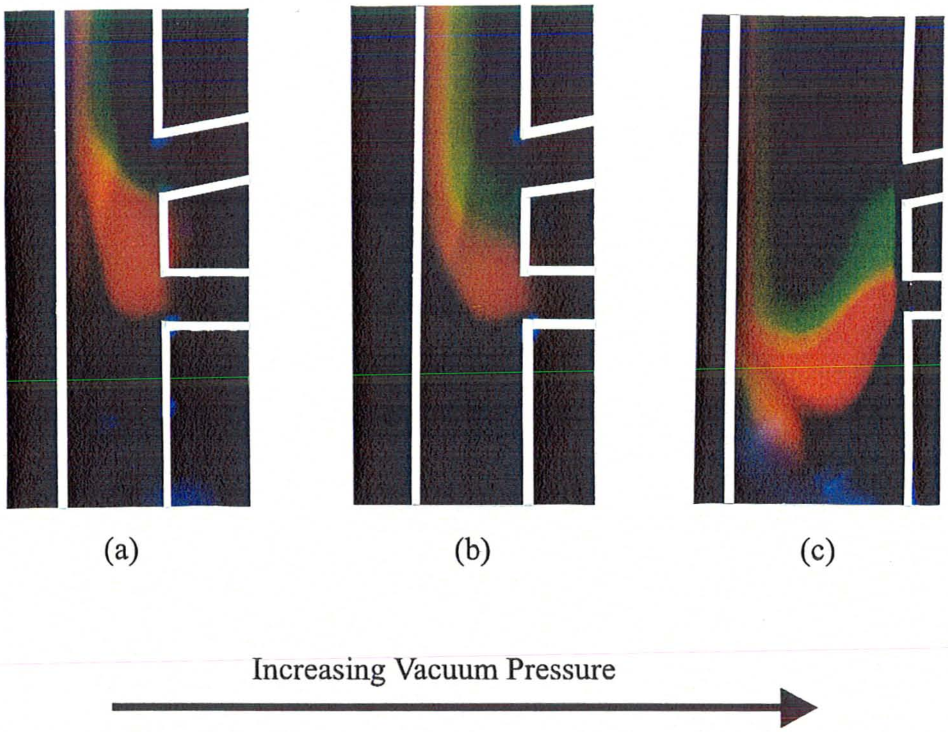

Figure 3.6: Effect of increasing vacuum on the shape and position of the interfacial region. Photo (a): t_U=50 μm, t_L=50 μm, μ_U= 39 cp, μ_L=39 cp, vac=4.5 cmH_2O, U=0.254 m/s, gap=203 μm. Photo (b): t_U=50 μm, t_L=50 μm, μ_U= 39 cp, μ_L=39 cp, vac=6.0 cmH_2O, U=0.254 m/s, gap=203 μm. Photo (c): t_U=50 μm, t_L=50 μm, μ_U= 39 cp, μ_L=39 cp, vac=2.7 cmH_2O, U=0.152 m/s, gap=381 μm.

region bent gradually downstream until it was parallel to the web surface. As the vacuum pressure was increased, the interfacial region moved upstream along the die face and formed a sharper bend or quarter circle (Figure 3.6b). The upstream meniscus and interfacial region were then pinned to their respective upstream corners as the vacuum was further increased. Here, the interfacial region formed the pocket described earlier (Figure 3.6c). The pocket length could be extended further into the upstream region of the coating bead by applying slightly more vacuum.

3.1.4 Effect of Line Speed

It was initially expected that the flow structure of the bead would change as the line speed was increased. However, there was no evidence of changes in the flow pattern between 0.152 m/s (30 ft/min) and 0.305 m/s (60 ft/min) for the square block geometry. The only observable effect of line speed was that greater vacuum pressures were required to stabilize the bead at higher line speeds.

3.1.5 Effect of Wet Thickness Ratio

The wet thickness ratio had no observable effect on the interfacial region. Switching from a 1:1 to a 2.5:1 thickness ratio did require an increase in the coating gap from 0.305 mm (0.012 inch) to 0.457 mm (0.018 inch) and eliminated the need for large vacuum pressures below the upstream meniscus. However, these effects are probably the direct result of an increased total wet thickness, from 100 μm (0.0039 inch) for the 1:1

wet thickness ratio to 175 μm (0.0069 inch) for the 10:1 ratio, and not the effect of the wet thickness ratio. The small vortex under the downstream die face was only clearly visible with the 2.5:1 wet thickness ratio and 1:1 viscosity ratio. At the 1:1 thickness ratio and 1:1 viscosity ratio, the recirculation was either too small to be visible or simply disappeared due to the reduced coating gap.

3.2 Knife Geometry

The coating bead created with the knife center block proved to be relatively difficult to stabilize. Stability refers to a coating bead that is devoid of any three-dimensional or transient flow patterns, such as rivulets, oscillations of the menisci, or air entrainment. There was only a narrow range of vacuum pressure and values of coating gap for which a stable coating bead could be obtained under the set operating conditions. For example, a uniform coating could only be obtained within a vacuum pressure of 0.2 to 3.7 cmH_2O for a 1:1 viscosity ratio and 2.5:1 wet thickness ratio. Continuous oscillation of the upstream meniscus was another sign of the instability of the bead created by the knife die lip. The oscillations were especially large near the dynamic contact line which would often move about 0.254 mm (0.010 inch) as it shifted its position along the moving web surface.

Layers of Equal Viscosity

For the coating runs of equal viscosity and wet thickness ratio, the interfacial region pinned to the knife edge and could not be moved from that position. Varying the vacuum pressure from 0.2 to 3.7 cmH_2O only changed the shape of the interfacial region. At lower vacuum pressures (about 1.5 cmH_2O at 0.152 m/s), the region formed a gentle arc pointing downstream and the upstream meniscus would move freely along the upstream die face. Higher vacuum pressures (about 2.5 cmH_2O at 0.152 m/s) would pin the upstream meniscus and force the interfacial region to form the pocket shape described earlier. However, the pocket shape showed signs of instability, oscillating between a shorter and longer shaped pocket. Figure 3.7 shows the effect of vacuum pressure on the shape of the interfacial region.

At a wet thickness ratio of 2.5:1, the interfacial region became unpinned from the knife edge and the liquid from the top layer invaded the upstream feed slot. Adjustments to the vacuum pressure and the coating gap could not force the interfacial region to pin to the knife edge.

Layers of Different Viscosity

For a 10:1 viscosity ratio, two different flow structures were possible within the coating bead. In the first structure (Figure 3.8a), the interfacial region began by pointing directly upstream from the knife edge and formed a long, narrow pocket that extended close to the upstream meniscus. The slim volume inside the pocket appeared to be filled with liquid from the top layer. This particular structure was unstable, showing strong oscillations in both the x and y directions. In the second structure (Figure 3.9b), the interfacial region pointed almost straight into the bead before turning gradually

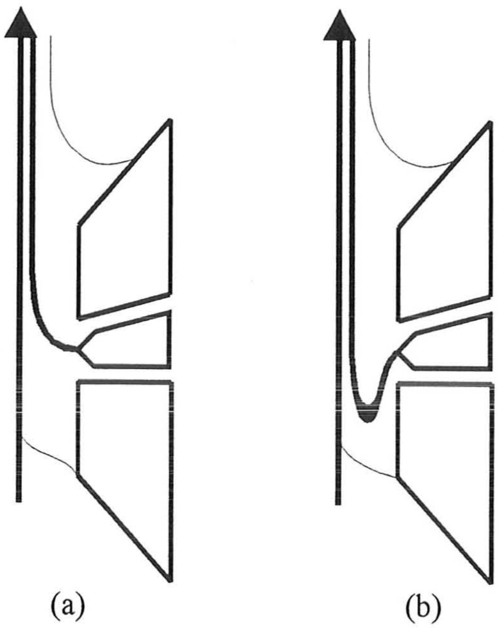

Figure 3.7: Effect of vacuum on the shape of the interfacial region created by the knife geometry for layers of equal viscosity. (a): t_U=50 μm, t_L=50 μm, μ_U= 39 cp, μ_L=39 cp, vac=1.5 cmH_2O, U=0.152 m/s, gap=305 μm. (b): t_U=50 μm, t_L=50 μm, μ_U= 39 cp, μ_L=39 cp, vac=2.5 cmH_2O, U=0.152 m/s, gap=305 μm.

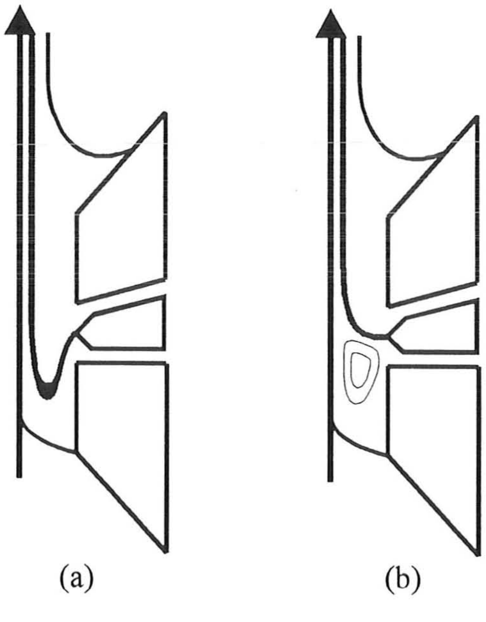

Figure 3.8: Observed shapes of the interfacial region created by the knife edge when the viscosity ratio was 10:1, independent of line speed and wet thickness ratio.
(a): long thin pocket. (b): recirculation.

downstream. A large vortex, rotating in a clockwise direction, formed in the bottom layer of the upstream feed slot region, S^U. Blurring made it difficult to determine if the liquids from both layers were mixing within the vortex. This second flow structure is similar to the flow field observed for a 10:1 viscosity ratio and square geometry.

Coating runs of 1:1 wet thickness ratio saw the occurrence of both structures (Figures 3.8a and 3.8b) with the flow field oscillating randomly between the two flow fields. When the wet thickness ratio was 2.5:1, only the second flow field (Figure 3.8b) was observed.

3.3 Bullet Geometry

The bullet shaped center piece showed some signs of instability, although the symptoms were less severe than those observed with the knife geometry. For example, there was only a slight oscillation of the upstream meniscus and the coating gap had to be reduced from 0.305 mm (0.012 inch) used for the square geometry to 0.254 mm (0.010 inch) for coating runs with 1:1 wet thickness ratio. The range of vacuum over which a uniform coating could be obtained was narrower than the square geometry vacuum range. It ranged from 1.5 cmH_2O to 6.0 cmH_2O for a 2.5:1 wet thickness ratio and 1:1 viscosity ratio.

Unlike the previous two geometries, the interfacial region created by the bullet geometry appeared to be a smooth line with no signs of oscillations or associated recirculations in the intermediate region, regardless of the viscosity ratio and wet thickness ratio. Vacuum pressure could be used to move the region around the curvature

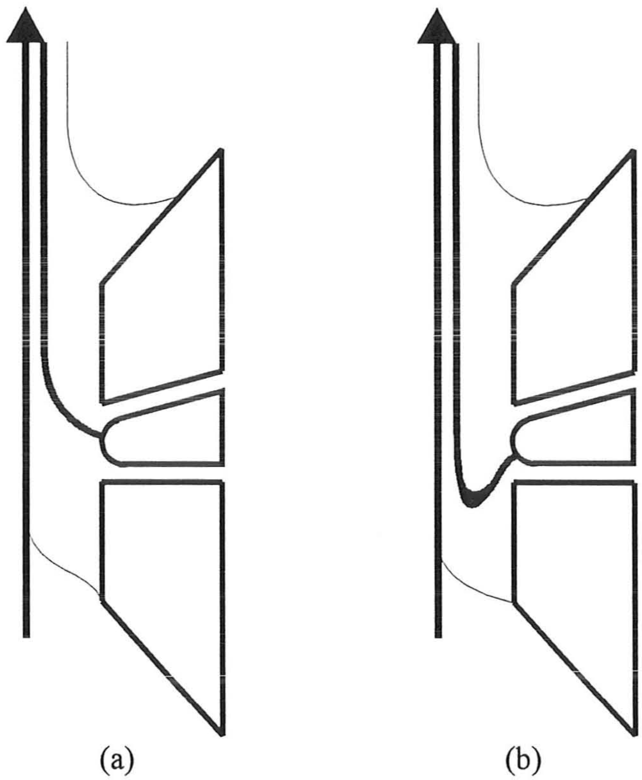

Figure 3.9: Shape of the interfacial region at low vacuum (a) and high vacuum (b) for the bullet geometry. (a): t_U=125 μm, t_L=50 μm, μ_U= 389 cp, μ_L=39 cp, vac=0.5 cmH_2O, U=0.305 m/s, gap=457 μm. (b): t_U=125 μm, t_L=50 μm, μ_U= 389 cp, μ_L=39 cp, vac=2.0 cmH_2O, U=0.305 m/s, gap=457 μm

of the bullet edge. At lower vacuums, the separation line (the line where the interfacial region contacts the die face) would rest on the downstream side of the bullet. Extending nearly perpendicular from the bullet face, the interfacial region formed a gentle arc that moved downstream until it became parallel to the web surface (Figure 3.9a). The separation line could then be moved upstream along the bullet edge by increasing the vacuum pressure under the upstream meniscus. At all points along the bullet face, the region would maintain a nearly 90^0 angle to the die face. When the separation line reached the upstream side of the bullet edge, the interfacial region would point upstream and form a wide pocket as it turned 180^0 to move downstream (Figure 3.9b).

Problems with the downstream injection port prevented the dye tracer from being injected into the top layer of liquid. The shape and position of the interfacial region had to be visualized using the bottom dye tracer only. Without the use of the second dye tracer, the occurrence of mixing along the interfacial region could not be determined.

3.4 Groove Geometry

The groove geometry was more stable than the knife or bullet geometries. There were no oscillations of the upstream meniscus or interfacial region and the range of vacuum over which a uniform coating was obtained was comparable to the vacuum range for the square geometry (about 0 to 6.0 cmH_2O). However, to obtain a stable bead, the coating gap had to be reduced to 356 μm (0.014 inch) for the 0.305 m/s (60 ft/min) coating runs of 10:1 viscosity ratio and 2.5:1 wet thickness ratio.

Layers of Equal Viscosity

Figure 3.10 shows that for layers of equal viscosity, the separation line would pin to the upstream edge of the groove. From this edge, the interfacial region would point straight into the coating bead before it turned upstream and moved into the upstream region of the bead. The region then turned 180^0 towards the web forming the

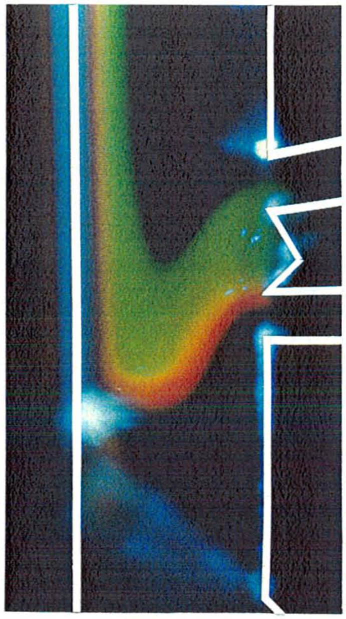

Figure 3.10: Pinning of the interfacial region on the upstream corner of the groove for layers of equal viscosity. t_U=125 μm, t_L=50 μm, μ_U= 39 cp, μ_L=39 cp, U=0.305 m/s, gap=457 μm.

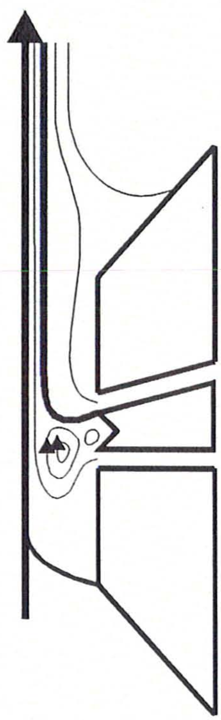

Figure 3.11: Pinning of the interfacial region on the downstream corner of the groove at a viscosity ratio of 10:1. t_U=50 μm, t_L=50 μm, μ_U= 388 cp, μ_L=39 cp, U=0.152 m/s, gap=305 μm.

characteristic pocket shape described earlier. The inside region of the pocket was filled with a thick line of fluorescein dye, indicating slow moving fluid in this portion of the top layer. While no recirculations were seen, a small vortex was expected to exist inside the groove. The vortex may still have existed but remained unseen due to its small size and the difficulty of observing the fluid flow in such a small corner of the coating bead.

A yellow streak was again seen along the interfacial region between the lines of sulforhodamine B and fluorescein dye tracers. The yellow line was especially thick along the pocket and then thinned as the fluid accelerated in the direction of the web.

Layers of Different Viscosity

The sketch in Figure 3.11 shows the interfacial region pinned to the downstream edge of the groove when the viscosity ratio was 10:1. The flow structure in the intermediate region was similar to the structure of the square geometry where the interfacial region formed an arc that turned immediately downstream and a pair of recirculations were formed in the bottom layer of the intermediate region I. The pair consisted of one tiny vortex inside the groove and a second, larger vortex centered in region I. Pictures of these flow fields were often blurred by the mixing of the top viscous layer (386 cp) with the less viscous bottom layer (39 cp) at the edge of the coating bead. The mixing at the edge became severe at higher line speed (0.305 m/s) causing the entire bead to become completely blurred.

For both viscosity ratios, the separation line could not be moved from either edge of the groove by changing the vacuum pressure. However, cycling of the vacuum pressure from 0 to 6.0 cmH_2O range caused the upstream meniscus to move freely along the upstream die face at lower vacuum pressures while causing weeping of the upstream meniscus at higher vacuum pressures.

3.5 General Observations of the Upstream Meniscus

Up to this point, the emphasis of the chapter has been on the interfacial region and very little attention has been given to the upstream meniscus. The upstream meniscus is important since it is more than just the lower boundary of fluid flow, but also partially determines the pressure and flow fields inside the coating bead. Thus, this section is devoted to describing a couple unique features of the upstream meniscus that may warrant further study.

Recirculation Zones

It was mentioned earlier that the bottom fluid flowed smoothly along the meniscus. However, small vortices may exist at the dynamic and static contact lines. There were glimpses of a tiny vortex near the dynamic contact line on number of coating runs at both 0.152 m/s (30 ft/min) and 0.305 m/s (60 ft/min). The photograph in Figure 3.12 show bright streaks of light created by particles trapped in a small recirculation at the dynamic contact line.

The conditions under which these vortices will repeatedly occur are not clearly known, although their presence is likely related to the flow rate, web speed, and the angle of contact with the surface. Cohen (1993) reported to have seen a vortex at an unpinned static contact line, although no recirculations were observed in his work where the static contact line was pinned to upstream corner of the die. Blake et. al (1994) observed that a vortex occurs at the dynamic contact line at low line speeds and high flow rates in curtain coaters. Dussan (1979) has also observed vortices at a moving contact line between two immiscible liquids within a capillary tube.

Meniscus Shape

Sketches of the coating bead often show the upstream meniscus as having an arc or semi-circular shape. Figure 3.13 show that this is not generally true. The meniscus is able the take on at least two possible shapes, a convex curve or an S-curve. The convex curve appears to be very similar to an arc of constant radius until it approaches the dynamic contact line where the meniscus begins to stretch and the radius of curvature begins to increase. Figure 3.13a is an example of a convex curve. The S-shaped meniscus begins with concave curve near the static contact line. The meniscus then passes through an inflection point near the middle of the coating gap where its shape changes to the convex curve required for the approach to the dynamic contact line. Figure 3.13b shows an example of an S-curve. Similar meniscus shapes were observed by Sartor (1990), although he only observed the S-shaped curve when the upstream static contact line moved freely along the die face.

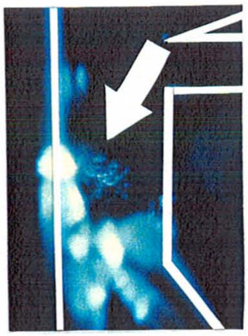

Figure 3.12: Tiny recirculation at the dynamic contact line. t_U=125 μm, t_L=50 μm, μ_U= 39 cp, μ_L=39 cp, vac=2.3 cmH_2O, U=0.305 m/s, gap=457 μm.

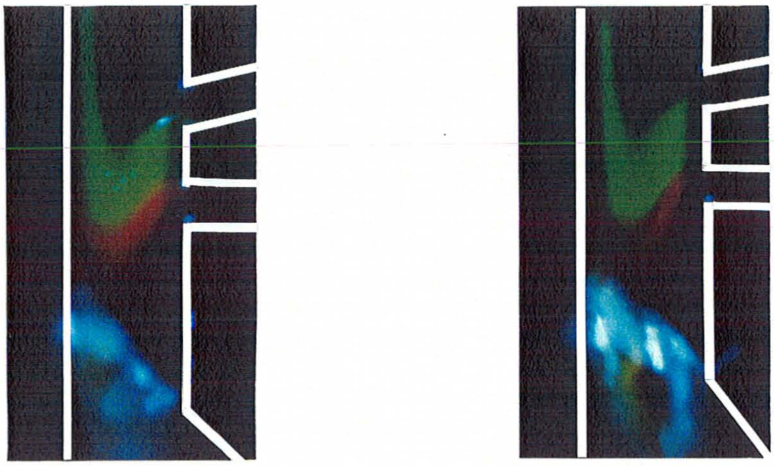

(a) (b)

Figure 3.13: Possible shapes of the upstream meniscus. Photo (a): convex shape t_U=125 μm, t_L=50 μm, μ_U= 39 cp, μ_L=39 cp, vac=1.6 cmH_2O, U=0.305 m/s, gap=457 μm. Photo (b): S-curve t_U=125 μm, t_L=50 μm, μ_U= 39 cp, μ_L=39 cp, vac=0.1 cmH_2O, U=0.152 m/s, gap=457 μm.

3.6 Flow Maps

A flow map of the observed flow fields under different operating conditions is provided in Figure 3.14. The flow map is accompanied by Table 3.1 that defines the range of operating conditions under which each flow field was observed. Only the major effects related to die geometry and viscosity ratio are shown. Line speed and the wet thickness ratio have been ignored since these effects were minor over the variable range that was tested. The only exception was the knife geometry where switching from a 1:1 to a 2.5:1 wet thickness ratio caused the top layer of liquid to invade the upstream feed slot when the layers were of equal viscosity.

The flow map also assumes that the vacuum was set to a pressure that would pin the upstream meniscus. However, the vacuum pressure did have a strong effect on the position of the separation line and the shape of the interfacial region. Low vacuum pressures led to an arc shaped interfacial region whereas higher vacuum pressures caused the region to form a pocket shape. The pocket grew longer, extending further upstream with increasing vacuum pressure. The length and width of the pocket depended on coating gap and the shape of the center die lip.

In Cohen's (1993) initial study of the two slot coater, he mentioned that it was almost impossible to obtain a coating bead devoid of recirculations over the range of variables tested. This appears to be true for the square, knife and groove geometries for the range of variables tested in this work. It was possible to eliminate all of the large recirculation zone in the middle of the coating bead using the bullet center die block, as well as control the position and shape of the interfacial region. However, tiny vortices may still exist at the dynamic and static contact lines.

Table 3.1: Range of operating conditions for which each flow field in Figure 3.14 was observed.

Flow Field in Figure 3.14	Geometry	Viscosity Ratio	Wet Thickness Ratio	Line Speed (m/s)	Coating Gap (μm)	Vacuum* (cmH_2O)
(a)	Square	1:1	1:1 to 2.5:1	0.152 to 0.305	203 to 508	0.2 to 3.0
(b)	Square	10:1	1:1 to 2.5:1	0.152 to 0.305	305 to 457	0.2 to 3.3
(c)	Knife	1:1	1:1 to 2.5:1	0.152 to 0.305	178 to 457	0.6 to 4.1
(d)	Knife	10:1	1:1 to 2.5:1	0.152 to 0.305	229 to 457	2.3 to 3.0
(e)	Bullet	1:1	1:1 to 2.5:1	0.152 to 0.305	152 to 457	1.9 to 2.3
(f)	Bullet	10:1	1:1 to 2.5:1	0.152 to 0.305	254 to 457	1.5 to 2.6
(g)	Groove	1:1	1:1 to 2.5:1	0.152 to 0.305	305 to 584	0 to 4.1
(h)	Groove	10:1	1:1 to 2.5:1	0.152 to 0.305	305 to 457	0 to 1.5

*This is the vacuum range needed to pin the upstream meniscus to the upstream corner of the die. A uniform coating bead can be obtained outside this specified range of vacuum.

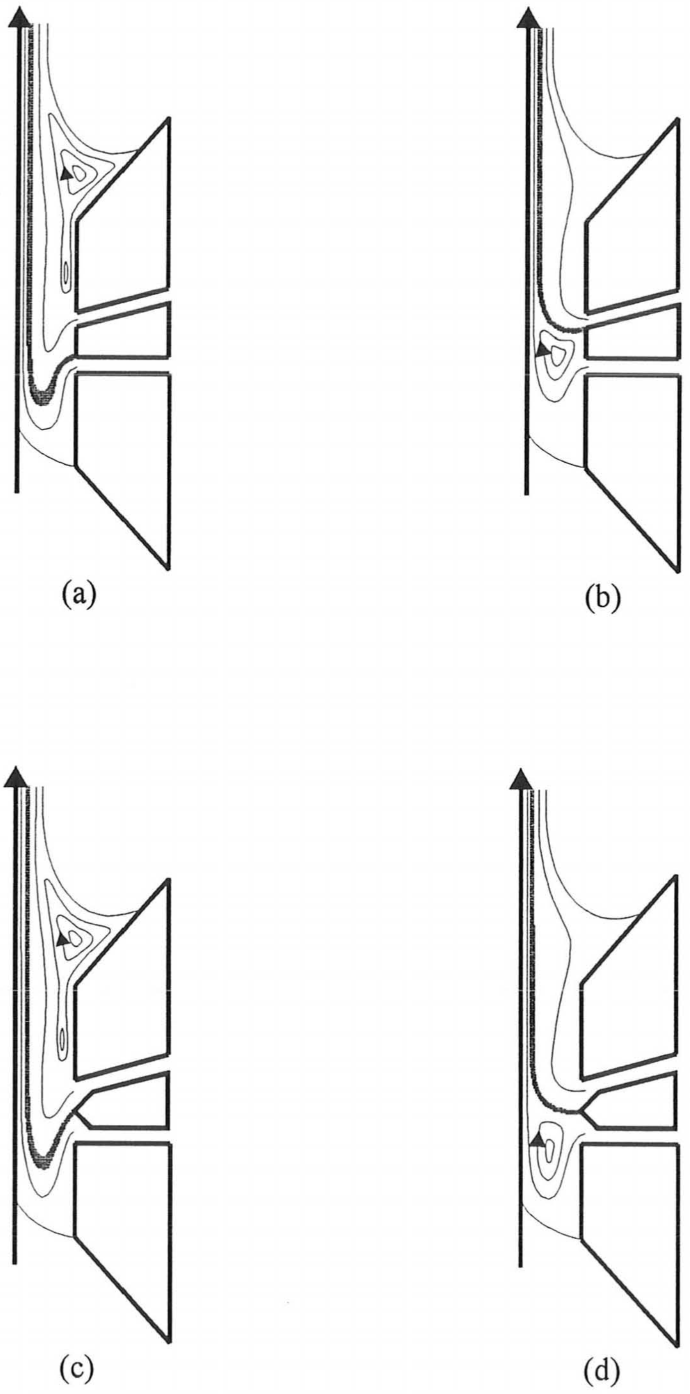

Figure 3.14: Flow map of viscosity and geometry effects on two slot coater.

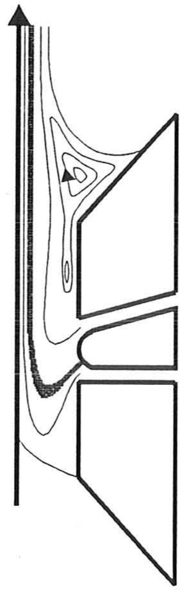

(e)

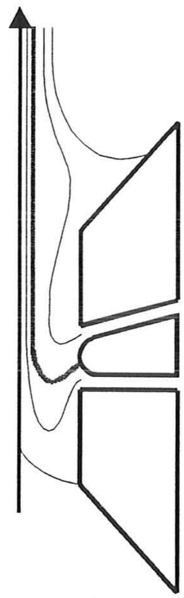

(f)

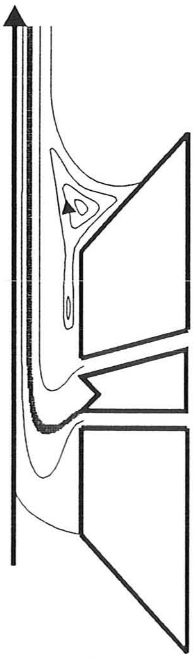

(g)

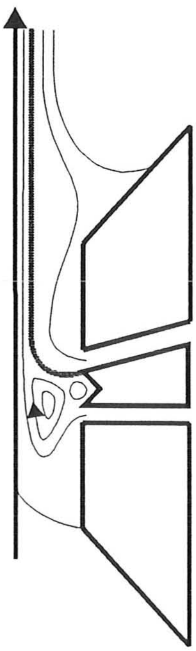

(h)

Figure 3.14 continued.

CHAPTER 4

SIMULATION OF A TWO SLOT COATER

The focus of the simulations will be to define the interfacial region between the two layers of miscible liquids. Previous approaches include the assumption that the interfacial region behaves like an interface of two immiscible liquids with a surface tension of zero (Scanlan, 1990). Another approach has been to add an additional tensor to the Navier-Stokes equations to account for the stress created by concentration differences across the interfacial region (Joseph, 1990). This second approach is the most fundamental, but it is also leads to a very difficult set of equations to solve.

A more empirical approach has been taken in this study. The fluid properties, namely the viscosity, of the individual layers has been linked to a false species concentration where the viscosity is a defined function of tracer concentration. The fluid layers could then be differentiated by their false species concentrations and the interfacial region separating the layers was defined as the narrow region between the highest and lowest concentration. The concentration profile through the interfacial region was determined from the mass transport equations.

This chapter focuses on the development of a numerical model of the two slot coater. The results are compared to the experimental observations made in the previous chapter to determine the validity of the model.

4.1 Numerical Technique

Two dimensional simulations of the two slot coater were carried out using the commercial computational fluid dynamics (CFD) package FIDAP^{TM} (v7.61, 1996). FIDAP^{TM} solves the fundamental equations of transport phenomena using the finite element method (FEM). The FEM is used to reduce continuum problems to the solution for the state variables on a discrete set of nodes using a system of algebraic equations. This is achieved by dividing the flow region of interest into a mesh made up of simply shaped regions or elements. The velocity, pressure, and other state variables are then solved through interpolation functions at a set of nodes within each element. A relevant review of FEM can be found in the FIDAP manuals (FDI, 1993) or Huebner and Thorton (1982).

4.1.1 Mesh

Modelling of the two slot coating bead was done using a mesh of 9-node quadrilateral elements. Velocity components were interpolated using a biquadratic approximation and pressure was linearly interpolated. The outline of the standard mesh used for all four centre die geometries (square, knife, groove, and bullet) is shown in Figure 4.1. Figure 4.2 shows the changes that were made to the mesh in the intermediate region to account for the different shaped centre die blocks. The meshes were refined by increasing the mesh density in the intermediate, downstream, and early portion of the film

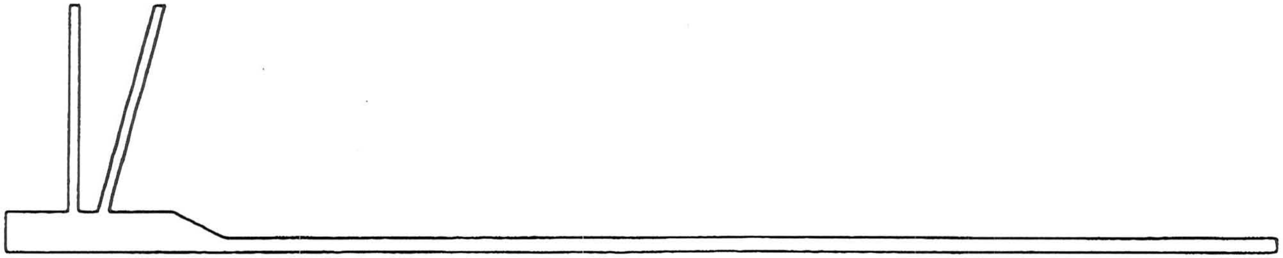

Figure 4.1: Outline of the standard mesh used in the simulation of the two slot coating bead.

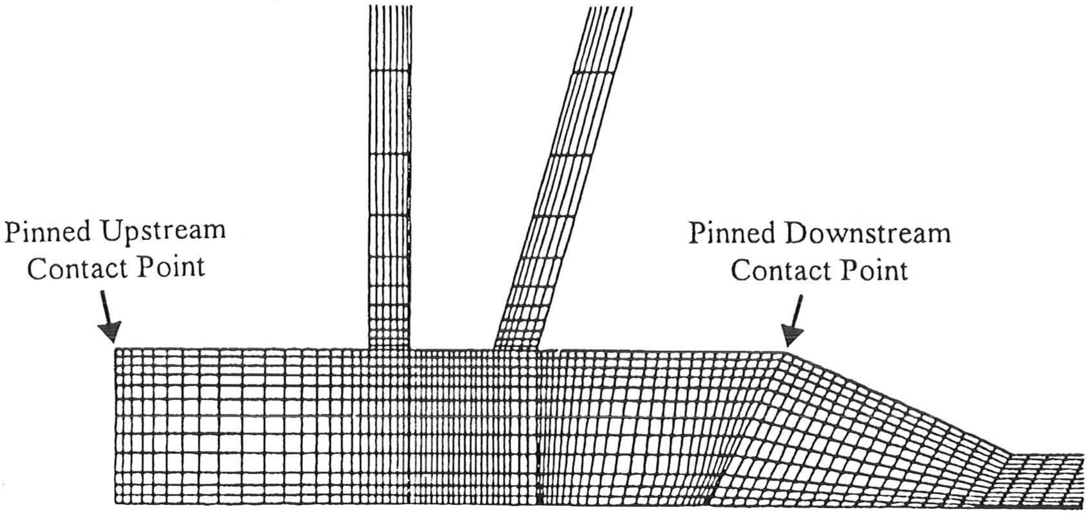

(a)

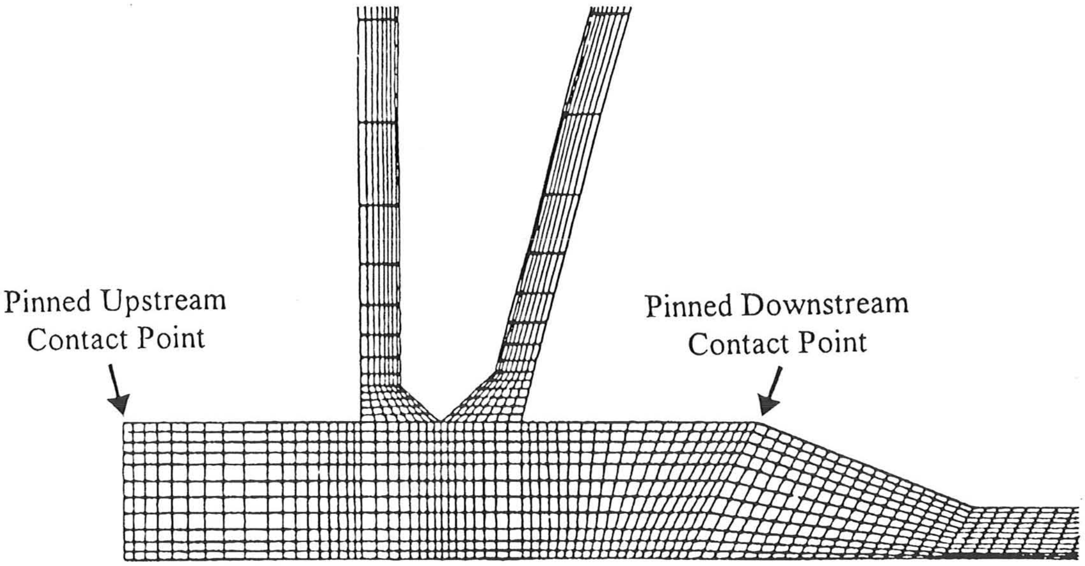

(b)

Figure 4.2: Close-up view of the initial mesh in the coating gap: (a) square geometry, (b) knife geometry, (c) bullet geometry, and (d) groove geometry.

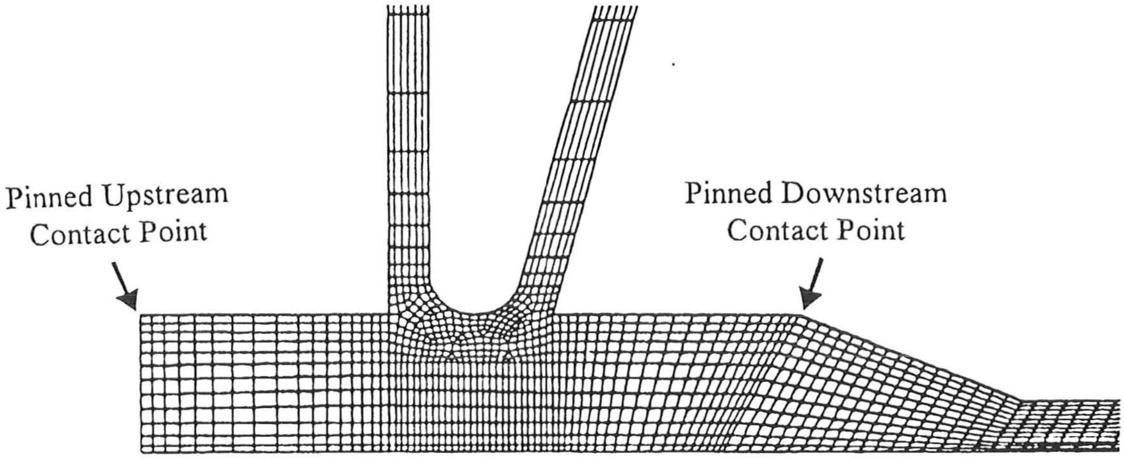

(c)

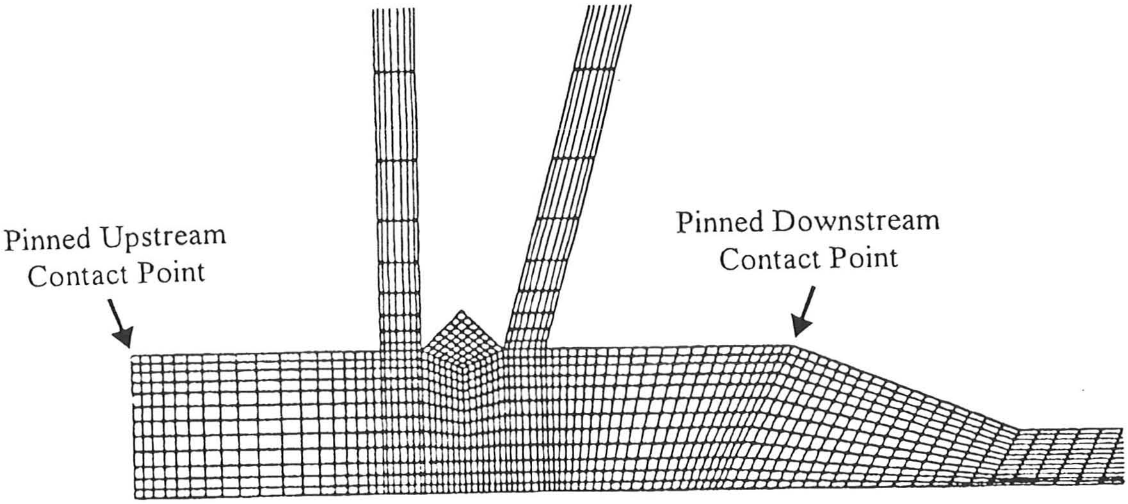

(d)

Figure 4.2 continued.

forming regions. A relatively coarse mesh was used in the feed slots and in the latter portion of the film forming region where the downstream meniscus was parallel to the web surface.

In all of the experimental flow fields, the upstream meniscus was pinned to the upstream corner of the die while the downstream meniscus moved freely along the downstream shoulder of the die. However, it is proposed that wetting of the downstream shoulder does not significantly affect the structure of the flow field within the coating gap. Thus, the coating bead could be simulated by assuming that both menisci are pinned to their respective corners, as shown in Figure 4.2. The validity of this assumption was tested using the mesh in Figure 4.3a which includes wetting of the downstream shoulder.

It was concluded in the flow visualizations that the wet thickness had no significant effect on the structure of the flow field. Thus, a constant wet thickness ratio (2.5:1) and corresponding gap (457 μm) were assumed for the simulations. This assumption was tested using a mesh with a narrow gap (305 μm) and operating conditions set for a 1:1 wet thickness ratio. The narrow gapped mesh is shown in Figure 4.3b.

Table 4.1 lists the total number of elements and nodes used for the meshes of each geometry. Simulations of the square geometry using a denser mesh (2314 instead of 2079 elements) showed that an increase in mesh density did not effect the streamlines or the interfacial region's position and thickness throughout the entire bead. Solutions could only be obtained for line speeds of 0.150 m/s (30 ft.min) or less since the simulation would diverge at higher line speeds.

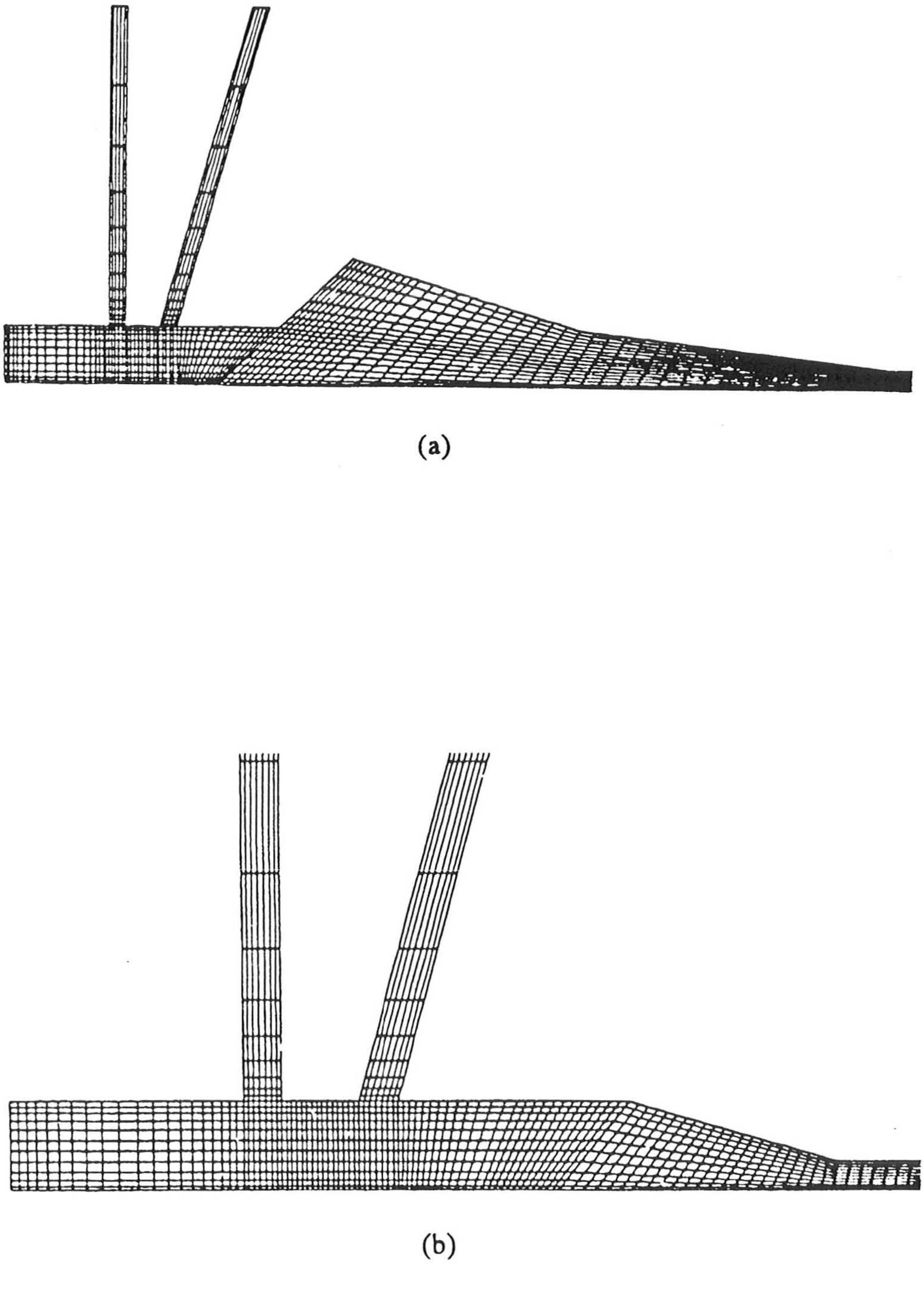

(a)

(b)

Figure 4.3: Close-up view of the initial meshes assuming (a) wetting of the downstream shoulder and (b) narrow gap.

Table 4.1: Number of elements and nodes for the meshes of each geometry.

Configuration	Number of Elements	Number of Nodes
Square Centre Block	2079	7303
Knife Centre Block	1801	6275
Groove Centre Block	2021	7131
Bullet Centre Block	2526	8959
Square Centre Block with Narrow Gap	2144	7491
Square Centre Block with Wetted Downstream Shoulder	1854	6535

4.1.2 Governing Equations

The coating bead was assumed to be an incompressible, laminar, steady state, two dimensional flow field. Due to the small volume of liquid contained in the coating gap, the force of gravity was ignored. The resulting continuity and momentum equations were, as follows:

$$\nabla \bullet \overline{\mathrm{U}} = 0 \tag{4.1}$$

$$\mathrm{Re}(\overline{\mathrm{U}} \bullet \nabla\overline{\mathrm{U}}) = \nabla \bullet \overline{\overline{\mathrm{T}}} \tag{4.2}$$

where

$$\overline{\overline{\mathrm{T}}} = -\overline{\overline{\mathrm{I}}}\mathrm{p} + \mu(\nabla\overline{\mathrm{U}} + (\nabla\overline{\mathrm{U}})^{\mathrm{T}}) \tag{4.3}$$

In order to track the shape and position of the interfacial region, a false species was introduced into the model. The viscosity, μ, was set as a function of a false species concentration, allowing for changes in fluid properties through the interfacial region. For

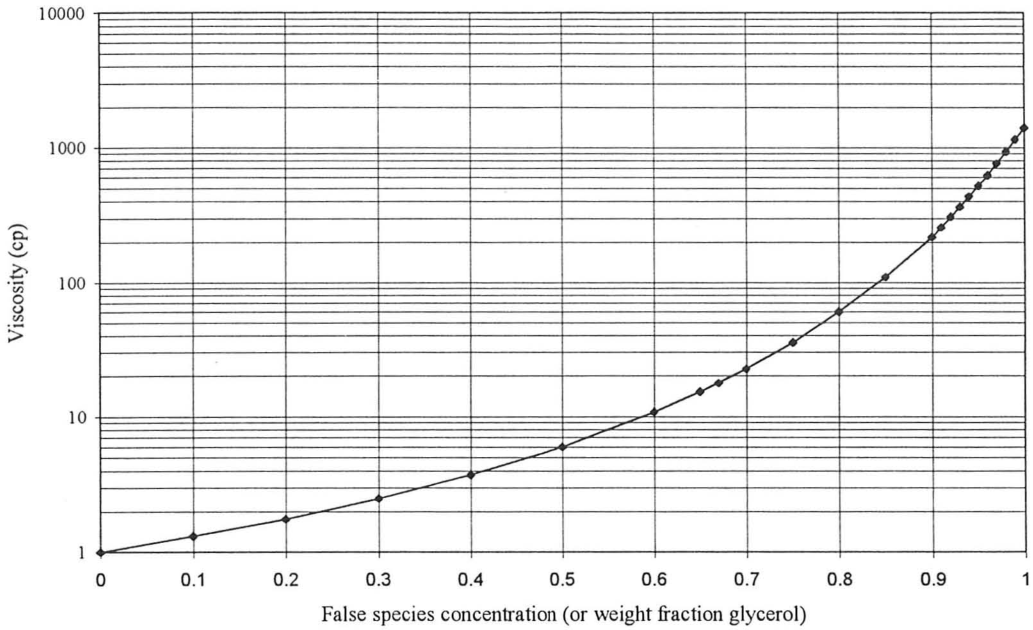

Figure 4.4: Viscosity as a function of false species concentration. Taken from the curve for viscosity as a function of wt% glycerol at 20^0C (CRC Handbook of Chemistry and Physics, 63rd Ed., 1982).

the cases of 1:1 viscosity ratio between the two layers, the viscosity was assumed to be a constant function (39 cp) of the species concentration. For the cases of viscosity ratio greater than 1:1, the viscosity curve for the concentration of glycerol in water was used where the false species concentration was set equal to the glycerol concentration. A series of twenty data points were read from the viscosity curve in Figure 4.4 and entered into the model. FIDAP™ then calculated the viscosity using linear interpolation for values between data points.

Assuming the problem was steady state, the mass transport equation was used for determining the false species concentration:

$$\bar{U} \bullet \nabla C = \nabla \bullet (\alpha \nabla C) \tag{4.4}$$

where C is the species concentration and α is the mass diffusivity of the false species.

4.1.3 Boundary Conditions

Parabolic velocity profiles were applied to the entries of the top and bottom layer feed slots:

$$\bar{u} = f(x)(\hat{i}, \hat{j}) \tag{4.5}$$

Uniform false species concentrations were also assumed at the entry of each feed slot. The no slip boundary condition was applied to the die walls and the moving web:

$$\bar{u} = 0 \qquad \text{and} \qquad \bar{u} = (U,0) \tag{4.6}$$

where U was the web speed.

At the outlet far downstream of the coating gap, the natural outflow (i.e. no traction) boundary condition was satisfied by forcing the downstream meniscus to be parallel to the web surface.

A number of boundary conditions were applied to the free surfaces. At the dynamic contact line, an angle of 120°C was assumed based on previous work by Hrymak and Stevanovic (1994) and Scanlan (1990) which indicated that angles in this range provided good solution convergence. Higher contact angles could be used but lead to greater difficulties in convergence. A zero normal velocity was also assumed at the dynamic contact point. Both the x- and y-component velocities were set to zero at the upstream and downstream static contact lines, pinning the menisci to their respective upstream and downstream corners of the die. Finally, the kinematic condition and stress balance equations were applied to the free surfaces:

$$\hat{n} \bullet \bar{u} = 0 \tag{4.7}$$

$$\hat{n} \bullet \bar{\bar{T}} = \frac{1}{Ca}\frac{d\hat{t}}{ds} - \hat{n}p \tag{4.8}$$

where the pressure, p, was set to zero at the downstream meniscus and from zero to some negative value for the vacuum below the upstream free surface.

4.1.4 Solution Method

Solving the two slot coating problem required four steps. The first step was to obtain an estimate of the velocity/pressure field at a relatively low web speed. At this point, the free surfaces were assumed to be fixed walls that allowed for slip. Once this estimate was obtained, the slip wall boundary condition for the downstream meniscus was replaced by the free surface boundary condition. This provided an approximation of the shape of the downstream free surface. The free surface boundary condition for the upstream meniscus, as well as the species equation and species boundary conditions, were introduced in the third stage. Finally, the web speed was ramped up to the desired value using the estimate of the flow field from the third stage as the initial condition for velocity, species concentration, and free surface position.

Solutions were obtained using the Newton-Raphson iterative method. The free surface position was adjusted using spines. The spine method allows the mesh to deform as the velocity components and pressures are calculated with the unknown free surface position as a degree of freedom. To reduce the risk of a diverging solution due to large movements in the free surface position during iteration, it was necessary to use a large relaxation factor of $\gamma = 0.9$. The relaxation factor was defined as follows:

$$\overline{W}_{i+1} = \gamma\overline{W}_i + (1-\gamma)\overline{W}^* \tag{4.9}$$

where $\overline{W}$ is the solution vector at iteration i and * denotes the calculated solution vector. The simulation was considered converged when the relative change in the solution vector was less than 0.0001. Total CPU time required to obtain a full solution was typically 475 minutes for a simulation of 1:1 viscosity ratio flow field. Increasing the viscosity ratio nearly doubled the required CPU time to about 830 minutes for a flow field with a viscosity ratio of 10:1. The simulations were performed on an IBM RS600 370 computer (92 Mb RAM, AIX 3.2).

4.1.5 Parameter Settings

Table 4.2 is a listing of the parameters held constant for all simulations. The physical property constants were based on typical values for high concentration glycerol solutions, like those used in the experiments. The simulated operating conditions match experimental operating conditions.

Table 4.2: Simulation constants.

Parameter	Value
Web Speed	150 mm/s (30 ft/min)
Wet Thickness Ratio	2.5:1
Wet Thickness: Top Layer Bottom Layer	125 μm 50 μm
Dynamic Contact Angle	120°
Surface Tension	68 mN/m
Specific Gravity	1.19
False Species Diffusivity	0.0078 mm^2/s

4.2 Results and Discussion

4.2.1 Sensitivity of False Species Diffusivity

The quality of the simulation results, especially the behaviour of the interfacial region, depends strongly on the value of the false species diffusivity. This parameter partially determines both the position and the thickness of the interfacial region. The criteria for choosing a false species diffusivity were smooth contours of species concentration and a reasonable estimate of the interfacial position and thickness. A reasonable estimate meant that the centre of the interfacial region must be 50 μm above the web surface at the outflow plane (i.e. corresponding to the bottom layer wet

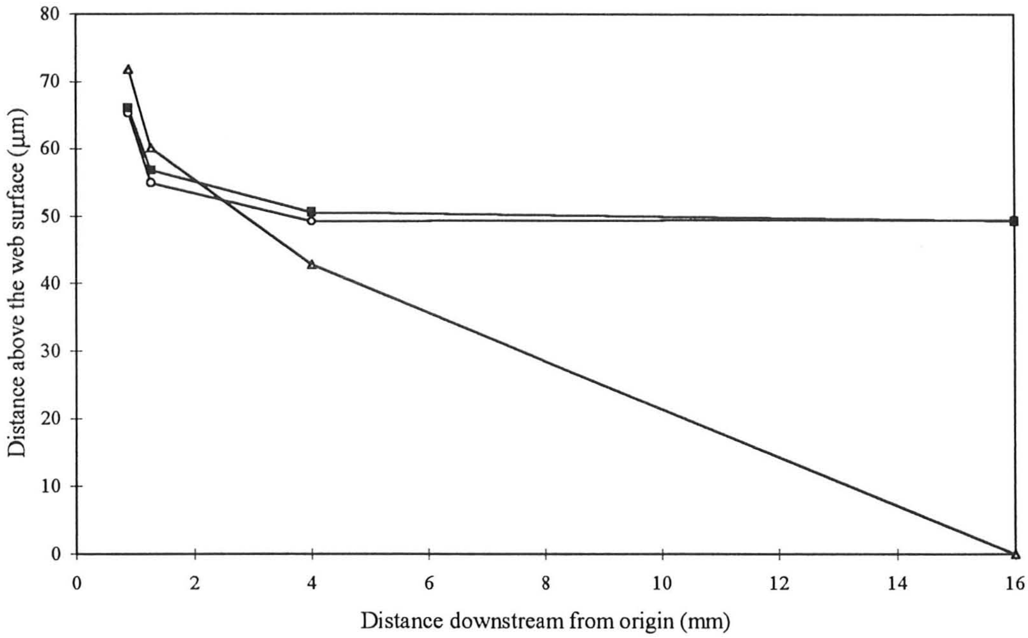

Figure 4.5: Position of interfacial region from just inside the coating gap to the outflow plane based on computer simulation. The origin is located below the upstream corner of the die (see Figure 2.5). O 7.8×10^{-6} m^2/s, ■ 7.8×10^{-5} m^2/s, Δ 7.8×10^{-4} m^2/s.

thickness) and the interfacial thickness must be significantly less than the total wet thickness of the coating at the outflow plane. The interfacial thickness was calculated as 90% of the difference in concentration between the top and bottom layer. A sensitivity study was done to determine a reasonable value for the false species diffusivity. Simulations were performed for values of 7.8×10^{-6} m^2/s, 7.8×10^{-5} m^2/s, and 7.8×10^{-4} m^2/s where the first value is the diffusivity of glycerol in water at infinite dilution (Reid and Sherwood, 1966). The large false species diffusivity produced smooth contours but gave

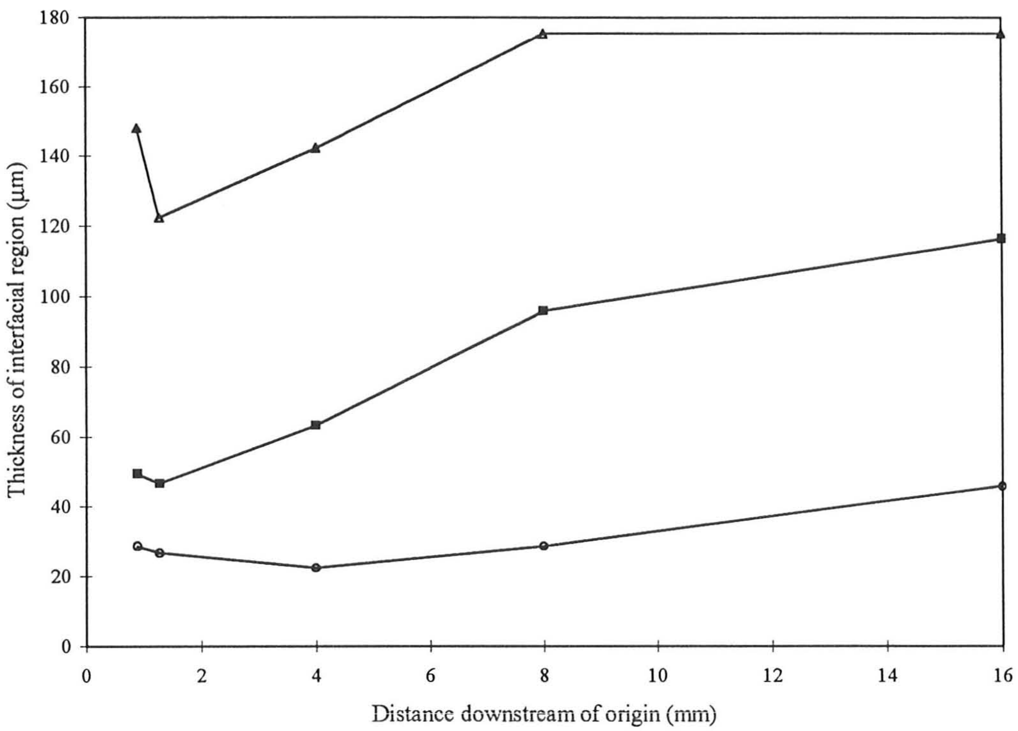

Figure 4.6: Predicted thickness of the interfacial region from inside the coating gap to the outflow plane based on computer simulation. The origin is located below the upstream corner of the die (see Figure 2.5). O $7.8x10^{-6}$ m^2/s, ■ $7.8x10^{-5}$ m^2/s, Δ $7.8x10^{-4}$ m^2/s.

unrealistic estimates of the interfacial region. Figure 4.5 shows that the large diffusivity predicted that the centre of the interfacial region eventually touched the web surface while Figure 4.6 indicates that the interfacial region thickness was equal to the wet thickness at the outflow plane.

The intermediate and lower diffusivities estimated the centre of the interfacial region to be positioned 50 μm above the web surface at the outflow plane (see Figure 4.5) and both produced reasonable estimates of the interfacial thickness (see Figure 4.6).

However, the low 7.8×10^{-6} m^2/s value produced a concentration contour diagram that was not smooth while the intermediate value provided a smooth contour diagram. Since the intermediate value of 7.8×10^{-5} m^2/s satisfied both criteria, it was chosen as a reasonable estimate of the false species diffusivity.

4.2.2 Square Geometry

The first geometry to be studied was the square centre block where both downstream and upstream menisci were assumed to be pinned to their respective die corners. Simulations were performed over a range of viscosity ratios from 1:1 to 10:1 of top layer: bottom layer viscosity. These results are summarised in Figures 4.7a-f which illustrate the effect of viscosity ratio on the interfacial layer via streamlines and contours of false species concentration. Only two contours of species concentration were used to outline the approximate shape and position of the interfacial region within the coating bead.

Simulation of the square geometry for a 1:1 viscosity ratio gave excellent agreement with the experimental photographs (refer to Figure 3.2). The streamlines show that fluid layers move immediately upstream after exiting from their respective feed slots. As the fluid layers turn downstream, they form the observed pocket region in the upstream section of the coating bead (see False Species Conrours in Figure 4.7a). Other comparable results include: the final thickness of the bottom layer (50 μm) was quickly approached once the fluid moved downstream of the pocket region, the separation line was located at the upstream corner of the centre die block and a required vacuum pressure of 3.06 cmH_20 (300 Pa). Thickening of the interfacial region at the bend of the pocket was also predicted; however, the effect was more pronounced in the experiments.

Wetting of Downstream Shoulder

The result of Figure 4.7a cannot yet be directly compared to the experimental photographs from Chapter 3 until consideration is given to the wetting of the downstream shoulder. Simulation results for the two slot coater with a wetted downstream shoulder is shown in Figure 4.8. These results, which indicate a large recirculation on the downstream shoulder, are comparable to the experimental photographs. A qualitative comparison between Figure 4.8 and Figure 4.7a indicates that this vortex had very little effect on the flow structure (ie. streamlines) within the coating gap and did not disturb the interfacial region (ie. no change in position or thickness). The only effect of wetting was a change in the curvature of the downstream meniscus which reduced the required vacuum pressure to 2.03 cmH_2O (200 Pa). The inability to predict the small, narrow vortex immediately below the downstream die block was the only point where the model did not match the experimental results for a 1:1 viscosity ratio.

Since the simulation showed that the recirculations at the downstream shoulder did not affect the streamlines or interfacial region within the coating bead, all remaining simulations assumed that the downstream meniscus was pinned and that these results were comparable to the experimental results.

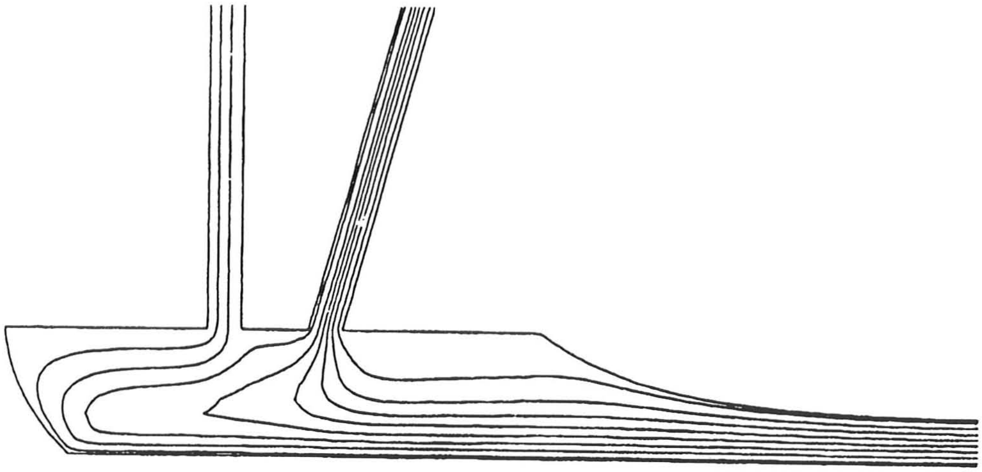

Streamline

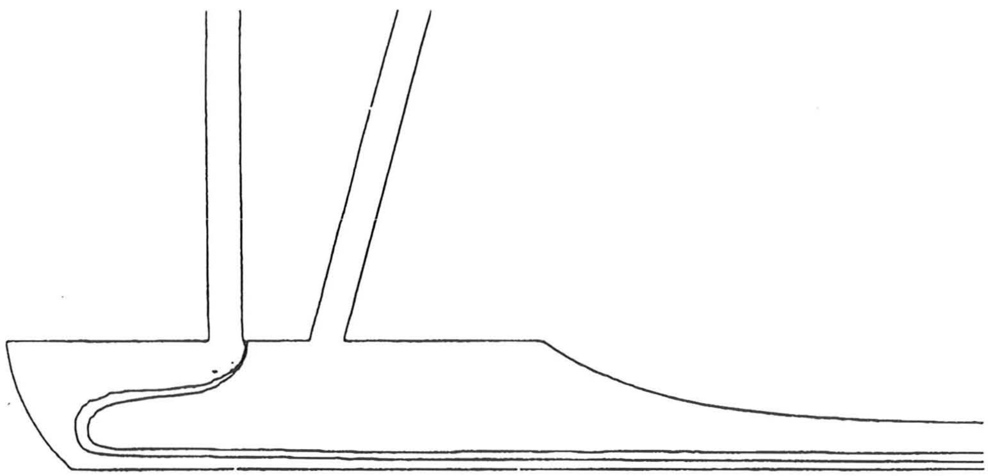

False Species Concentration

(a)

Figure 4.7: Streamlines and false species concentration contours for the square geometry at the following viscosity ratios: (a) 1:1, (b) 2:1, (c) 4:1, (d) 6:1, (e) 8:1, and (f)10:1.

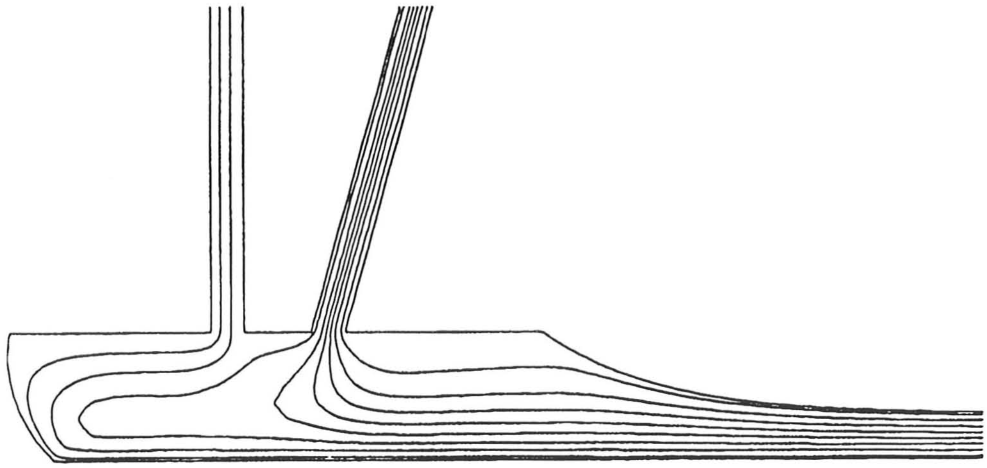

Streamline

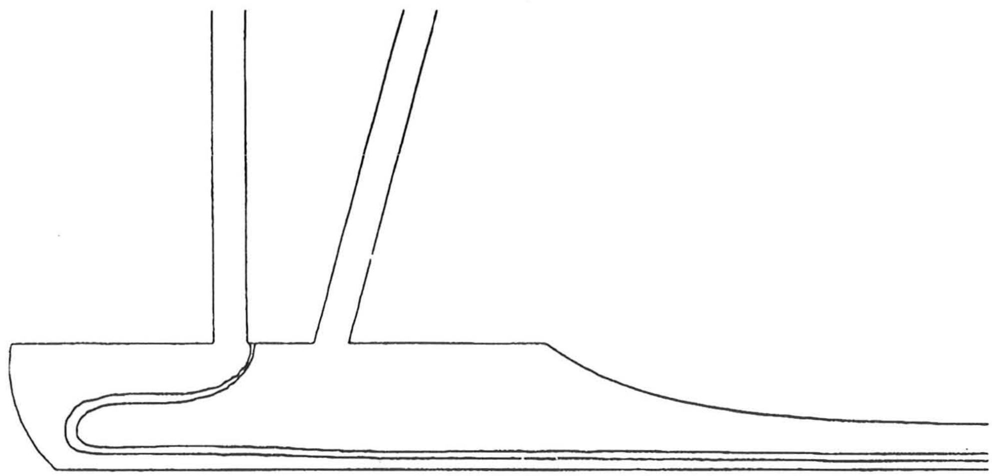

False Species Concentration

(b)

Figure 4.7 continued.

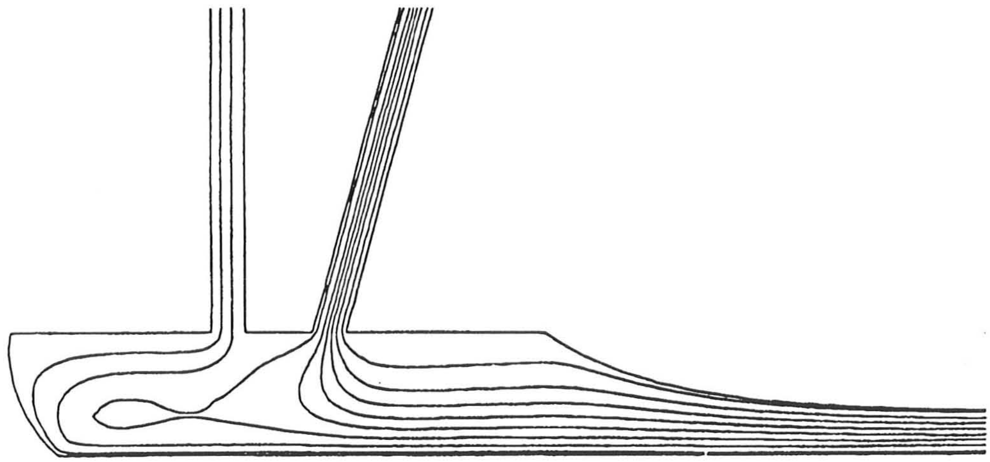

Streamline

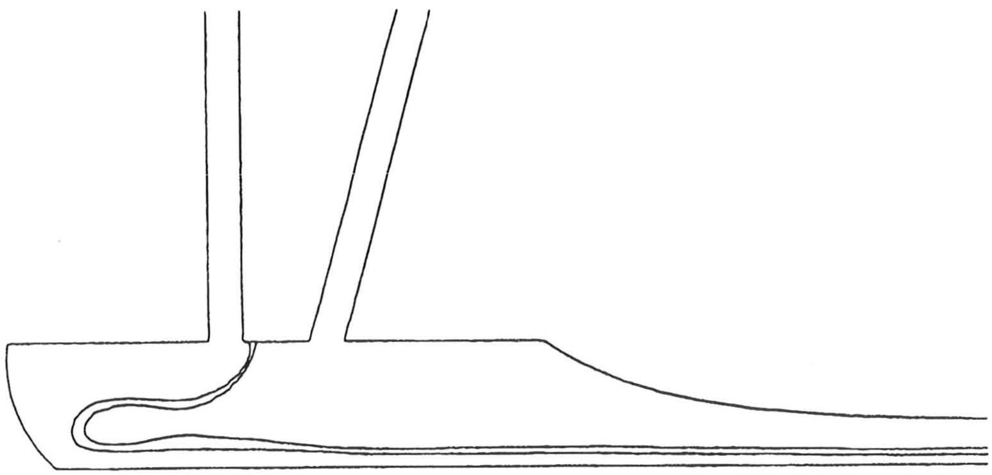

False Species Concentration

(c)

Figure 4.7 continued.

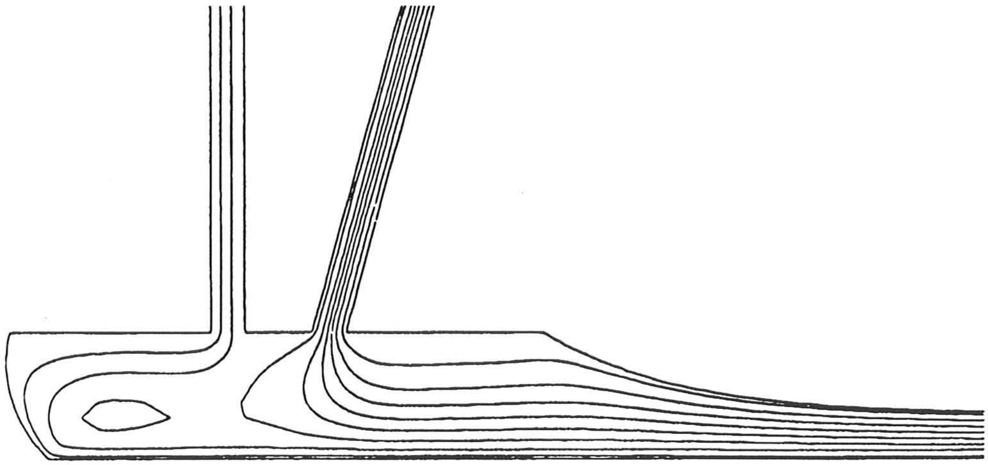

Streamline

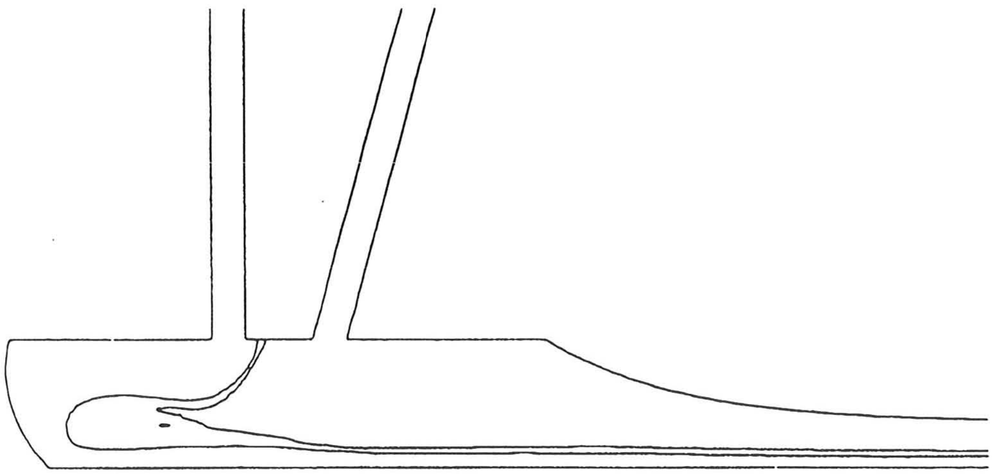

False Species Concentration

(d)

Figure 4.7 continued.

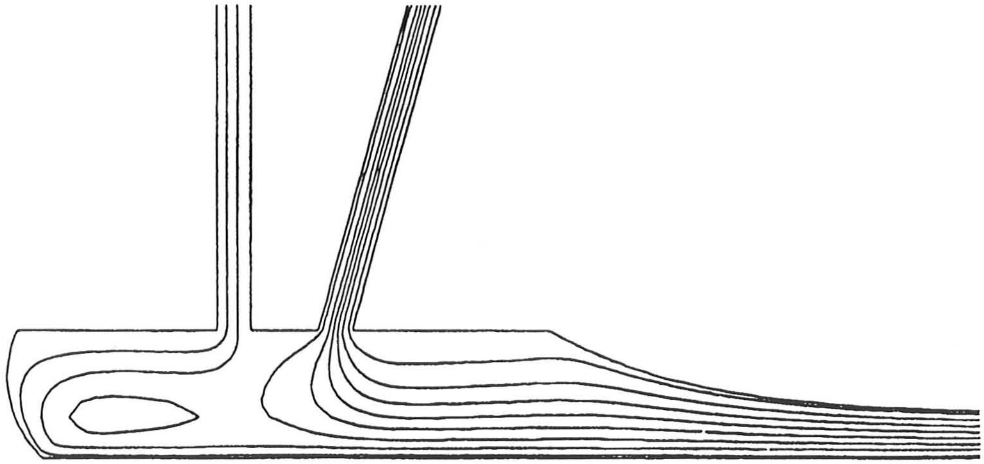

Streamline

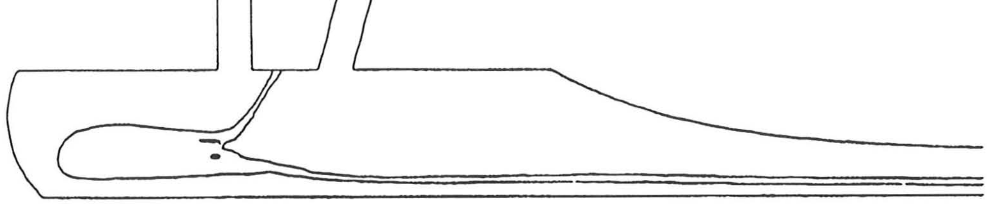

False Species Concentration

(e)

Figure 4.7 continued.

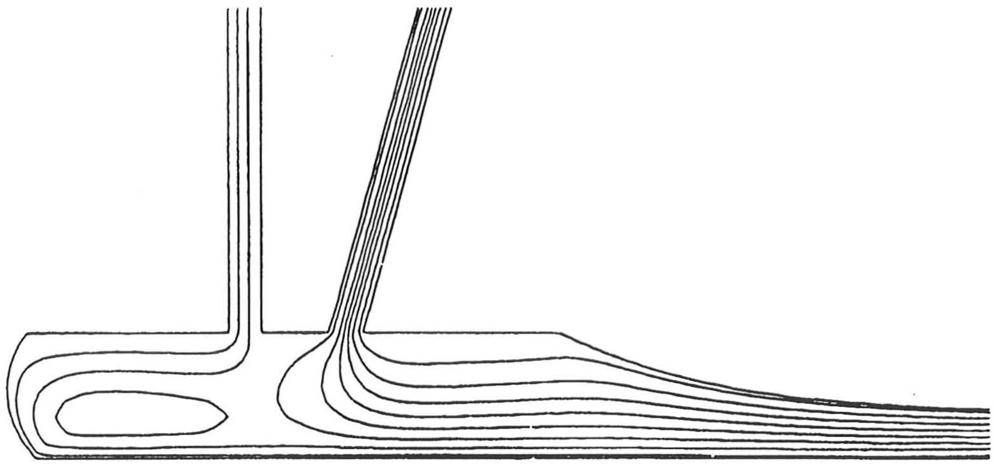

Streamline

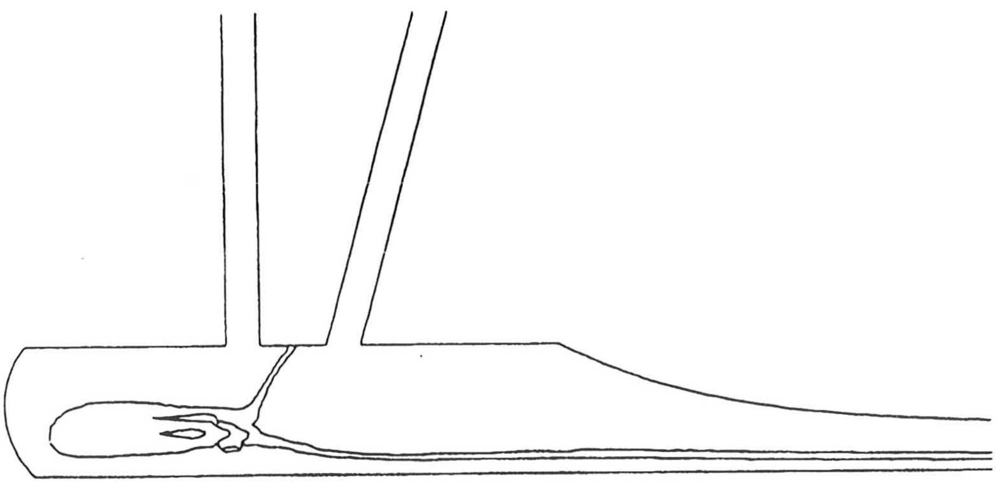

False Species Concentration

(f)

Figure 4.7 continued.

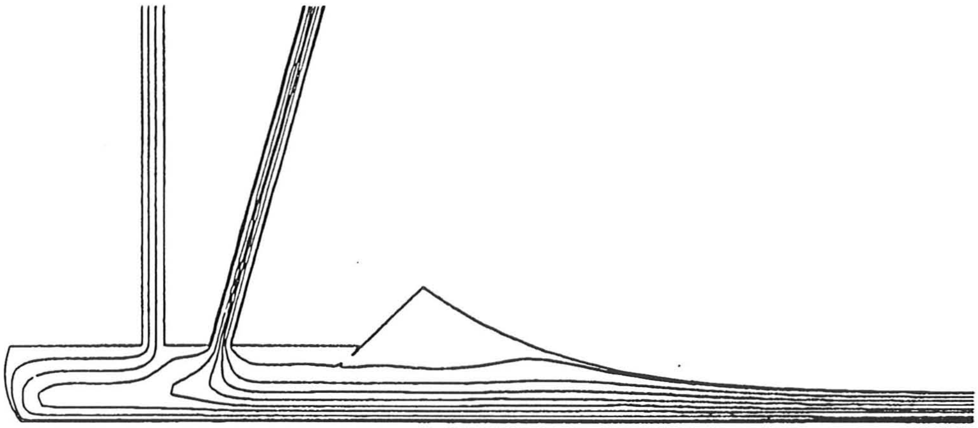

Streamline

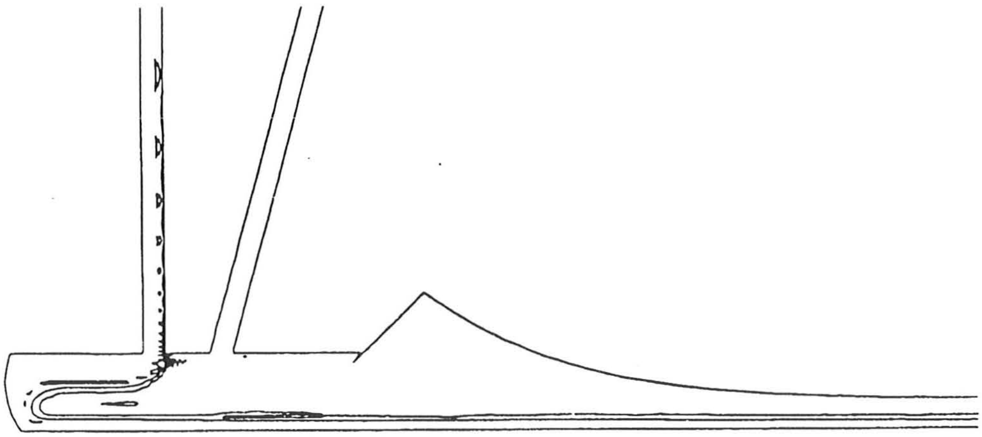

False Species Concentration

Figure 4.8: Streamlines and false species concentration contours of the two slot coater with a square centre block and wetting of the downstream shoulder.

Reduced Wet Thickness Ratio

In the experimental portion of this study, the wet thickness ratio had no significant effect on the structure of the flow field within the coating bead for the range of variables tested. Also, the reduced total wet thickness led to an increased vacuum pressure and reduced the required gap. Similar results were observed in the simulation of the coating bead with a reduced gap and a 1:1 wet thickness ratio.

The contour maps in Figure 4.9, when compared to Figure 4.7a, indicate that the wet thickness ratio had only minor effects on the flow field. Most noticeable is the reduced size of the pocket region which, with the reduced gap, extends only to the upstream feed slot. The smaller total wet thickness simulation required an increase in vacuum to 4.09 cmH20 (400 Pa), an effect also observed in the experiments where the vacuum was increased from 1.0 cmH_2O for a 175 μm thickness (2.5:1 wet thickness ratio) to 3.5 cmH_2O for a 100 μm thickness (1:1 wet thickness ratio).

Effect of Viscosity Ratio

The viscosity ratio is one of the most important parameters in multilayer coating since it has a strong effect on the structure of the flow field. This effect can be easily seen by comparing the series of contour maps given in Figures 4.7a-f.

Relatively small viscosity ratios, such as 2:1, had little effect on the coating bead; the flow structure in Figure 4.7b was nearly identical to the structure for a 1:1 viscosity ratio of Figure 4.7a. Increasing the viscosity ratio beyond 2:1 had a dramatic effect on

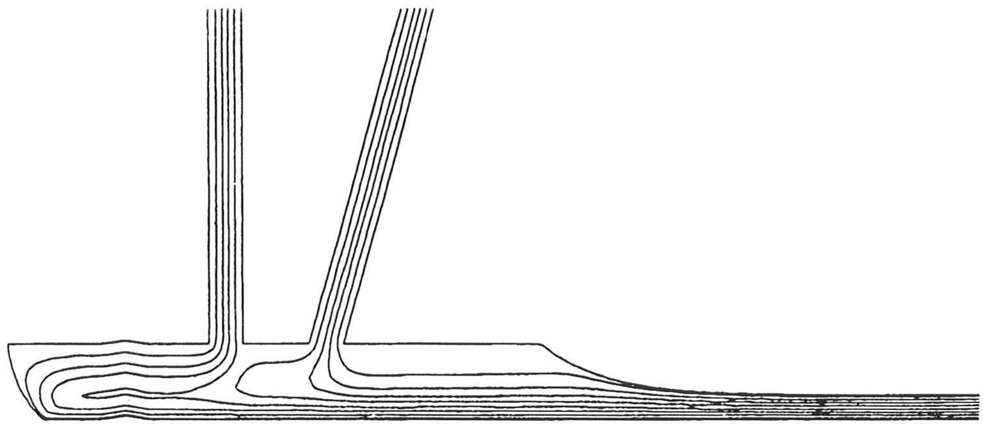

Streamline

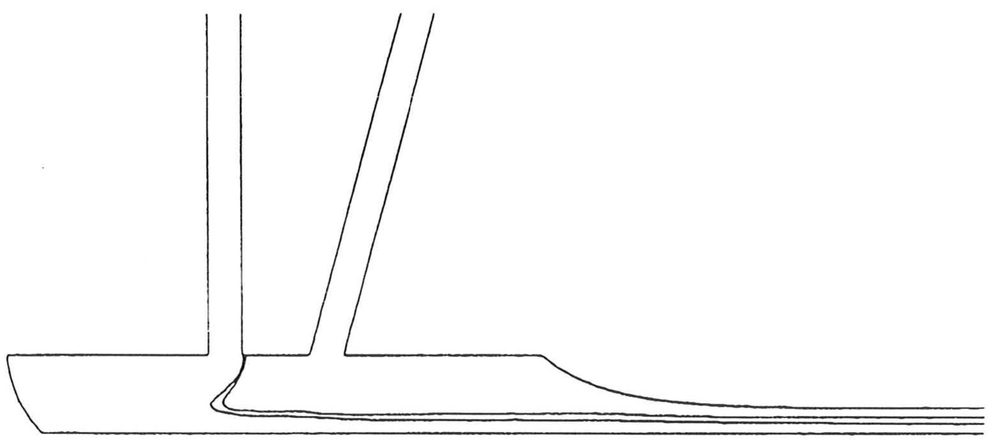

False Species Concentration

Figure 4.9: Contours of the two slot coater with a reduced coating gap and 1:1 wet thickness ratio.

the coating bead. At 4:1, a small vortex was formed in the pocket region that entrained liquid from both layers resulting in large mixing zone, dramatically increasing the size of the interfacial region (Figure 4.7c). Mixing within this zone was nearly complete as indicated by the uniform species concentration calculated to be an about the average of the top and bottom layer concentrations. Increasing the viscosity further saw the size of the recirculation and mixing zone increase to cover a large portion of the upstream region of the bead (Figures 4.7d-f). This large vortex was also observed in the experiments. The simulations also confirm some of suspicions raised in the experimental results section that a mixing zone, and not a second vortex, must occur for continuity to be satisfied.

As the viscosity ratio approached 10:1, the species concentration within the mixing zone did not increase with the average of the top and bottom layer concentrations. Instead, the species concentration within the mixing zone began to approach the lower layer species concentration which indicated that less top layer fluid was being entrained by the vortex. One would expect that further increases in the viscosity ratio, both experimental and numerically, would lead to the elimination of the large mixing zone at the interfacial region and the vortex would become an exclusive part of the bottom layer, having no influence on the top layer fluid.

Another noticeable effect of the viscosity ratio was the change in the separation line position. At lower ratios of 1:1 and 2:1, the separation line was pinned to the upstream corner of the square centre die block. The separation then became unpinned and gradually shifted downstream to the middle of the die block as the viscosity ratio was increased to 10:1. A similar effect was observed in the experiments where the switch to a

10:1 ratio saw the separation line migrate to the downstream corner of the centre die block (refer to Figure 3.5). Note that all the simulations were performed under constant vacuum pressure of 300 Pa whereas the experimental vacuum pressure was reduced as the ratio was changed from 1:1 to 10:1. Pinning of the separation line to the downstream corner of the centre die block could not be predicted by the model for the 10:1 viscosity ratio. Even when the vacuum pressure was lowered to zero, the simulation predicted only that the separation line shifted closer to the downstream corner of the centre die block.

4.2.3 Knife Geometry

Simulations of the two slot coating bead generated by the knife geometry showed good agreement with the experimental results. Again, simulations were performed over a range of viscosity ratios from 1:1 to 10:1 (top layer:bottom layer viscosity). The vacuum pressure was held constant in the simulations at 3.6 cmH_2O (350 Pa), slightly lower than the vacuum pressure used in the experiments. The simulation results are displayed in the series of contour plots of Figures 4.10a-f.

The first set of plots (Figure 4.10a) show good agreement with the experimental results, predicting that the separation line would be pinned to the knife edge and that a long pocket region would be formed in upstream region of the bead. The simulation even captured the slight thickening of the interfacial region at the bend of the pocket region. However, there were a number of subtle effects that were not captured by the simulations. For example, the bead of 1:1 viscosity ratio and 2.5:1 wet thickness ratio should result in the invasion of the upstream feed slot by the top layer fluid as well as show oscillation of the upstream meniscus and the pocket region. Both of these effects can not be captured by a steady state model, indicating a need for a transient (or stability) analysis of the knife geometry.

Small increases in the viscosity ratio had no significant effect of the predicted flow structure (Figure 4.10b). When the viscosity ratio reaches 4:1, a small recirculation appeared in the upstream region of the bead turning the pocket region into a large mixing zone (Figure 4.10c). Convective mixing of the two layers led to a false species concentration within the mixing zone that was roughly the average concentration of the two liquid layers. Again, the size of the vortex and related mixing zone grew larger with increasing viscosity ratio (Figure 4.10d). However, at a viscosity ratio of 8:1, the vortex begins to separate from the interfacial region to become a part of the bottom layer; only a small amount of convective mixing can be seen in the species contour plot of Figure 4.10e. Figure 4.10f indicates that the vortex became completely separate from the interfacial region when the viscosity ratio reached 10:1. Under these conditions, the vortex occupied a large portion of the upstream region and the interfacial reformed as a narrow band of fluid. The pocket region no longer existed, giving way to a band that extend only downstream of the knife edge. This flow structure exactly matches one of the two flow structures observed in the experiments where the viscosity ratio was 10:1 (refer to Figure 3.9b). The steady state model falls short in predicting the second of the two observed structures. Again, this second structure may be predicted by a transient analysis of the knife.

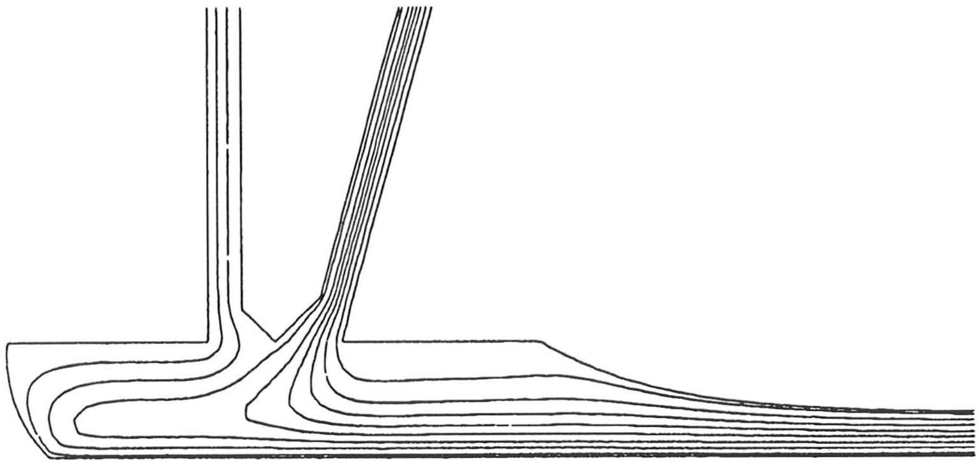

Streamline

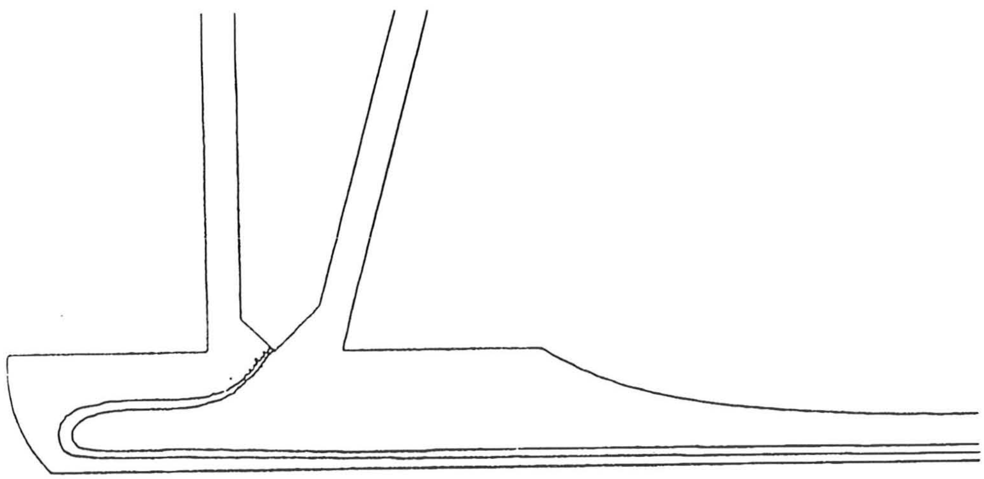

False Species Concentration

(a)

Figure 4.10: Streamlines and false species concentration contours for the knife geometry at the following viscosity ratios: (a) 1:1, (b) 2:1, (c) 4:1, (d) 6:1, (e) 8:1, and (f)10:1.

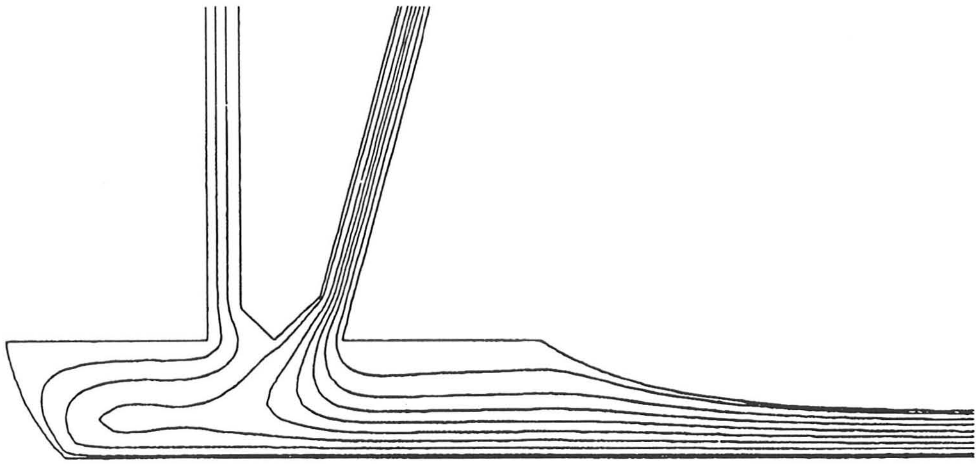

Streamline

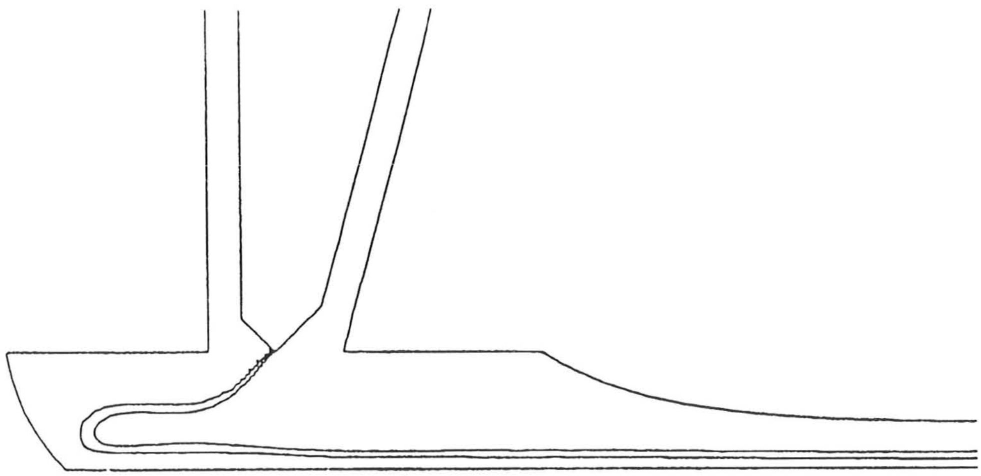

False Species Concentration

(b)

Figure 4.10 continued.

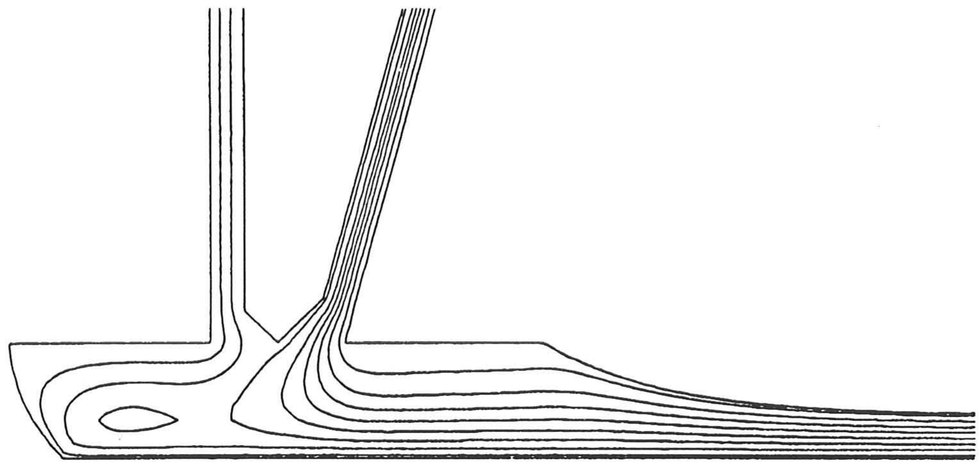

Streamline

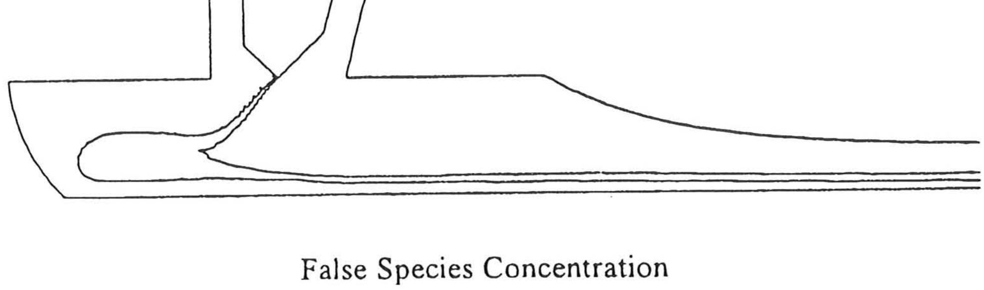

False Species Concentration

(c)

Figure 4.10 continued.

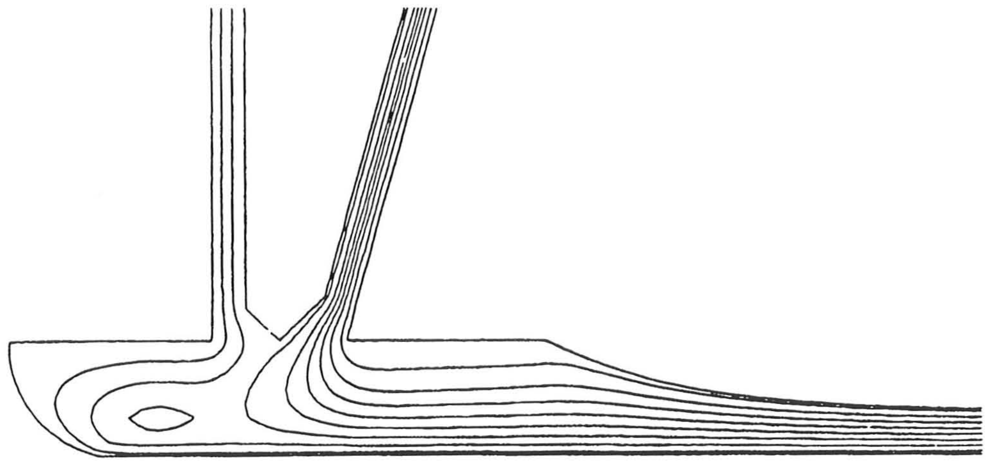

Streamline

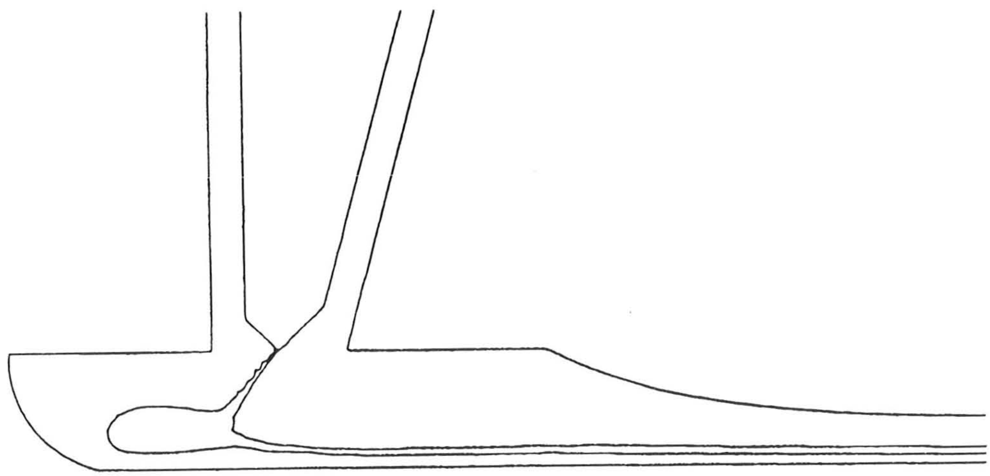

False Species Concentration

(d)

Figure 4.10 continued.

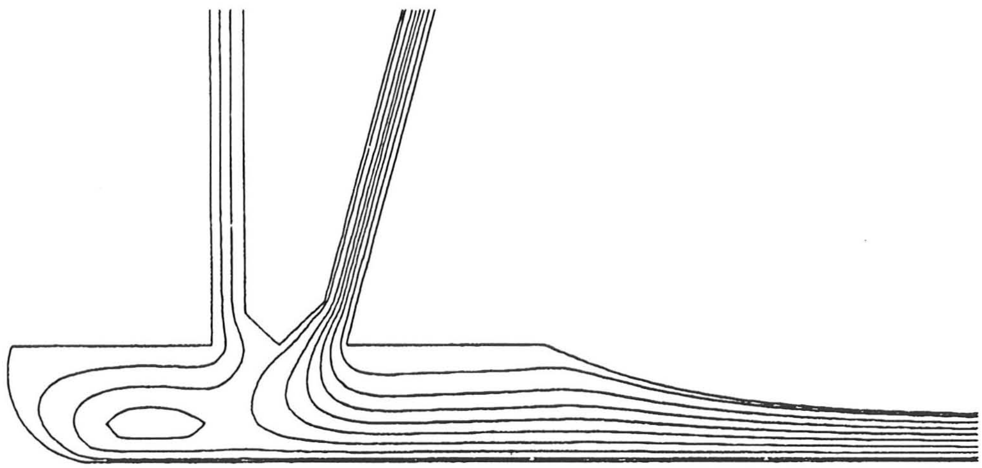

Streamline

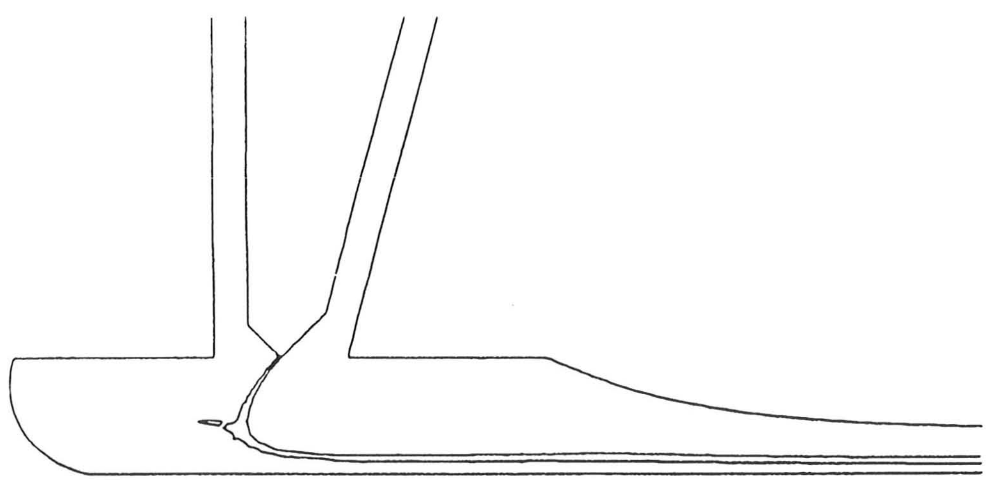

False Species Concentration

(e)

Figure 4.10 continued.

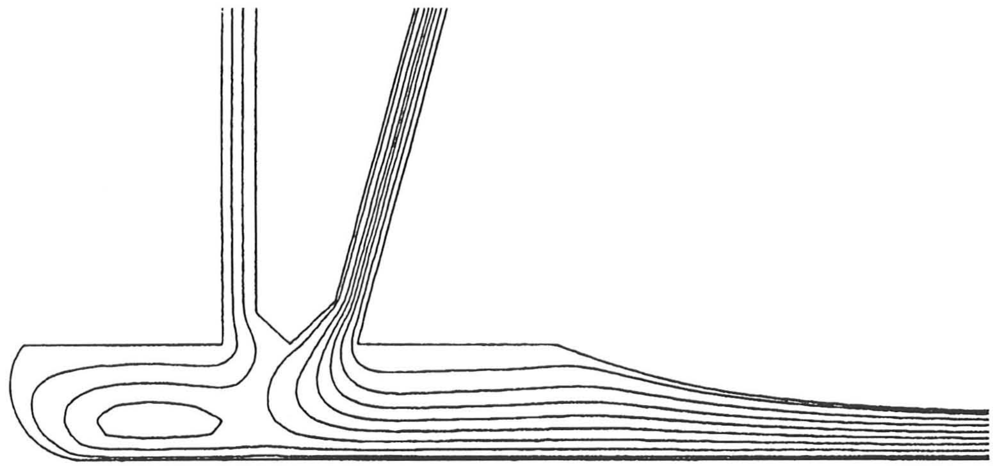

Streamline

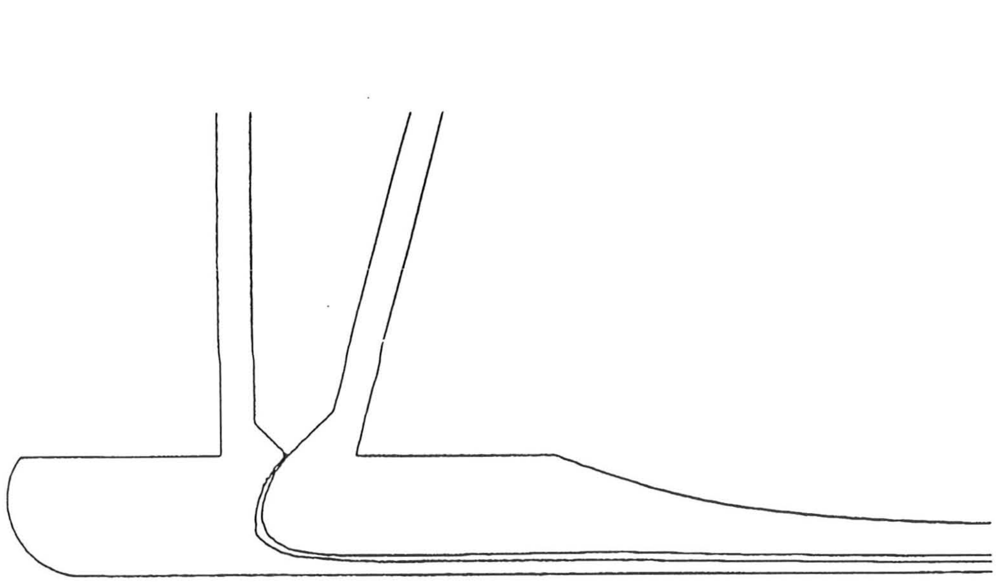

False Species Concentration

(f)

Figure 4.10 continued.

4.2.4 Bullet Geometry

The most promising die design from the experiments was the bullet centre block. The interfacial region was always a smooth line that formed a small pocket as it came off the upstream side of the bullet, extending just inside the upstream region of the bead. This result was independent of the wet thickness ratio or viscosity ratio. Simulations of the bullet geometry showed excellent agreement at low viscosity ratios but only reasonable agreement with the experiments at high viscosity ratios. The simulations are summarised in the series of contour maps in Figures 4.11a-f. Again, the vacuum was held constant at 3.06 cmH_2O (300 Pa) over the range viscosity ratios studied.

Simulation of the 1:1 viscosity ratio flow field was in excellent agreement with the experiments. Figure 4.11a shows that the pocket region was formed in the upstream region of the bead, although the size of the pocket was slightly over estimated. The species contour also indicated that the interfacial region came into contact with the centre block at about a 90° angle on the upstream side of the bullet, an effect also seen in the visualizations. Increasing the viscosity ratio saw the formation of a small vortex in the upstream region of the bead for a viscosity ratio of 4:1 (Figure 4.11c). The vortex turned the pocket region into a mixing zone that effectively created a large interfacial region in the upstream and intermediate sections of the bead. Both the vortex and mixing zone continued to grow as the viscosity ratio was increased to 6:1 (Figure 4.11d). The mixing zone disappeared at an 8:1 viscosity ratio returning the interfacial region to thin band (Figure 4.11e). The vortex continued to increase in size and separated from the interfacial region to become an exclusive part of the bottom liquid layer.

The simulations indicated that the large vortex persisted to occupy a large portion of the upstream region of the bead at a viscosity ratio of 10:1 (Figure 4.11f). Reducing the vacuum pressure to 1.02 cmH_2O (100 Pa) in the simulation could not eliminate the vortex, but only reduced it in the size. It is on this single point that the simulation contradicts the visualizations where no such vortex was observed. There is agreement on the position and general shape of the interfacial region, the simulation predicting that it remained a thin band throughout the bead. The separation line remained on the upstream side of the bullet edge, making contact with the centre block at nearly a 90° angle.

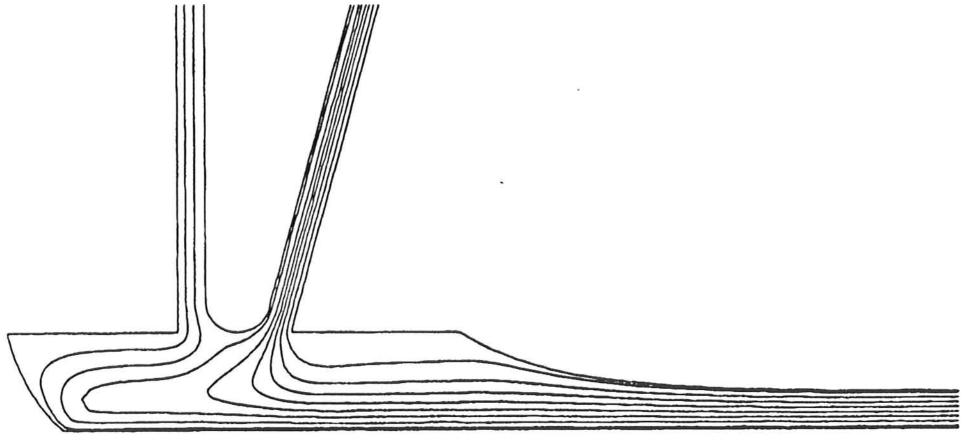

Streamline

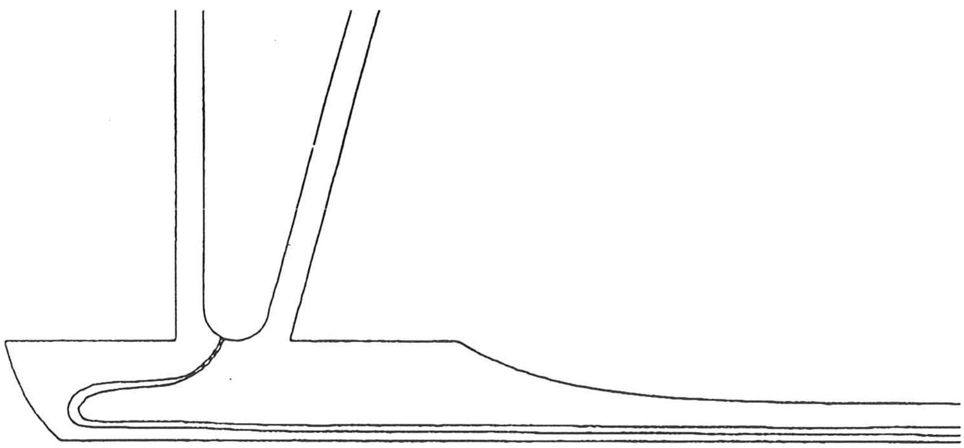

False Species Concentration

(a)

Figure 4.11: Streamlines and false species concentration contours for the bullet geometry at the following viscosity ratios: (a) 1:1, (b) 2:1, (c) 4:1, (d) 6:1, (e) 8:1, and (f)10:1.

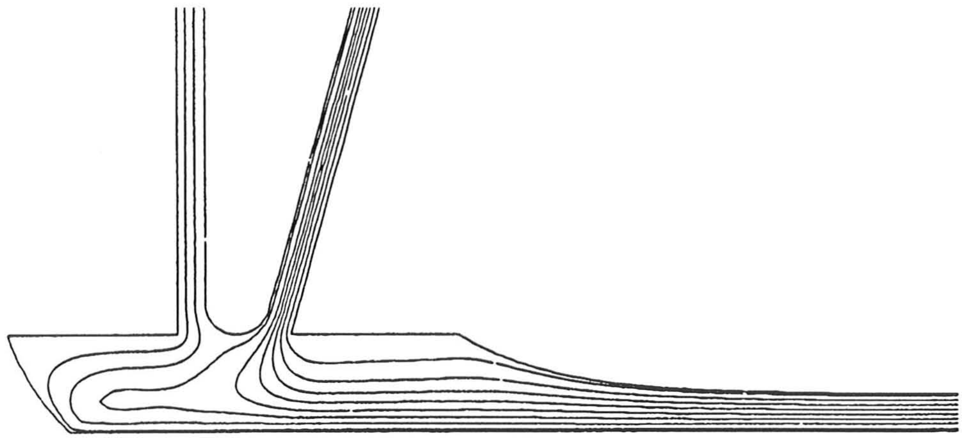

Streamline

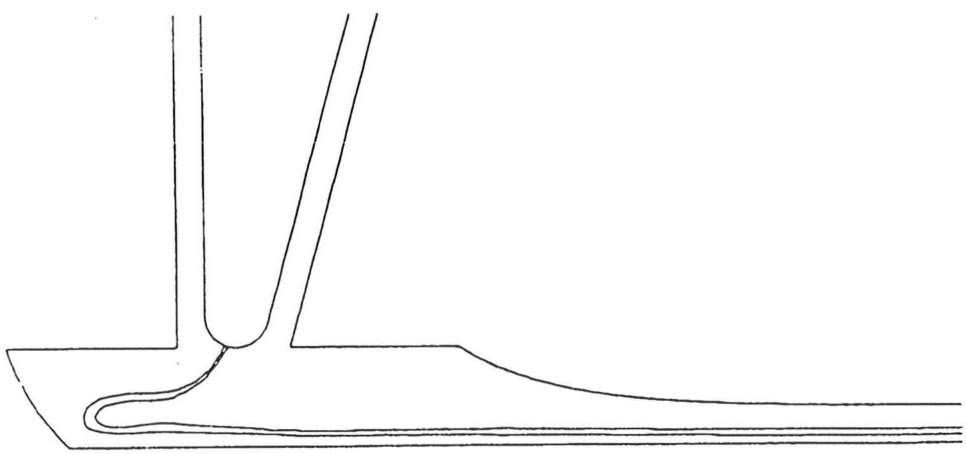

False Species Concentration

(b)

Figure 4.11 continued.

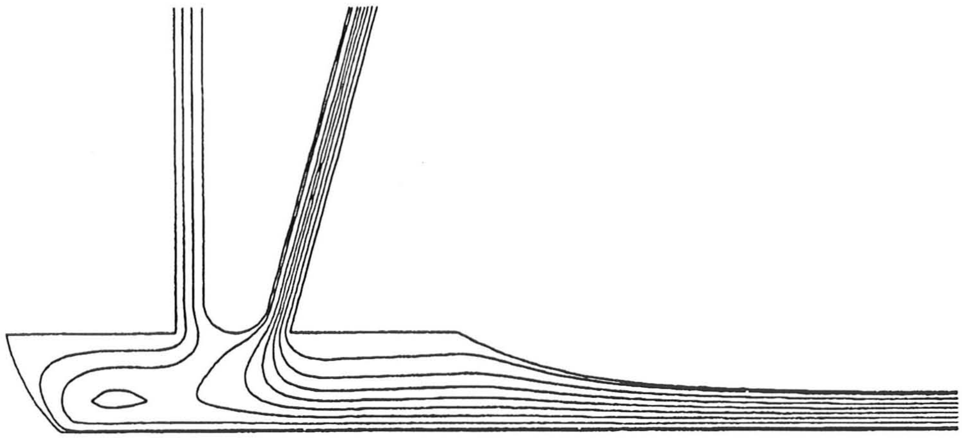

Streamline

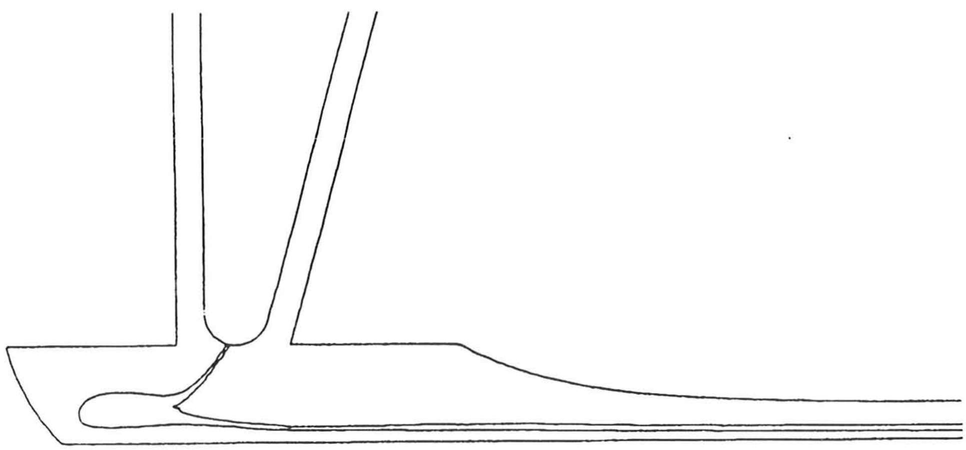

False Species Concentration

(c)

Figure 4.11 continued.

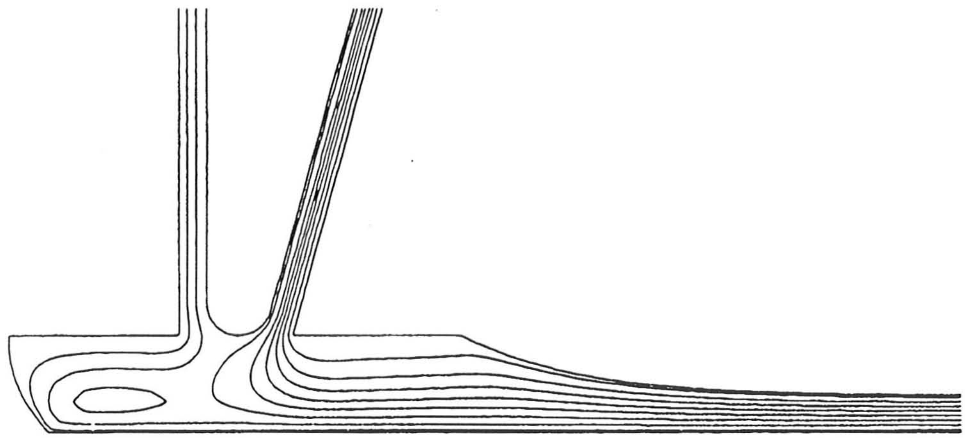

Streamline

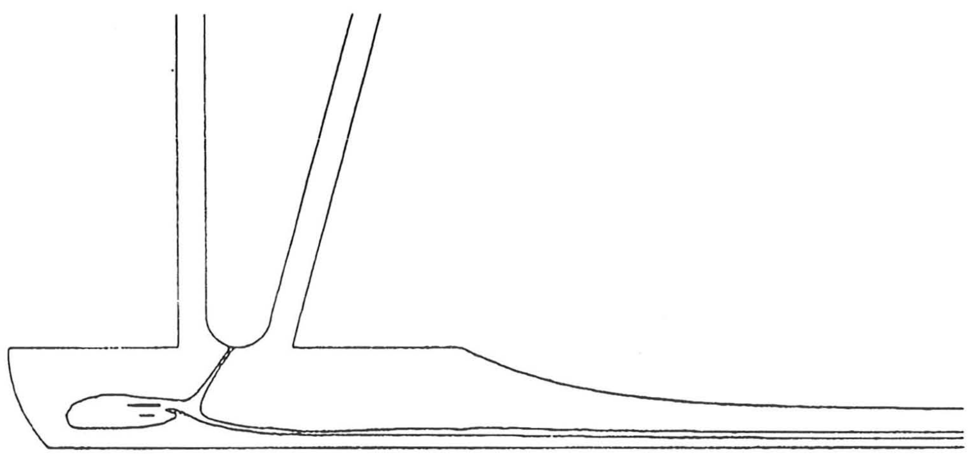

False Species Concentration

(d)

Figure 4.11 continued.

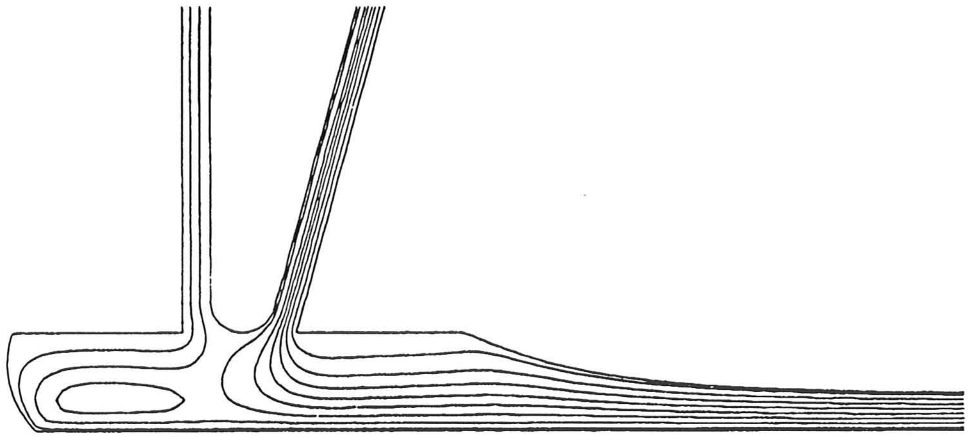

Streamline

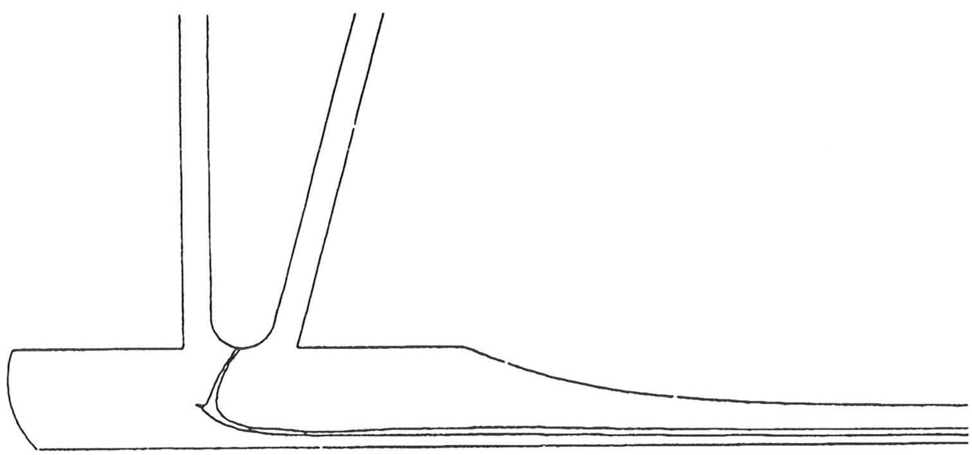

False Species Concentration

(e)

Figure 4.11 continued.

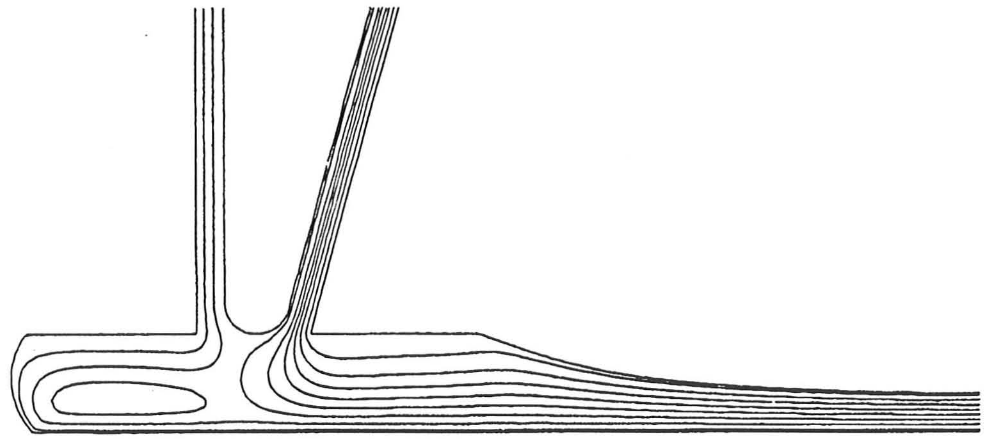

Streamline

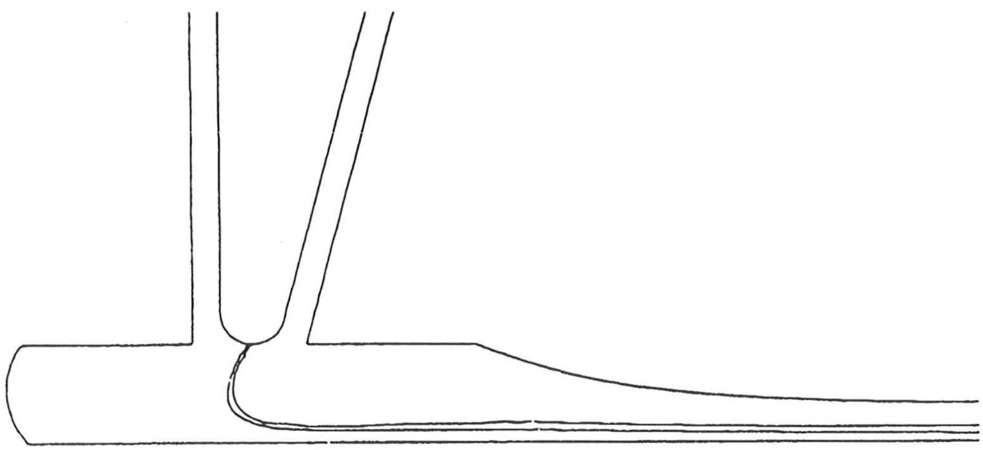

False Species Concentration

(f)

Figure 4.11 continued.

4.2.5 Groove Geometry

The simulations of the groove geometry provided excellent agreement with the visualization results, especially around the groove edge itself. The vacuum was held constant at 3.06 cmH_2O (300 Pa) for the entire range of viscosity ratios studied. Simulation results are presented in a series of contours in Figures 4.12a-f and Figures 4.13a-f.

The contours for the 1:1 viscosity ratio (Figure 4.12a) indicated that the separation line was pinned to the upstream edge of the groove. The simulations also predicted that the interfacial region formed a pocket in the upstream region of the bead. Both of these results exactly match the flow visualizations. It was also confirmed that a tiny vortex exists inside the groove itself (Figure 4.13a), a phenomena that could not be confirmed experimentally. Changing the viscosity ratio to 2:1 had little effect on the flow structure of the coating bead except to increase the size of the vortex inside the groove (Figure 4.13b).

Increasing the ratio to 4:1 had some fascinating effects on the structure of the coating bead. Once again, a small recirculation was formed in the upstream region of the bead but unlike previous geometries, only a small amount of convective mixing occurred between the two liquid layers. The general shape of the pocket still existed in the upstream region (Figure 4.12c). However, the separation no longer clearly defined since the growing vortex inside the groove (Figure 4.13c) created a second mixing zone within the groove itself. This second mixing zone was only temporary, since the separation line was quickly re-established on the downstream edge of groove when the viscosity ratio was raised to 6:1 (Figure 4.12d). At this ratio, the vortex inside the groove began to move out of the groove and into the intermediate section of the bead (Figure 4.13d). The recirculation in the upstream region increased in size and the convective mixing between the two liquid layers became more complete. Thus, the pocket region was again replaced by a large mixing zone that became a part of the interfacial region.

When the viscosity ratio was increased to 8:1, only trace amounts of convective mixing could be seen between the two liquid layers (Figure 4.12e). The large mixing zone in the upstream region was almost non-existent. At a 10:1 ratio, the mixing zone was completely eliminated, replaced by a thin band for the interfacial region. The interfacial region started at the separation line, pinned to the downstream edge of the groove, and then turned immediately downstream (Figure 4.12f). The recirculation still occupied a large portion of the upstream region of the bead and was completely contained within the bottom liquid layer. The second, small vortex that originated inside the groove was positioned in the middle of the coating bead, coupled with the large recirculation (Figure 4.13f). Both of these predictions match the visualizations very well (refer to Figure 3.12).

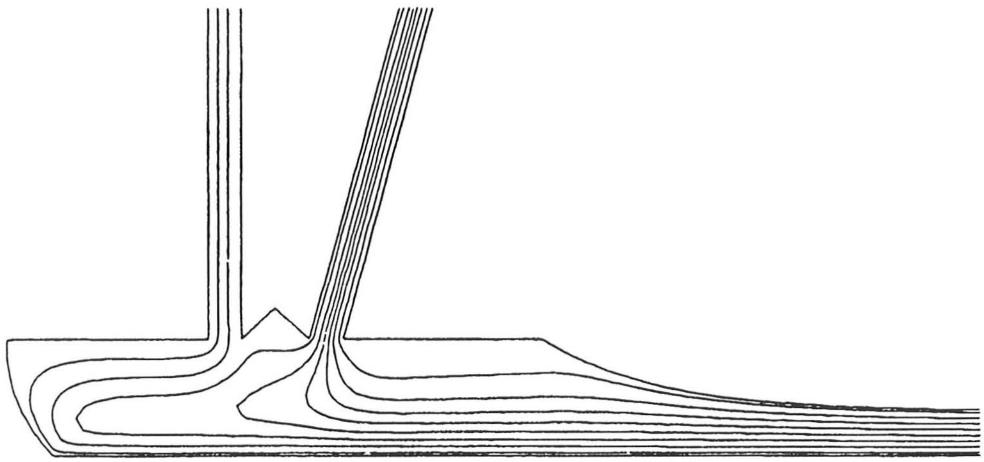

Streamline

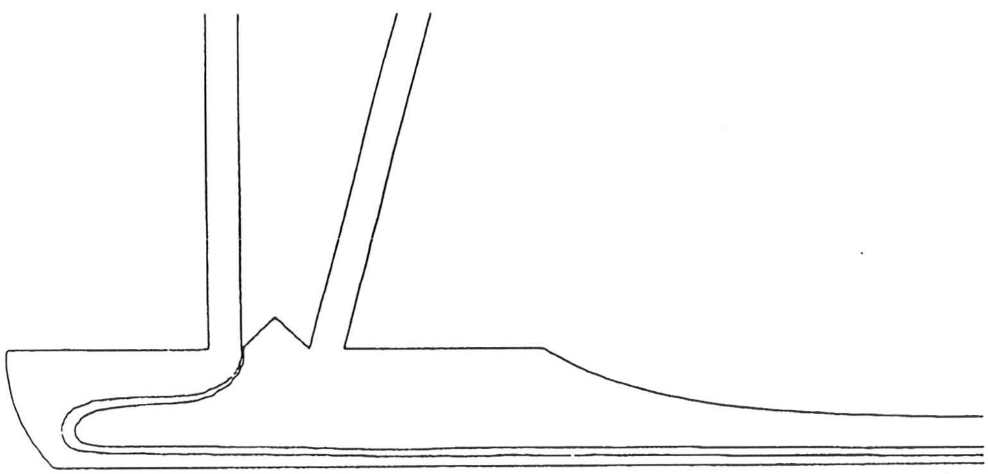

False Species Concentration

(a)

Figure 4.12: Streamlines and false species concentration contours for the groove geometry at the following viscosity ratios: (a) 1:1, (b) 2:1, (c) 4:1, (d) 6:1, (e) 8:1, and (f)10:1.

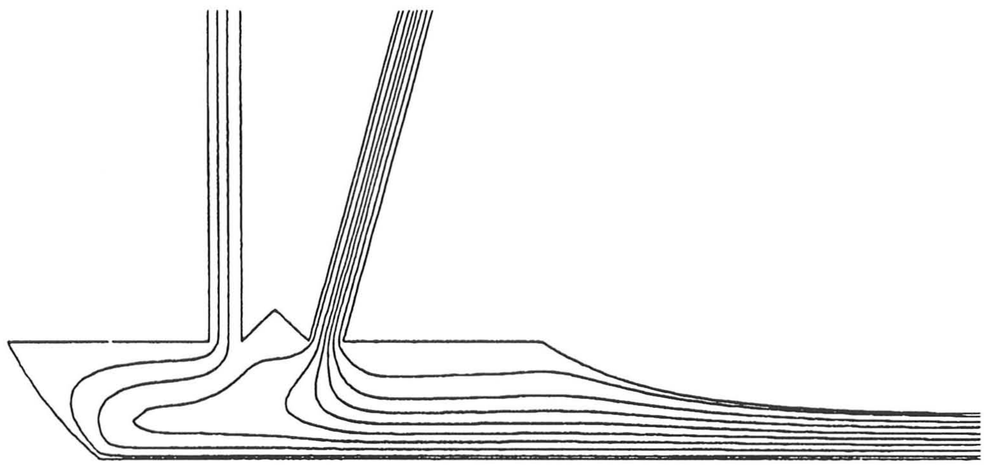

Streamline

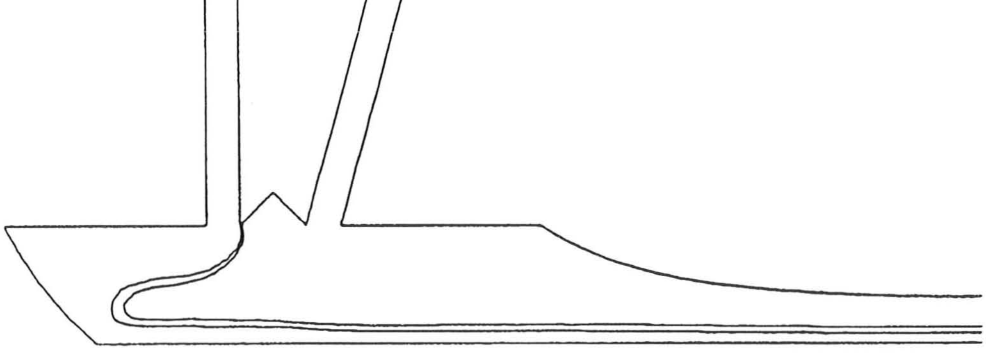

False Species Concentration

(b)

Figure 4.12 continued.

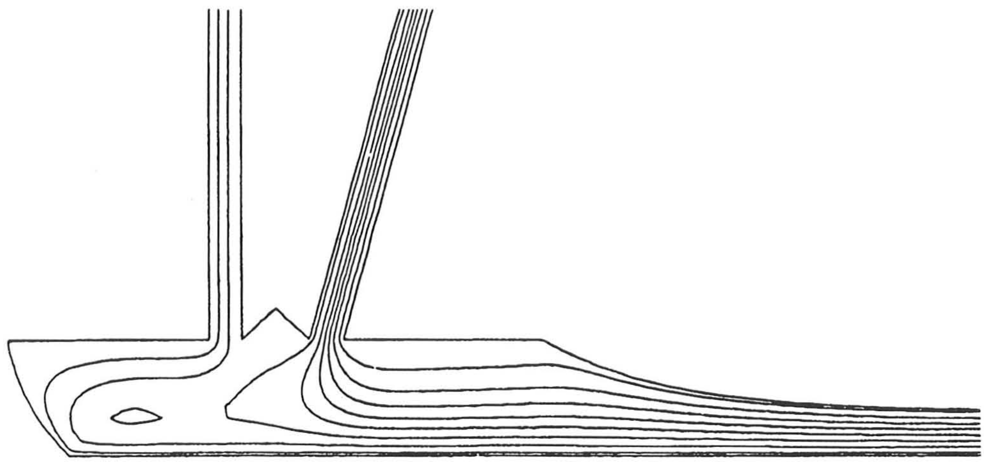

Streamline

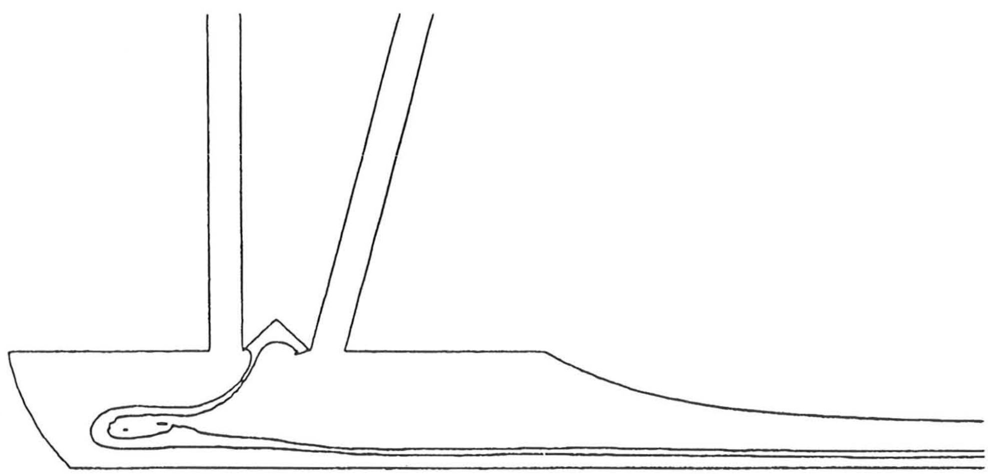

False Species Concentration

(c)

Figure 4.12 continued.

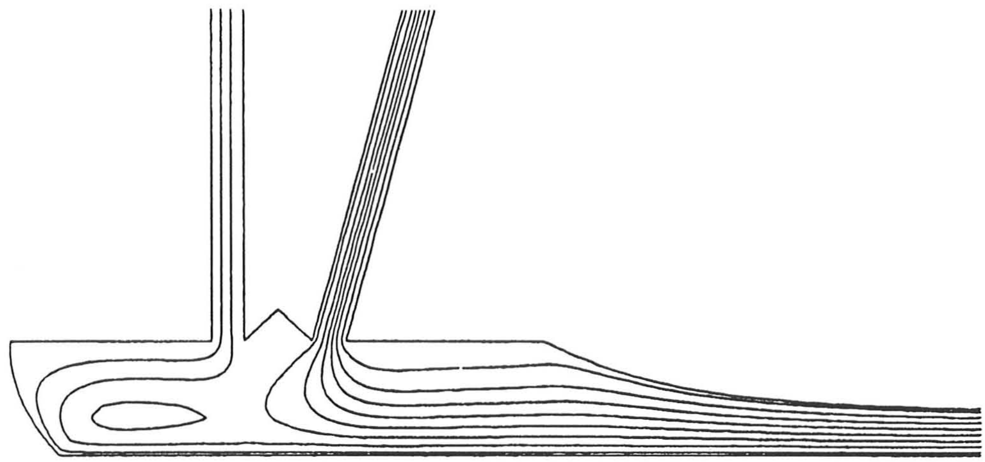

Streamline

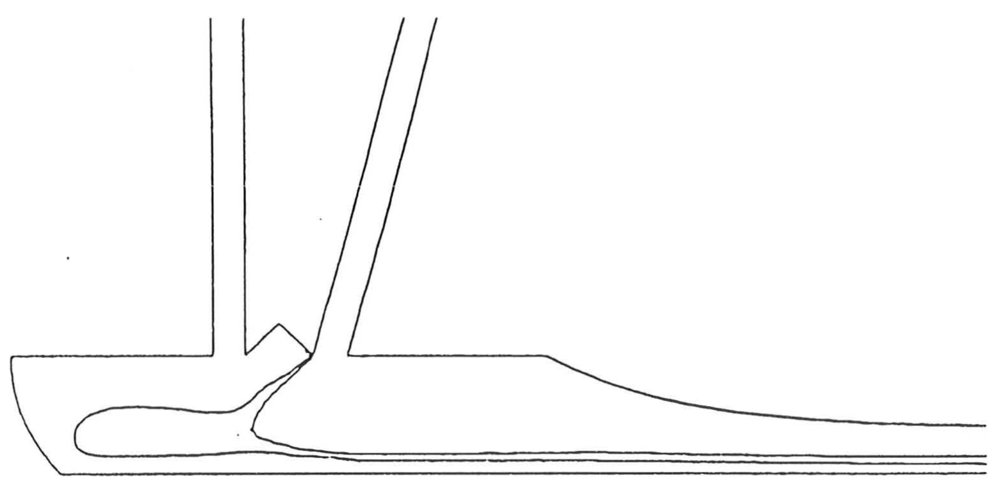

False Species Concentration

(d)

Figure 4.12 continued.

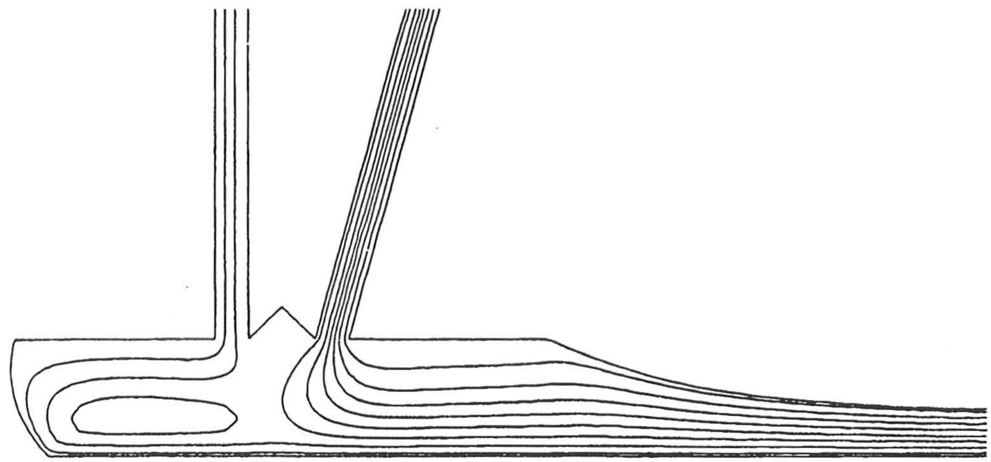

Streamline

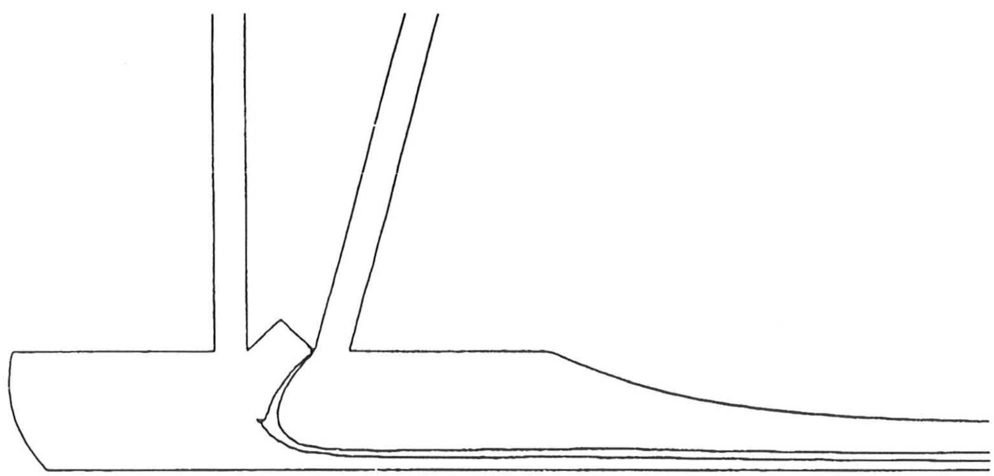

False Species Concentration

(e)

Figure 4.12 continued.

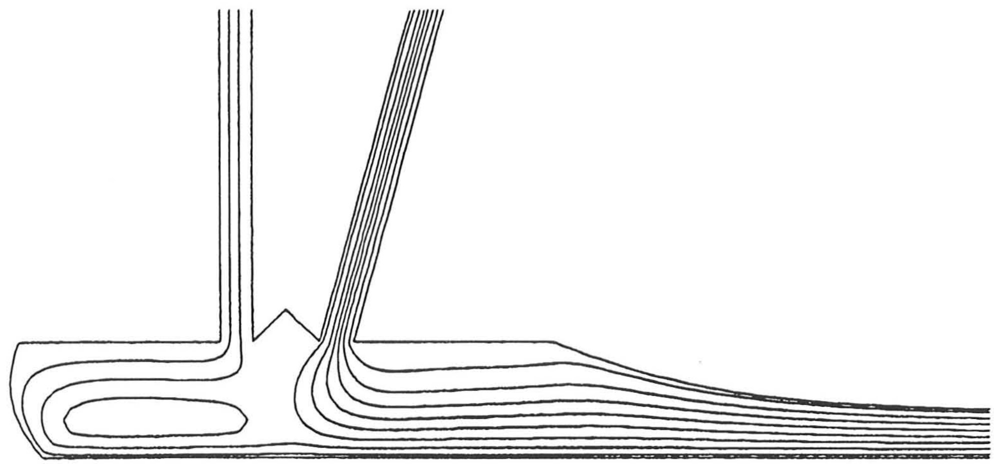

Streamline

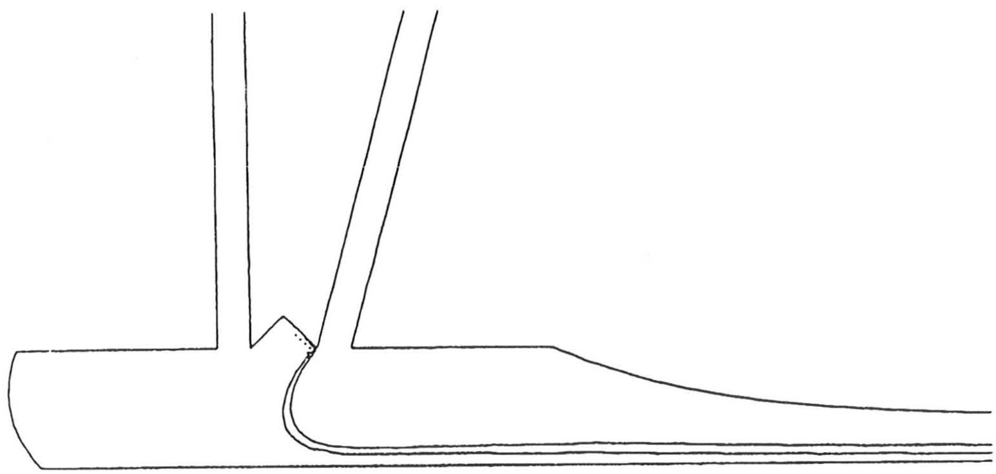

False Species Concentration

(f)

Figure 4.12 continued.

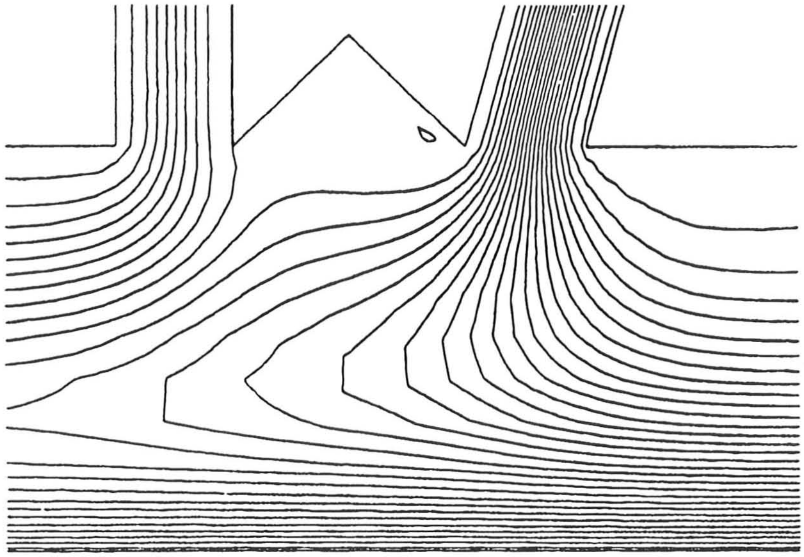

(a)

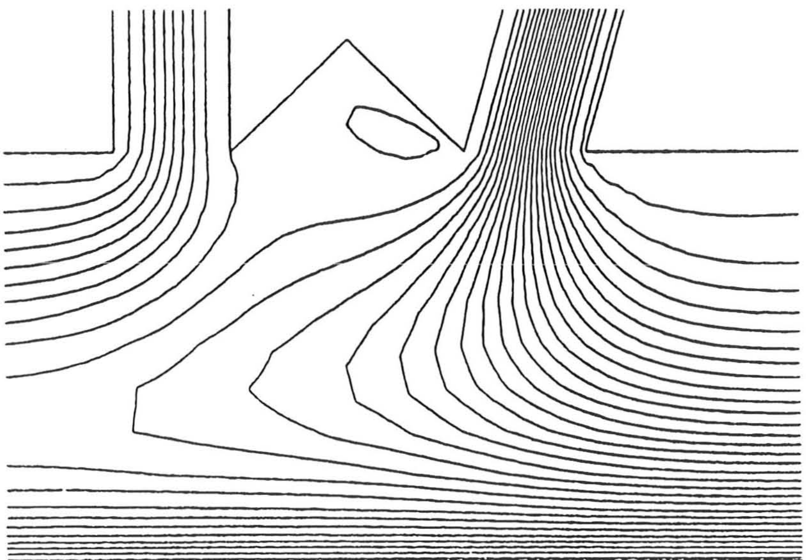

(b)

Figure 4.13: Streamlines indicate a tiny vortex inside or near the groove of the centre die block at the following viscosity ratios: (a) 1:1, (b) 2:1, (c) 4:1, (d) 6:1, (e) 8:1, and (f)10:1.

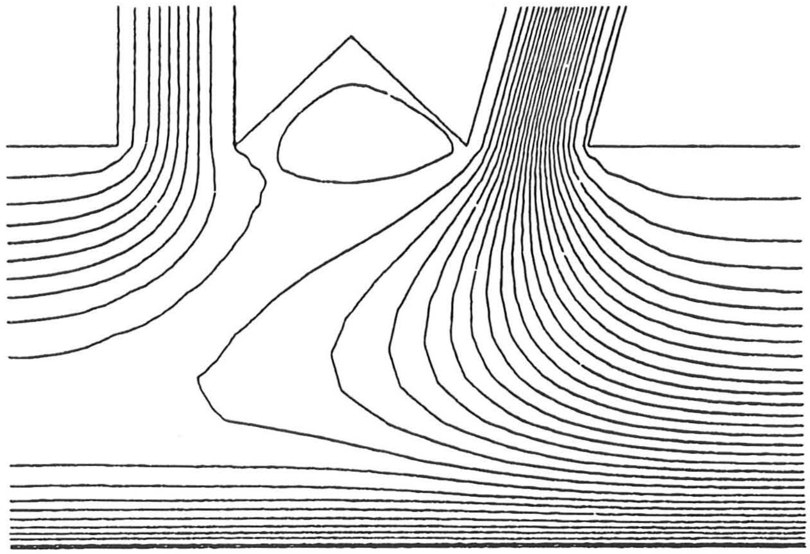

(c)

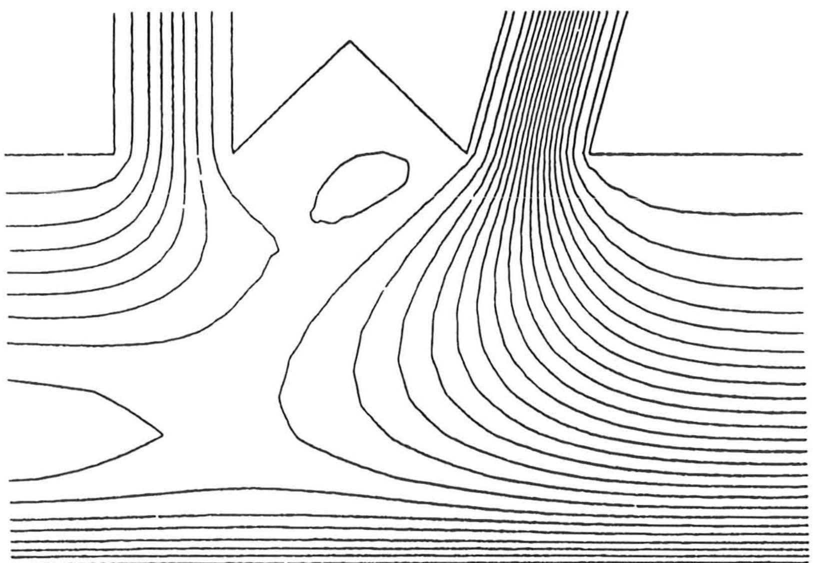

(d)

Figure 4.13 continued.

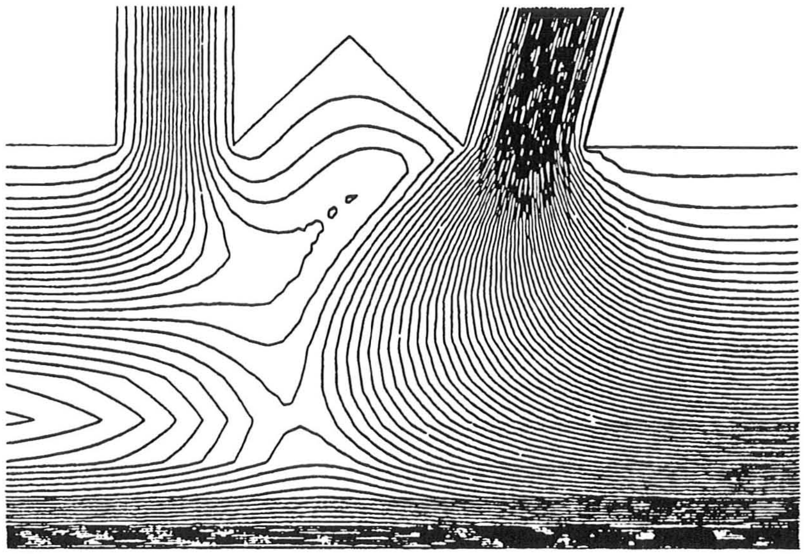

(e)

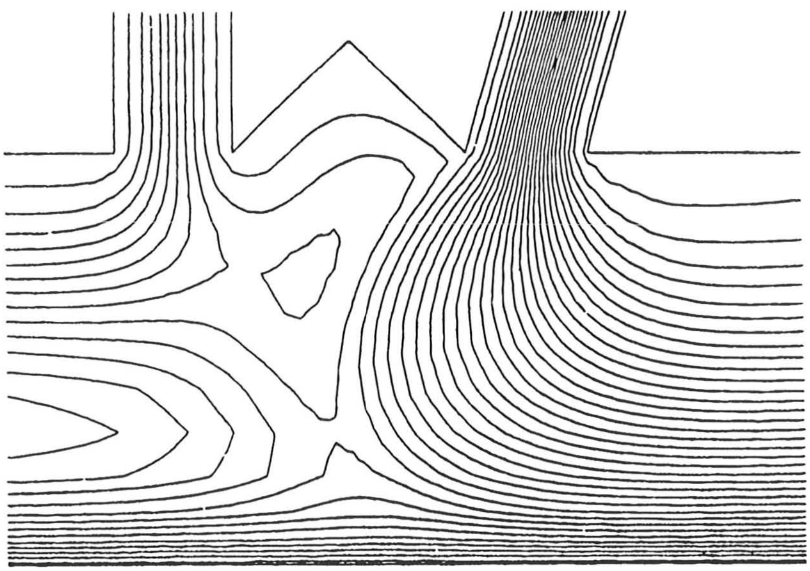

(f)

Figure 4.13 continued.

CHAPTER 5

CONCLUSIONS AND RECOMMENDATIONS

5.1 Conclusions

The objective of this work was to determine if significant mixing occurred between the miscible liquid layers of a two slot coater and how the shape of the centre die block effects the shape, position, and thickness of the interfacial region. Flow visualizations and numerical modelling of the coating bead revealed that diffusional and convective mixing can occur at the interfacial region. The viscosity ratio appeared to have the greatest effect on the shape and position of the interfacial region.

Flow visualizations of the coating bead showed the presence of mixing by a yellow region created by the mixing of fluorescein and sulforhodamine B. In coating beads created by the conventional square centre block, a thin yellow region was observed at the interfacial region to indicate diffusional mixing between the layers of equal viscosity. The yellow region was especially thick in the pocket region where the slow moving fluid turned and accelerated in the web direction. The interfacial region was also observed pinned to the upstream corner of the centre die block. Similar results were reported by Cohen(1993) who observed and predicted the interfacial region would pin to the upstream corner of the square centre block for flow rate ratios of 1:1 or greater. Increasing the viscosity ratio to 10:1 caused the interfacial region to pin to the downstream corner of the centre block and created a vortex near the interfacial region below the centre block itself.

Attempts were made to remove the vortex and reduce the thickening in the pocket area by changing the shape of the centre die block. The groove geometry only introduced a second, smaller vortex below the centre block while the knife geometry was often unstable for the tested operating conditions. On the other hand, the bullet geometry produced a stable bead with smooth streamlines and no vortices below the centre block at viscosity ratios of 1:1 and 10:1.

A two dimensional model was developed on FIDAP™ with the main feature of the model being the calculation of a false species concentration using the transport equation. Liquid viscosity was set as a function of the false species concentration, thus allowing for a gradient in fluid properties across the interfacial region. The interfacial region was defined as the region between the upper and lower contours false species concentration.

There was excellent agreement with the experiments for the square and groove geometries as well as good agreement for the knife and bullet centre blocks. For all four geometries, a vortex appeared below the centre die block for viscosity ratios of 4:1 to 10:1. This vortex led to convective mixing between the two liquid layers at viscosity ratios of 4:1 and 6:1 for all geometries and up to a ratio of 10:1 for the square geometry. The main drawback of using a steady state model was its inherent inability to predict transient behaviour, especially for the knife geometry. The model also fell short in predicting completely smooth flow for the bullet geometry.

5.2 Recommendations

While there are still several unanswered questions about multilayer slot coating, two particular areas appear to be important in understanding and improving the die design of a slot coater: curved die faces and viscosity.

The use of the curved die face (i.e. bullet geometry) has shown some advantages over the conventional flat die face (i.e. square geometry). Experimentally forcing the interfacial region to pin to an edge, such as the knife edge or the corner of the square centre block, leads to instability problems or convective mixing of the two layers. It appears that these problems might be avoided by allowing the interfacial region to move freely along a curved surface. However, the evidence to support this idea is limited to only a small range of operating parameters, such as low line speeds. Future efforts should be directed towards studying curved shaped die faces in more detail to determine the effects of radius of curvature and curved centre and downstream die blocks. There is also a need to establish an operating window for the bullet geometry through a full study of flow rate ratio, viscosity ratio, line speed, gap and vacuum.

Both experiments and modelling have shown that large shear rates often occur within the coating bead, thus making apparent viscosity very important. All published visualization studies, including this work, have been limited to studying Newtonian fluids. However, it is common for industry to use shear thinning solutions in their coating flows, making one question the validity of Newtonian studies to practical coating situations. Thus, future work should be directed at determining the effect of shear thinning fluids on the structure of the flow field within the coating bead.

REFERENCES

Barlett, L. C., Krall, H. J., US Patent 2,932,855, Eastman Kodak Company, Rochester, New York, 1960.

Beck, R. H., US Patent 2,901,770, E. I. du Pont de Nemeurs and Company, Wilmington, Delaware, 1959.

Beguin, A. E., US Patent 2,681,294, Eastman Kodak Co., Rochester, NY, 1954.

Blake, T. D., Clarke, A., Ruschak, K. J., "Hydrodynamic Assist of Dynamic Wetting", AIChE Journal, Vol. 40, No. 2, 229-242, 1994.

Cameron, E., Wills, P. A. R., US Patent 3,413,143, Ilford Limited, Essex, England, 1968.

Chen, K. S., Studies of Multilayer Slide Coating and Related Processes, PhD Thesis, University of Minnesota, 1992.

Chino, N., Hiraki, Y., Shibata, N., Sato, T., US Patent 5,030,484, Fuji Photo Film Co., Ltd., Kanagawa, Japan, 1991.

Cohen, D., Two Layer Slot Coating: Flow Visualization and Modelling, M.Sc. Thesis, University of Minnesota, 1993.

Cohen, E., Gutoff, E., eds, Modern Coating and Drying Technology, VCH Publishers, New York, NY, 1992.

Dheur, J., Crochet, M. J., "Newtonian Stratified Slow Through an Abrupt Expansion", Rheologica Acta Vol. 26, 401-413, 1987.

Dussan, E. B., "On the Spreading of Liquids on Solid Surfaces: Static and Dynamic Contact Lines", Annual Review of Fluid Mechanics, Vol. 11, 371-400, 1979.

Edwards, D. A., Brenner, H., Wason, D. T., Interfacial Transport Processes and Rheology, Butterworth-Heinemann, Boston, 1991.

Fluid Dynamics International (FDI), FIDAP 7.0 Manual, 1993.

Galdi, G. P., Joseph, D. D., Preziosi, L., Rionero, S., "Mathematical Problems for Miscible, Incompressible Fluids with Korteweg Stresses", European Journal of Mechanics, B/Fluids, Vol 10, No 3, 253-267, 1991.

Goldstein, R. J., Fluid Mechanics Measurements, Hemisphere Publishing Corporation, New York, 1983.

Gutoff, E. B., Kendrick, C. E., "Dynamic Contact Angles", AIChE Journal, Vol. 28, No. 3, 459-466, 1982.

Higgins, B. G., Capillary Hydrodynamics and Coating Beads, Ph.D. Thesis, University of Minnesota, 1980.

Hrymak, A. N., Stevanovic, M., 7th Annual Coating Symposium, AIChE Spring National Meeting, 1994.

Huebner, K. H., Thornton, E. A., The Finite Element Method for Engineers, 2nd Edition, John Wiley & Sons, Inc., New York, 1982.

Ishiwata, M., Uchida, Y., Nagai, Y., US Patent 3,573,965, Fuji Shashin Film Kabushiki Kaisha, Minami Ashigara-machi, Ashigara-Kamigun, Kanagawa, Japan.

Ishizuka, S., European Patent 0,313,043, Fuji Photo Film Co., Kanagawa, Japan, 1989.

Isrealachvili, J., Intermolecular and Surface Forces, 2nd Ed., Academic Press Limited, San Diego, 1992.

Joseph, D. D., "Fluid Dynamics of Two Miscible Liquids wtih Diffusion and Gradient Stresses", European Journal of Mechanics, B/Liquids, Vol 9, No 6, 565-596, 1990.

Kageyama, T., Yoshida, M., UK Patent 2,120,132B, Konishiroku Photo Industry Co., Tokyo, Japan, 1986.

Kistler, S. F., Scriven, L. E., "The Teapot Effect: Sheet-Forming Flows with Deflection, Wetting, and Hysteresis", Journal of Fluid Mechanics, Vol. 263, 19-62, 1994.

Korteweg, D., "Sur la forme que prennent les équations du mouvement des fluides si l'on tient compte des forces capillaires causées par des variations de densité", Arch. Néerl. Sci. Ex. Nat., Series II, Vol. 6, 1-24, 1901.

Miller, F. D., Wheeler, J. J., US Patent 3,206,323, Eastman Kodak Comapny, Rochester, New York, 1965.

Nagai, Y., Uchida, Y., US Patent 3,584,600, Ashigara Kamigun, Japan, 1971.

Reid, R. C., Sherwood, T. K., eds., The Properties of Gases and Liquids, 2nd Edition, McGraw-Hill, Toronto, 1966.

Russel, T. A., US Patent 2,761,791, Eastman Kodak Company, Rochester, New York, 1956.

Sartor, L., Slot Coating: Fluid Mechanics and Slot Design, Ph.D. Thesis, University of Minnesota, 1990.

Scanlan, D. J., Two-Slot Coater Analysis: Inner Layer Separation Issues in Two-Layer Coating, Masters Thesis, University of Minnesota, 1990.

Schweizer, P.M., "Visualization of Coating Flow", Journal of Fluid Mechanics, Vol 193, 285-302, 1988.

Scriven, L. E., Suszynski, W. J., "Take a Closer Look at Coating Problems", Chemical Engineering Progress, Vol. 86 No. 9, 24-29, 1990.

Shibata, N., Takeda, H., Sato, T., Tanaka, Y., US Patent 4,681,062, Fuji Photo Film Co., Ltd., Kanagawa, Japan, 1987.

Silliman, W. J., Viscous Film Flows with Contact Lines: Finite Element Simulation, a Basis for Stability Assessment and Design Optimization, Ph.D., University of Minnesota, 1979.

Smith, P. G., van de Ven, T. G. M., Mason, S. G., "The Transient Interfacial Tension between Two Miscible Fluids", Journal of Colloid and Interface Science, Vol 80, No 1, 302-303, 1981.

Thompson, E., "Use of Pseudo-Concentrations to Follow Creeping Viscous Flows During Transient Analysis", International Journal for Numerical Methods in Fluids, Vol 6, 749-761, 1986.

Umemura, M., Setsuko, K., Takemasa, N., Seiichi, T., Shigetochi, K., Nakajima, T., Nakano, Y., Koyama, N., US Patent 5,097,792, Konica Corporation, Tokyo, Japan, 1992.

Weast, R. C., ed. CRC Handbook of Chemistry and Physics, 63rd Edition, CRC Press, Inc., Boca Raton, Florida, 1982.

Woods, D. W., "Surfaces, Colloids and Unit Operations", Course Notes, McMaster University, 1995.

Yang, C., Li, D., "A Method of Determining the Thickness of Liquid-Liquid Interfaces", Colloids and Surfaces A: Physicochemical and Engineering Aspects, Vol 113, 51-59, 1996.

APPENDIX A

RECTILINEAR MODEL OF TWO SLOT COATER

The two slot coating bead can be modelled as rectilinear flow by ignoring the two dimensional flow near the feed slot. The main flow characteristics are obtained by dividing the bead into three sections: upstream, intermediate, and downstream (see Figure A.1). Each section can then be modelled as Couette flow of two liquid layers between parallel plates (see Figure A.2). Combining the results of each section will give any overall picture of coating bead.

Ignoring any body forces and convective terms, the Navier-Stokes equations for two Newtonian fluids simplify to become:

$$\frac{\partial p}{\partial x} = \mu_i \frac{\partial^2 u_i}{\partial y^2} \qquad \text{where } i = A, B \tag{A.1}$$

$$\frac{\partial p}{\partial y} = 0 \tag{A.2}$$

Equations A.1 and A.1put into dimensionless form by defining the following variables:

$$x' = \frac{x}{L} \quad y' = \frac{y}{h} \quad u' = \frac{u}{U} \tag{A.3}$$

where L is the section length, h is the height of the coating gap and U is the web speed. Equation (1.24) can then be written in dimensionless form:

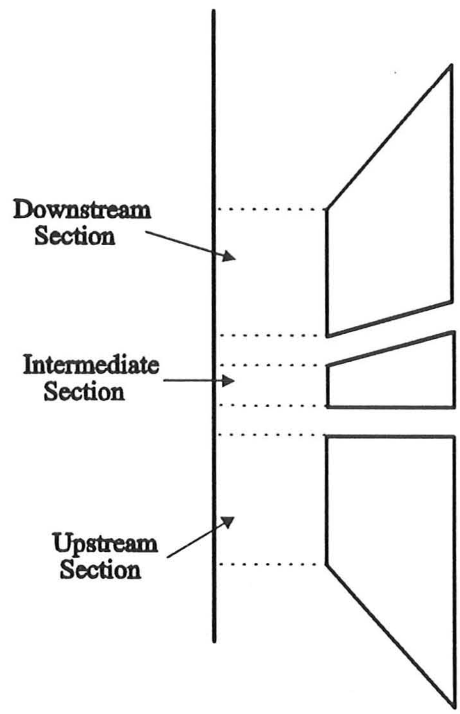

Figure A.1: The separation of a two slot coating bead into three sections (Cohen, 1993).

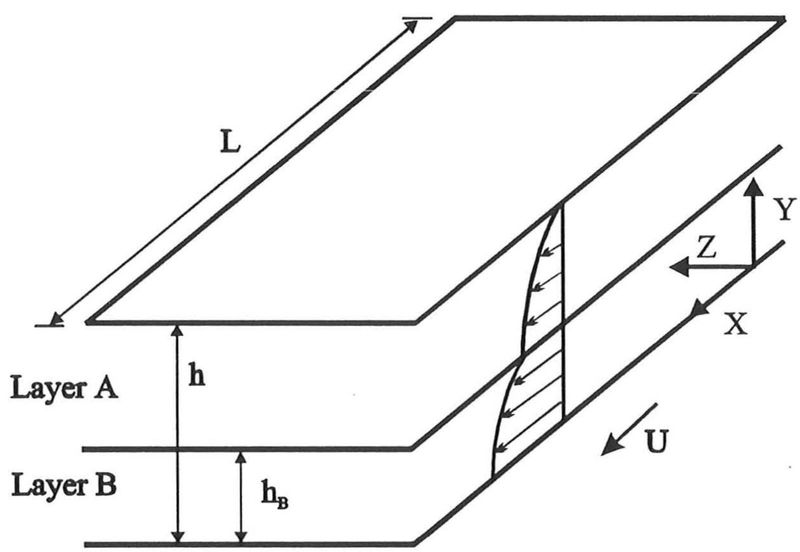

Figure A.2: Sketch of two layer parallel plate model.

$$\frac{d^2 u'_A}{dy'^2} = -P_s \qquad \frac{d^2 u'_B}{dy'^2} = -m P_s \tag{A.4}$$

where P_s is the Poiseulle number:

$$P_s \equiv \frac{\frac{-dp}{dx'} h^2}{\mu_A UL} \tag{A.5}$$

The boundary conditions are:

$$u'_B = 1 \text{ at } y' = 0 \tag{A.6}$$

$$u'_A = 0 \text{ at } y' = 1 \tag{A.7}$$

$$u'_A = u'_B \text{ at } y' = s = \frac{h_B}{h} \tag{A.8}$$

$$m\frac{du'_A}{dy'} = \frac{du'_B}{dy'} \text{ at } y' = s \tag{A.9}$$

The analytical solution for the velocity profile can then be obtained by integrating equation (A.4):

$$u_A = -P_s\frac{y'^2}{2} + \alpha_1 y' + \alpha_2 \qquad u_B = -mP_s\frac{y'^2}{2} + \beta_1 y' + \beta_2 \tag{A.10}$$

The constants (α_i, β_i) are determined by applying the no-slip condition at the solid surfaces and forcing the continuity of velocity and shear stress at the fluid-fluid interface. The pressure profile in each section is then obtained by simply integrating the pressure gradient over the section length:

$$\Delta p = \int_0^L \frac{-P_s \mu_A UL}{h^2} dx \tag{A.11}$$

Finally, the pressure change from the upstream to the downstream meniscus is the sum of the pressure change in each section:

$$\Delta p_{bead} = \Delta p_{upstream} + \Delta p_{intermediate} + \Delta p_{downstream} \tag{A.12}$$

After all the substitutions, the overall pressure change can be expressed in the following form:

$$\Delta p_{bead} = 6\mu_A V \left[\frac{1}{m} \int_0^{L_U} \frac{ds}{h^2} + \int_0^{L_i} \frac{(1-s^2\delta) - 2q_L(1-s\delta)}{h^2 f(s,\delta)} dx + \int_0^{L_d} \frac{(1-s^2\delta) - 2q_t(1-s\delta)}{h^2 f(s,\delta)} dx \right] \tag{A.13}$$

where d, i, u refer to the downstream, intermediate, and upstream sections, $s=h_L/h$ is the interface position and $\delta=1-m$. q_B, q_t are the dimensionless lower layer and overall flow rates, defined as:

$$q_B = \frac{Q_B}{Uh_B} \quad \text{and} \quad q_t = \frac{Q_t}{Uh} \tag{A.14}$$

where Q_B and Q_t are the volumetric flow rates per unit width. The function, f, is defined as:

$$f(s,\delta) \equiv 1 - 4s\delta + 6s^2\delta - 4s^3\delta + s^4\delta^2 \tag{A.15}$$

APPENDIX B

TRACER PREPARATION

Tracers are one of the basis to experimental fluid mechanics. Tracers enable the researcher to observe detailed flow patterns and, with the proper equipment, measure velocities at any given point in a flow field. However, care must be used in selecting the proper tracer for each experiment. A good tracer will follow the movement of the fluid and reflect (or emit) enough light to be visible to a recording device. For example, larger particles will reflect light well but will not follow the flow around bends due to the large momentum of the particle itself.

In this work, two types of tracers were used to study the flow pattern in the coating bead: particles and fluorescent dyes. Before these tracers could be used, some preparation was required to alter the tracers into a form (solution or suspension) that would not affect the flow structure of the bead. It is important that, when injected into the flow, the tracers did not create any density or viscosity gradients which would change the structure of the coating flow and thus, result in a false measurement.

Particle Tracers

A rheoscopic fluid (AQ-1000, Kalliroscope Corporation) was used as the source of particles for the visualization. The fluid contained a high concentration of particles, such as titanium oxide and mica, suspended in an aqueous solution. The density and viscosity of the fluid was equivalent to that of water and hence, could not be injected directly into the coating flow without causing problems. The density and viscosity of the fluid were adjusted by mixing glycerin (99.5 %wt) and the rheoscopic fluid together in the same proportions as the coating solutions: 77 %wt glycerin for the low viscosity solution and 96.5 %wt glycerin for the high viscosity solution. These new solutions were then injected directly into the coating flow. Due to the preparation procedure, the low viscosity particle solution resulted in better visualizations because more particles were added to the solution.

Fluorescent Dye Tracers

Fluorescein disodium salt and sulforhodamine B (laser grade) were selected as the dye tracers since both were soluble in water and fluoresced brightly at low concentrations when exposed to blue-green light. Both dyes were stored in powder form and as such, could not be inserted directly into coating flow. Instead, the dyes had to be dissolved into a liquid before being injected into the flow field. The dye solutions were prepared as follows:

1. Take two-1 liter samples of the low viscosity (39 cp) glycerin solution stored in the pressure pots.
2. Dissolve 2.0 mg of fluorescein disodium salt into one sample and 5.0 mg of sulforhodamine B into the other sample.
3. Repeat steps 1 and 2 using the high viscosity (386 cp) glycerin solution.

The dye tracer solutions could then be injected directly into the coating flow.

APPENDIX C

SUMMARY OF EXPERIMENTAL OPERATING CONDITIONS

The following series of tables provide a list of the all the flow visualizations completed and the values of every operating variable for each run. The layer viscosity, wet thickness of each layer, and the line speed were set according the ratios specified in Table 2.2. The gap was held constant at 305 μm and 457 μm for total wet thicknesses of 100 μm and 175 μm, respectively. However, the gap was increased or decreased for some operating conditions where a stable coating bead was difficult to obtain or to avoid severe wetting of the downstream shoulder.

Table C.1: Visualizations of the Square Geometry

Run #	Top Layer Viscosity (cp)	Top Layer Wet Thickness (μm)	Bottom Layer Viscosity (cp)	Bottom Layer Wet Thickness (μm)	Line Speed (m/s)	Coating Gap (μm)	Vacuum (cmH_20)
1	39	50	39	50	30	305	0.2
2	39	50	39	50	60	203	3.0
3	39	125	39	50	30	457	0.1
4	39	125	39	50	60	457	1.6
5	389	50	39	50	30	305	3.3
6	389	50	39	50	60	305	2.7
7	390	125	39	50	30	457	0.6
8	390	125	39	50	60	457	0.2
9	38	125	39	50	30	686	0
10	38	125	39	50	30	508	0.5
11	406	125	35	50	30	457	0
12	406	125	35	50	60	457	0
13	406	125	35	50	30	457	0
14	406	125	35	50	60	457	1.6
15	39	50	39	50	30	381	2.2 to 2.7
16	39	50	39	50	50	203	4.5 to 6.0
17	39	50	39	50	30	305	1.8
18	39	50	39	50	50	203	5.3

Table C.2: Visualizations of the Knife Geometry

Run #	Top Layer Viscosity (cp)	Top Layer Wet Thickness (μm)	Bottom Layer Viscosity (cp)	Bottom Layer Wet Thickness (μm)	Line Speed (m/s)	Coating Gap (μm)	Vacuum (cmH_2O)
1	39	50	39	50	30	305	2.5
2	39	50	39	50	60	178	4.1
3	39	125	39	50	30	457	0.6
4	39	125	39	50	60	457	2.1
5	388	50	39	50	30	305	2.6
6	388	50	39	50	60	229	2.8
7	388	125	39	50	30	457	2.3
8	388	125	39	50	60	457	2.7
9	39	125	39	50	30	457	0.3
10	388	125	39	50	30	457	3.0

Table C.3: Visualizations of the Bullet Geometry

Run #	Top Layer Viscosity (cp)	Top Layer Wet Thickness (μm)	Bottom Layer Viscosity (cp)	Bottom Layer Wet Thickness (μm)	Line Speed (m/s)	Coating Gap (μm)	Vacuum (cmH_2O)
1	39	50	39	50	30	279	1.9
2	39	50	39	50	60	152	2.3
3	39	125	39	50	30	457	3.0
4	39	125	39	50	60	457	2.3
5	389	50	39	50	30	254	2.6
6	389	50	39	50	60	305	2.4
7	389	125	39	50	30	457	1.5
8	389	125	39	50	60	457	1.8

Table C.4: Visualizations of the Groove Geometry

Run #	Top Layer Viscosity (cp)	Top Layer Wet Thickness (μm)	Bottom Layer Viscosity (cp)	Bottom Layer Wet Thickness (μm)	Line Speed (m/s)	Coating Gap (μm)	Vacuum (cmH_2O)
1	39	50	39	50	30	305	3.1
2	39	50	39	50	60	305	4.1
3	39	125	39	50	30	584	0
4	39	125	39	50	60	457	0.6
5	388	50	39	50	30	305	1.0
6	388	50	39	50	60	not stable	-
7	388	125	39	50	30	457	0
8	388	125	39	50	60	356	0